การวิเคราะห์ตัวประกอบความเข้มของความเค้นสำหรับคานรูปตัวไอที่มีรอยร้าวโดยผิวรอยร้าวไม่ซ้อนทับกัน

นายฮู ชิ มา

วิทยานิพนธ์นี้เป็นส่วนหนึ่งของการศึกษาตามหลักสูตรปริญญาวิศวกรรมศาสตรมหาบัณฑิต
สาขาวิชาวิศวกรรมโยธา ภาควิชาวิศวกรรมโยธา
คณะวิศวกรรมศาสตร์ จุฬาลงกรณ์มหาวิทยาลัย
ปีการศึกษา 2559

ANALYSIS OF STRESS INTESITY FACTORS FOR CRACKED I-BEAMS WITH NON-OVERLAPPING CRACK SURFACES

Mr. Hieu Chi Ma

A Thesis Submitted in Partial Fulfillment of the Requirements
for the Degree of Master of Engineering Program in Civil Engineering
Department of Civil Engineering
Faculty of Engineering
Chulalongkorn University
Academic Year 2016

Thesis Title	ANALYSIS OF STRESS INTESITY FACTORS FOR CRACKED I-BEAMS WITH NON-OVERLAPPING CRACK SURFACES
By	Mr. Hieu Chi Ma
Field of Study	Civil Engineering
Thesis Advisor	Associate Professor Akhrawat Lenwari, Ph.D.

Accepted by the Faculty of Engineering, Chulalongkorn University in Partial Fulfillment of the Requirements for the Master's Degree

.....Dean of the Faculty of Engineering

(Associate Professor Supot Teachavorasinskun, D.Eng.)

THESIS COMMITTEE

.....Chairman

(Professor Thaksin Thepchatri, Ph.D.)

.....Thesis Advisor

(Associate Professor Akhrawat Lenwari, Ph.D.)

.....Examiner

(Professor Teerapong Senjuntichai, Ph.D.)

.....External Examiner

(Associate Professor Piya Chotickai, Ph.D.)

ฮู ชิ มา : การวิเคราะห์ตัวประกอบความเข้มของความเค้นสำหรับคานรูปตัวไอที่มีรอยร้าวโดยผิวรอยร้าวไม่ซ้อนทับกัน (ANALYSIS OF STRESS INTESITY FACTORS FOR CRACKED I-BEAMS WITH NON-OVERLAPPING CRACK SURFACES) อ.ที่ปรึกษาวิทยานิพนธ์หลัก: รศ. ดร. อัครวัชร เล่นวารี, 111 หน้า.

งานวิจัยนี้นำเสนอการวิเคราะห์ตัวประกอบความเข้มของความเค้น (SIFs) สำหรับรอยร้าวในคานเหล็กรูปตัวไอ วิธีไฟไนต์เอลิเมนต์ถูกใช้ในการคำนวนหาค่าตัวประกอบความเข้มของความเค้นที่ปลายรอยร้าวในแผ่นเอวของคานเหล็กรูปตัวไอ โดยพิจารณาพฤติกรรมแบบไม่ซ้อนทับกัน กล่าวคือการไม่ให้ผิวของรอยร้าวซ้อนทับกัน งานวิจัยที่ผ่านมาได้ชี้ให้เห็นว่าผลเฉลย SIFs ที่ปลายรอยร้าวด้านรับแรงดึงกรณีรอยร้าวกึ่งกลางในแผ่นขนาดอนันต์และความกว้างจำกัดภายใต้แรงดัด มีค่าไม่ปลอดภัยเมื่อไม่พิจารณาถึงพฤติกรรมการซ้อนทับกัน การวิเคราะห์ได้ใช้วิธีไฟไนต์เอลิเมนต์ 3 มิติโดยใช้วิธีกลศาสตร์การแตกหักแบบยืดหยุ่นเชิงเส้น โดยทำการตรวจสอบความเหมาะสมกับผลวิเคราะห์ SIFs ของรอยร้าวที่กึ่งกลางในแผ่นที่มีความกว้างจำกัดที่พิจารณาการไม่ซ้อนทับกันของผิวรอยร้าว (วิธี weight function) และผลวิเคราะห์ SIFs ของรอยร้าวในแผ่นเอวของคานเหล็กรูปตัวไอภายใต้แรงดัดที่ไม่พิจารณาการไม่ซ้อนทับกันของผิวรอยร้าว (วิธีไฟไนต์เอลิเมนต์) นอกจากนี้วิธีไฟไนต์เอลิเมนต์ที่นำเสนอนี้ยังถูกตรวจสอบความเหมาะสมกับผลการวิเคราะห์เชิงตัวเลขที่ใช้ผลเฉลย SIFs สำหรับรอยร้าวในแผ่นเอวของคานรูปตัวไอที่ไม่พิจารณาการไม่ซ้อนทับกันของผิวรอยร้าวจากวิธีไฟไนต์เอลิเมนต์ในอดีต ผลกระทบของตัวแปรคือ ความยาวของคานรูปตัวไอ ขนาดของแรงดัด ความยาวของรอยร้าว อัตราส่วนของพื้นที่แผ่นปีกต่อพื้นที่แผ่นเอวของหน้าตัดและระยะเยื้องของรอยร้าวจากกึ่งกลางความลึกของคานต่อผลเฉลย SIFs ที่ปลายรอยร้าวรับแรงดึง ได้ถูกศึกษาในงานวิจัยนี้ด้วย

ภาควิชา วิศวกรรมโยธา ลายมือชื่อนิสิต .....

สาขาวิชา วิศวกรรมโยธา ลายมือชื่อ อ.ที่ปรึกษาหลัก .....

ปีการศึกษา 2559

5870316021 : MAJOR CIVIL ENGINEERING

KEYWORDS: LINEAR ELASTIC FRACTURE MECHANICS, STRESS INTENSITY FACTORS, I-BEAMS, TWO-TIP WEB CRACK, FINITE ELEMENT METHOD, NON-OVERLAPPING BEHAVIOR

HIEU CHI MA: ANALYSIS OF STRESS INTESITY FACTORS FOR CRACKED I-BEAMS WITH NON-OVERLAPPING CRACK SURFACES. ADVISOR: ASSOC. PROF. AKHRAWAT LENWARI, Ph.D., 111 pp.

The physically acceptable analysis of stress intensity factors (SIFs) for cracked steel I-beams was presented in this research. The finite element method was used to calculate the stress intensity factors of two-tip web cracks in steel I-beams with non-overlapping behavior, i.e., crack surfaces were not allowed to overlap. For the center-cracked infinite and finite-width plates under bending, previous studies indicated that the SIF solutions at the tension-side crack tips are not conservative if non-overlapping behavior is not considered. Three-dimensional finite element analyses based on linear elastic fracture mechanics (LEFM) were performed and verified with SIF results from the non-overlapping center-cracked finite-width plates (weight function method) and the overlapping two-tip web crack in I-beams under bending (finite element method). Furthermore, a numerical analysis obtained from the previous finite element solution of overlapping cracked I-beams was then carried out to verify the present finite element model. The effects of parameters including the length of I-beams, magnitude of applied moment, web crack length, flange-to-web area ratio and crack eccentricity on the non-overlapping SIF solutions at tension-side crack tip were also examined in the study.

Department:	Civil Engineering	Student's Signature	.....
Field of Study:	Civil Engineering	Advisor's Signature	.....
Academic Year:	2016		

ACKNOWLEDGEMENTS

I would like to acknowledge the enormous help given to me in completion of this thesis. For their enthusiasm and their assistance, I wish to thank Mr. Chung, Phong, Thi, Thuc, Linh, Quynh, Tuan, Pond Chanachai Thongchom and many of my friends and colleagues for the duration of my studies in Thailand. Also, special thank to AUN-SEED Net Scholarship and Chulalongkorn University for giving me the great opportunity to study here. And, with great respect for their help, sincere thank to all committee members including Professor Dr. Thaksin Thepchatri, Professor Dr. Teerapong Senjuntichai, Associate Professor Dr. Akhrawat Lenwari and Associate Professor Dr. Piya Chotickai.

Mostly, my deep gratitude to Associate Professor Dr. Akhrawat Lenwari, my advisor, for his academic guidance, his patience, and his encouragement.

CONTENTS

Page

Page

LIST OF FIGURES

LIST OF TABLES

CHAPTER 1
INTRODUCTION

1.1 General

To date, stress intensity factor (SIF), which characterizes the magnitude of the singular stress field in the vicinity of crack tip, is still a significant problem in fatigue and fracture analysis of steel structures. By applying linear elastic fracture mechanics (LEFM), the static strength of cracked steel structures, as well as the fatigue crack growth rate under cyclic loading condition, can be calculated if SIF value is known. For steel structures, the I-beams play an important role due to their extensive applications. It is therefore essential to study the fracture behavior in structural I-beams with crack.

Many researchers have attempted to find the SIF of cracked structural I-beams. Nevertheless, the effects of crack surface interference (non-overlapping behavior) were commonly neglected in the analyses of these existing studies. Consequently, the SIF at the tension-side crack tip, as well as the crack opening displacement (COD) profile, which can be significantly influenced by non-overlapping crack surfaces, have not been studied.

This present research will fulfill the gaps in knowledge by performing a finite element analysis (FEA) of the stress intensity factors for cracked I-beams with non-overlapping crack surfaces. The finite element method was selected to simulate the crack behavior in I-beams. The non-overlapping models utilizing the commercial finite element program ANSYS were used to investigate various configurations of structural I-beams under in-plane bending. The analyses were based on linear elastic fracture mechanics. The *J*-integral method was subsequently applied to calculate the SIF values at the crack tips. The contact elements were employed to include the non-overlapping behavior of the crack.

1.2 Research objectives and scope

The objectives of this study are: (1) to perform a finite element analysis to develop a physically acceptable stress intensity factor solutions for structural I-beams that

contain through-thickness cracks; (2) to evaluate the effect of non-overlapping behavior on the opening-mode (mode I) stress intensity factors at the tension-side crack tips; (3) to investigate the effects of various parameters: the normalized web crack length, the flange-to-web area ratio and the normalized crack eccentricity.

The scope of this research was as follows

The analyses of non-overlapping models were based on linear elastic fracture mechanics (LEFM).

The W- shapes in the Manual of steel construction were selected.

The opening-mode (mode I) correction factor solutions for structural I-beams with through-thickness cracks under bending were calculated at tension-side crack tip. The crack configuration is a two tip crack in the web of W-shape.

The three-dimensional (3D) finite element analyses were performed with various parameters: the normalized web crack length, the flange-to-web area ratio and the normalized crack eccentricity. Besides, the effects of the parameters depth-to-width ratio on the correction factor and the magnitude of the applied load on the COD profile are also examined.

CHAPTER 2

LITERATURE REVIEW

2.1. Stress intensity factors for finite-width cracked plates with overlapping crack surface

Overlapping SIF of commonly finite-width cracked plates, which are subjected to tension or bending, are presented in this section. Figure 2.1 illustrates the configurations of the finite-width plates.

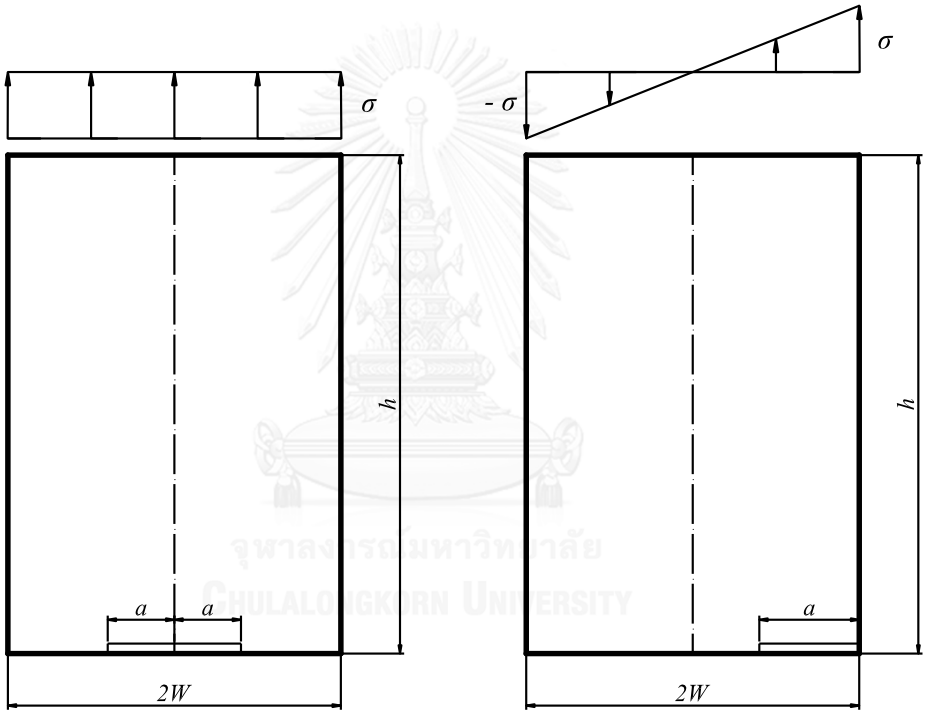

Figure 2.1. Configurations of the finite-width plates: (a) Center-cracked plate under tension; (b) edge-cracked plate under bending

The SIF solution is expressed as

$$K = f(\lambda)\sigma\sqrt{\pi a} \tag{2.1}$$

where $f(\lambda)$: correction factor of the SIF

σ : remote axial or bending stress, MPa

$\lambda = a / W$: normalized crack length

a : crack length, mm

The functions $f(\lambda)$ are listed in the Table 2.1.

Table 2.1. Correction factors for center-cracked and edge cracked plates

Description	Reference	$f(\lambda)$
A center-cracked plate under tension	*Irwin [1]*	$\sqrt{\frac{2}{\pi\lambda}\tan\frac{\pi\lambda}{2}}$
	Koiter [2]	$\frac{1-0.5\lambda+0.32\lambda^2}{\sqrt{1-\lambda}}$
	Brown [3]	$1+0.128\lambda-0.288\lambda^2+1.525\lambda^3$
	Fedderson [4]	$\sqrt{\sec\frac{\pi\lambda}{2}}$
	Tada et al. [5]	$(1-0.0025\lambda^2+0.06\lambda^4)\sqrt{\sec\frac{\pi\lambda}{2}}$
A edge-cracked plate under tension	*Brown [3]*	$1.122-0.231\lambda+10.550\lambda^2-21.710\lambda^3+30.382\lambda^4$
	Tada et al. [5]	$\sqrt{\frac{2}{\pi\lambda}\tan\frac{\pi\lambda}{2}}\frac{0.752+2.02\lambda+0.37\left(1-\sin\frac{\pi\lambda}{2}\right)^3}{\cos\frac{\pi\lambda}{2}}$
A edge-cracked plate under bending	*Brown* [3]	$1.122-1.40\lambda+7.33\lambda^2-13.08\lambda^3+14.0\lambda^4$
	Tada et al. [5]	$\sqrt{\frac{2}{\pi\lambda}\tan\frac{\pi\lambda}{2}}\frac{0.923+0.199\left(1-\sin\frac{\pi\lambda}{2}\right)^4}{\cos\frac{\pi\lambda}{2}}$

2.2. Stress intensity factor for cracked I-beams

Greif and Sanders [6] initially studied the problem of the cracked plate with zero-flexural-stiffness edge stiffeners under tensile loading. The plane stress analysis was conducted using the complex variable approach of Muskhelishvili to derive an integral equation which is then solved by numerical method, e.g. Simpson's rule.

Subsequently, the same problem including both axial and flexural rigidities was investigated by *Isida [7]*. The method was based on the Laurent expansions of the complex stress potentials. The perturbation technique was applied to determine their coefficients from the boundary conditions. The studied problem shown in Figure 2.2.

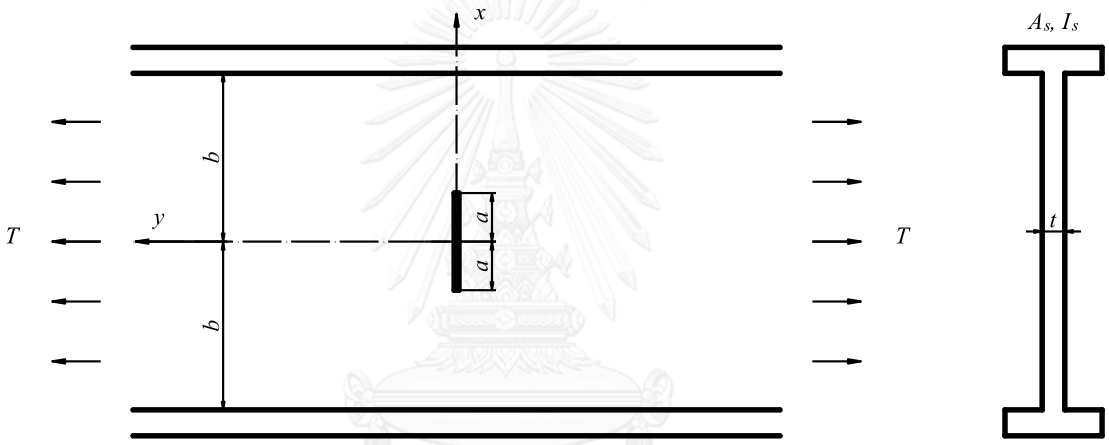

Figure 2.2. Centrally cracked strip with stiffened edges [7]

The stress intensity factors K_I were obtained by 36 term power series of λ^2 in the following equations

$$K_I = T\sqrt{\pi a}F(\alpha,\beta,\lambda) \tag{2.2}$$

$$F(\alpha,\beta,\lambda) = 1+\sum_{n=1}^{35} C_{2n}\lambda^{2n} \tag{2.3}$$

where $\alpha = (E_s / E).(I_s / b^3 t)$: dimensionless inertia parameter

$\beta = (E_s / E).(A_s / bt)$: dimensionless extensional rigidity

A_s: sectional area of stringer

I_s: moment of inertia of stringer section for in-plane bending

$\lambda = a / b$: crack ratio

and the coefficients $c_2, c_4, \ldots$ are functions of α and β .

It was noted that the constraining effect, which is characterized by the dimensionless parameters α and β, became pronounced for a long crack when the crack tip was close to the stiffeners.

Of the two researches of *Greif and Sanders [6]* and *Isida [7]*, the dimensionless extensional rigidity of stringers, which is the cross-sectional area ratio of the stiffener-to-plate, was the major factor affecting the stress intensity factor around the crack tip. As the unstressed edge stiffeners were assumed, it is impossible to apply these solution to I-beams.

Kienzler and Hermann [8] studied the stress intensity factors for cracked beams with a rectangular cross section and different crack geometries, using the conservation laws and elementary beam theory. Based on the remarkably applicable method in this study, several researchers have investigated the stress intensity factors of various cross-sectional shapes with many different loading conditions, e.g., *Hermann and Sosa [9], Gao and Hermann [10], Dunn et al. [11], Muller et al. [12], Ricci and Viola [13], Ghafoori and Motavalli [14].* Of these studies, *Dunn et al. [11]* utilized an extension work of *Kienzler and Hermann [8]*, associated with dimensional considerations and a finite element calibration to investigate the SIF of I-beams under a bending moment. Figure 2.3 illustrates the geometry of the cracked I-beam.

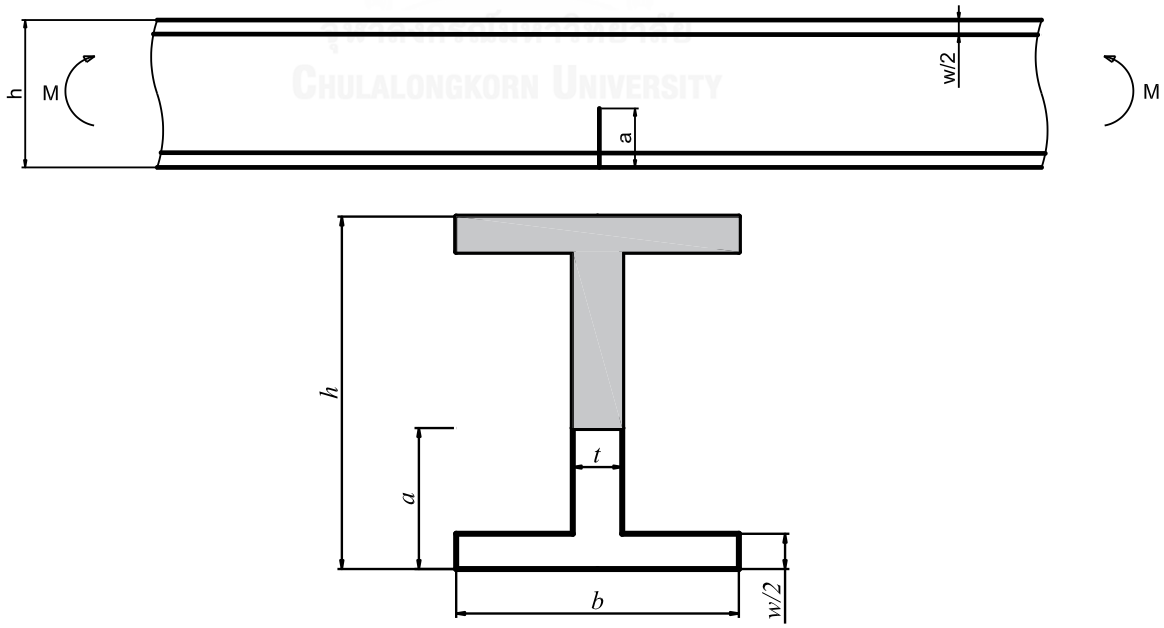

Figure 2.3. Geometry of the cracked I-beam [11]

The following dimensionless terms were utilized to compute the K_I values

$$K_I^* = \frac{K_I t h^{3/2}}{6M}, \xi_1 = \frac{a}{h}, \xi_2 = \frac{t}{b}, \xi_3 = \frac{w}{h} \tag{2.4}$$

where K_I^* : Non-dimensional loading variable.

ξ_1 , ξ_2 and ξ_3 : Non-dimensional geometric variables.

The non-dimensional stress intensity factor was represented as follows:

$$K_I^* = \sqrt{\frac{\beta\xi_2}{3}\left[\frac{1}{4(1-\xi_2)^3 + R(\xi_1,\xi_2,\xi_3)} - \frac{1}{1+(1-\xi_2)(\xi_3-1)^3}\right]} \tag{2.5}$$

where

$$R(\xi_1,\xi_2,\xi_3) = \frac{(1-\xi_2)\left[\xi_3 - -2(1-\xi_1)\right]^3}{2} + \frac{3\left\{4(1-\xi_1)\xi_3 - \xi_3^2 + \xi_2\left[\xi_3 - 2(1-\xi_1)\right]^2\right\}^2}{8\left\{\xi_2\left[\xi_3 - 2(1-\xi_1)\right] - \xi_3\right\}} \tag{2.6}$$

Besides, they also proposed a simple procedure to estimate the non-dimensional parameter β , using solutions from Equation (2.4) to Equation (2.6) fitted with the finite element results. The numerical solution for β is given as

$$\beta(\xi_1,\xi_2,\xi_3) = 1.16\xi_1^{-0.374}\xi_2^{-0.025} \tag{2.7}$$

More recently, *Xie et al. [15-17]* proposed another approach called *G**-integral method, based on conservation laws and the concept of crack mouth widening energy release rate, to calculate the SIF of cracked structures. Based on the *G**-integral method, *Ghafoori and Motavalli [14]* investigated the analytical solution of the SIF for cracked steel I-beams subjected to both bending and tension loadings, as shown in Figure 2.4. The analytical solution of the SIF for a plane strain condition, utilizing *G**-integral method, can be obtained as

$$K_I = \left[\left(-\frac{N^2}{A} - \frac{\left(M_c - Y_c.N\right)}{I} + N^2(\lambda_1+\lambda_2) + M_c^2(\eta_1+\eta_2)\right)\frac{\pi}{t_w(1-\nu^2)}\right]^{1/2} \tag{2.8}$$

where ν : Poisson's ratio

$$\lambda_1 = \int_0^{\mu}\frac{1}{A_1(\gamma)}d\gamma \ , \ \lambda_2 = \int_{\mu}^{1}\frac{1}{A_2(\gamma)}d\gamma \ , \ \eta_1 = \int_0^{\mu}\frac{1}{I_1(\gamma)}d\gamma \ , \ \eta_2 = \int_{\mu}^{1}\frac{1}{I_2(\gamma)}d\gamma \tag{2.9}$$

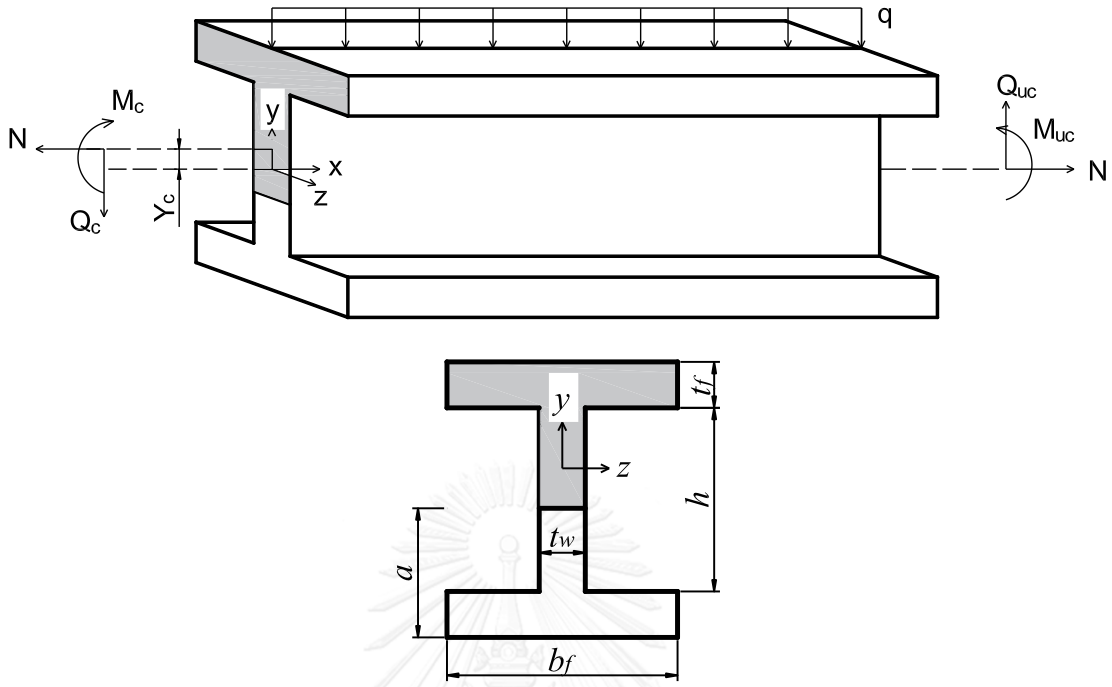

Figure 2.4. A half-length cracked I-beam; Y_C is the movement of the neutral axis for a crack length of a. x-z is the plane of the symmetry of the beam. [14]

γ and μ are given by $\gamma = \frac{x}{b}$ and $\mu = \frac{c}{b} = \sqrt{1-\left(\frac{t_f}{a}\right)^2}$

b and c : position of intersection between the lower and upper edges of bottom flange and the elliptic hole, respectively.

$A_1(\gamma)$ and $A_2(\gamma)$: area of cracked section for $0 \le x \le c$ and $c < x \le b$, respectively.

$I_1(\gamma)$ and $I_2(\gamma)$: moment of inertia of cracked section for $0 \le x \le c$ and $c < x \le b$, respectively.

Beside the analytical approaches, numerical techniques were also efficient ways to investigate the SIF solutions of cracked I-beams. *Tian et al. [18]* performed a three-dimensional SGBEM (Symmetric Galerkin Boundary Element Method)-FEM to compute the mixed mode SIF varied through the crack front and fatigue crack growth rate in cracked I-beams. Mixed mode SIFs were examined for the I-beams with an inclined

crack in the web or a slant edge crack in the flange subjected to torsion loading (Figure 2.5).

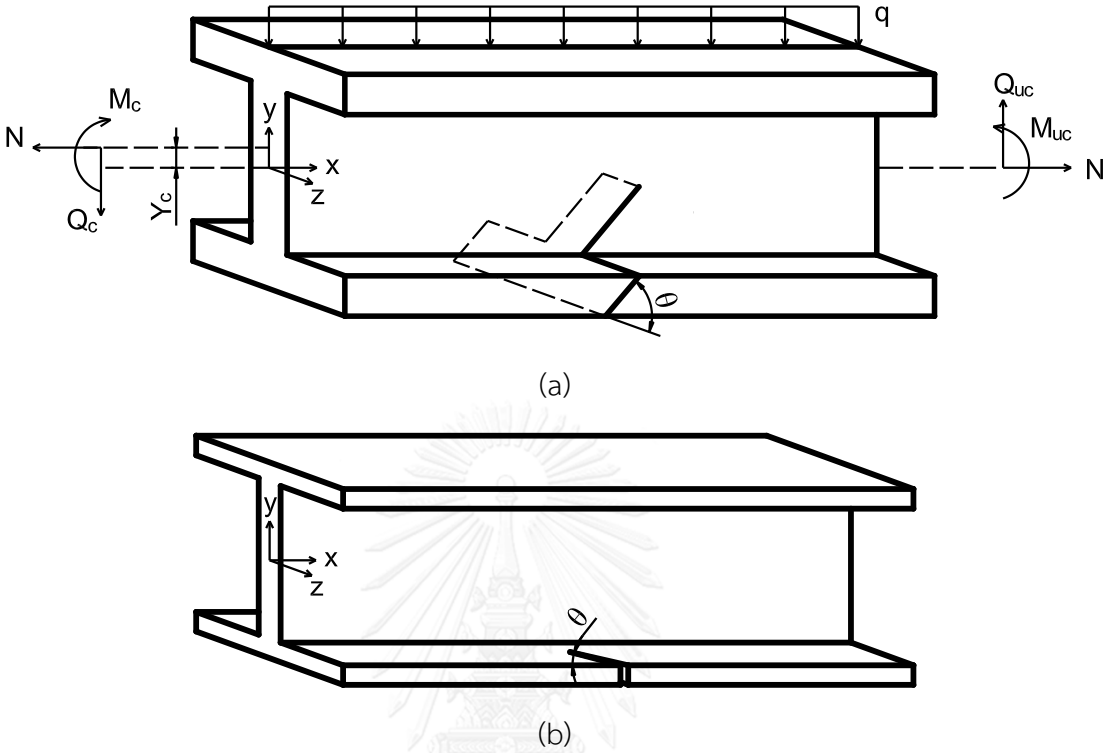

Figure 2.5. Schematics of I-beams: (a) With an inclined crack in the web; (b) with a slant edge crack in the flange subjected to torsional forces. [18]

In recent years, an extensive amount of researches focused on the application of advanced composites, e.g. carbon fiber-reinforced polymer (CFRP), as an apparently effective method to enhance the load capacity and fatigue life of steel I-beams. *Hmidan et al. [19, 20]* developed the three dimensional finite element solution for the SIFs of cracked steel girders (W-shapes) strengthened with carbon fiber-reinforced polymer (CFRP) sheets under bending. Figure 2.6 shows the W-shape geometry and strengthening details.

The SIF solutions for cracked W-shape girders with and without CFRP strengthening were proposed as follows

$K_I = Y(\lambda, \zeta)\sigma\sqrt{\pi a_0}$ for an un-strengthened W-shape (2.10)

$K_I = Y(\lambda, \zeta, \psi, \eta)\sigma\sqrt{\pi a_0}$ for a CFRP-strengthened W-shape (2.11)

Where K_I : mode I stress intensity factor, N/mm$^{3/2}$

Y : correction factor of the SIF

σ : remote stress of the un-cracked section subjected to tension, MPa

a_o: the depth of the crack, mm

$\lambda = A_f / A_w$: Flange-to-web ratio, where A_f and A_w are the cross-sectional area of the flange and the web, respectively.

$\zeta = a_o / h$: Normalized crack depth.

$\psi = A_c / A_s$: CFRP-to-steel area ratio, where A_c and A_s are the cross-sectional area of the CFRP and steel, respectively.

$\eta = E_f / E_s$: CFRP-to-steel modular ratio, where E_f and E_s are the elastic modulus of the CFRP and steel, respectively.

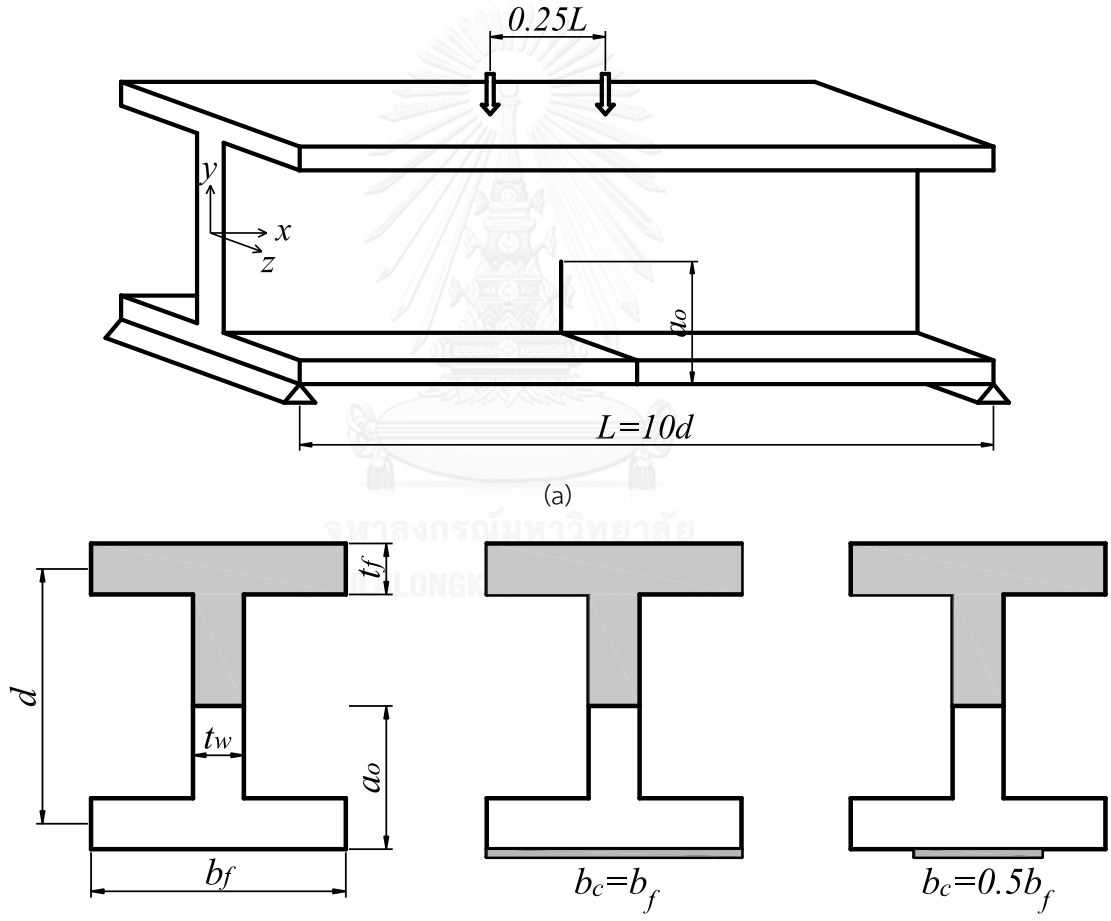

Figure 2.6. W-shape details: (a) Geometry; (b) un-strengthened; (c) full-flange strengthened; (d) half-flange strengthened. [20]

Correction factors of stress intensity factors

- Un-strengthened W-shape

$$Y(\lambda,\zeta) = 4.69 - 32.55\zeta + 2.83\lambda - 2.63\zeta\lambda - 0.36\lambda^2 + 47.12\zeta^2 - 0.06\lambda^2\zeta + 8.96\zeta^2\lambda \tag{2.12}$$

- Strengthened W-shape

$$\begin{aligned} Y(\lambda,\zeta,\psi) = {} & c_1 + c_2\zeta + c_3\lambda + c_4\psi + c_5\psi\lambda + c_6\zeta\psi + c_7\zeta\lambda \\ & + c_8\psi^2 + c_9\lambda^2 + c_{10}\zeta^2 + c_{11}\zeta\lambda\psi + c_{12}\psi^2\lambda \\ & + c_{13}\zeta\psi^2 + c_{14}\psi\lambda^2 + c_{15}\zeta\lambda^2 + c_{16}\zeta^2\psi + c_{17}\zeta^2\lambda \end{aligned} \tag{2.13}$$

where c_1 to c_{17} are curve-fitting coefficients, as shown in Table 2.2.

On the other hand, previous experimental researches of steel bridge details under fatigue loadings were investigated by *Fisher et al. [21, 22]*. It was pointed out that the origination of fatigue cracks usually starts at the welded details. For the steel I-beams with transverse stiffeners welded on the web, the two-tip web cracks can be formed at the bottom end of the stiffener, with upper crack tip A and lower crack tip B growing up and down the web, respectively. Because of the eccentricity of two-tip web cracks, the SIFs at the upper and lower crack tips are usually unequal. The two-tip web crack propagated gradually before the lower tip grew across the flange width to form a three-tip crack in I-beam. It was noted that three-tip cracks are usually symmetric in I-beams. Figure 2.7 shows the stages of fatigue crack in the I-beam with a stiffener welded to the web.

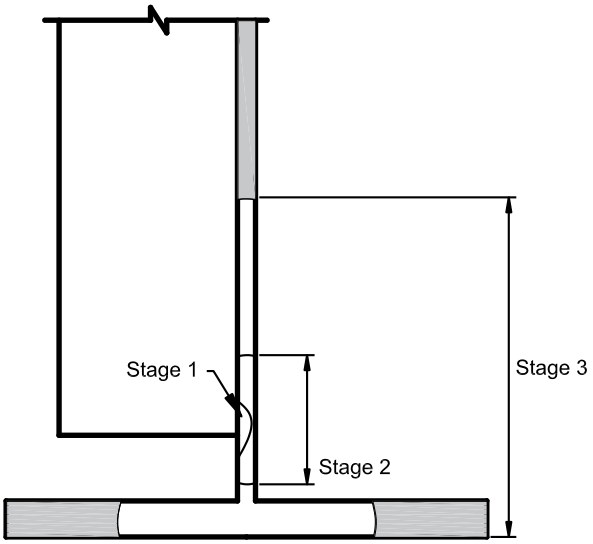

Figure 2.7. Stage of fatigue crack growth in a stiffener welded to the web [23]

Table 2.2. Coefficients of correction factors for λ = 0.91 to 2.01. [20]

Coefficient	Full flange			Half flange		
	$\eta = E_f / E_s$			$\eta = E_f / E_s$		
	0.75	1.125	1.5	0.75	1.125	1.5
C_1	0.26	0.65	0.87	0.16	0.84	0.69
C_2	4.37	3.21	2.48	5.72	4.48	3.65
C_3	2.18	2.01	1.95	2.07	1.52	2.14
C_4	211.78	138.27	59.03	272.72	111.82	85.09
C_5	-53.98	-94.37	-107.88	-88.74	-25.46	-148.50
C_6	-1393.84	-1218.76	-1042.38	-1516.15	-1352.67	-1161.49
C_7	2.32	1.69	1.00	1.96	1.52	0.67
C_8	-18.930	-12.166	-3757	-20.518	-10746	-903.73
C_9	-0.29	-0.17	-0.13	-0.21	0.02	-0.20
C_{10}	-3.01	-2.88	-2.71	-3.41	-3.28	-2.97
C_{11}	-163.31	-104.23	-60.94	-140.74	-53.41	-0.79
C_{12}	8999.36	10289.00	7704.27	8445.87	7856.95	6121.60
C_{13}	62279	42164	29930	70.234	46901	30528
C_{14}	-19.91	-18.29	-10.49	-10.14	-38.34	4.04
C_{15}	0.47	0.37	0.29	0.40	0.28	0.37
C_{16}	637.47	749.62	731.56	583.85	716.72	726.77
C_{17}	-3.48	-3.18	-2.59	-3.19	-3.16	-2.84

Albrecht et al. [23] developed the SIF solutions for two-tip web cracks and symmetric three-tip cracks in I-beams under tension or bending. Figure 2.8 illustrates cross-sectional information of cracked I-beams.

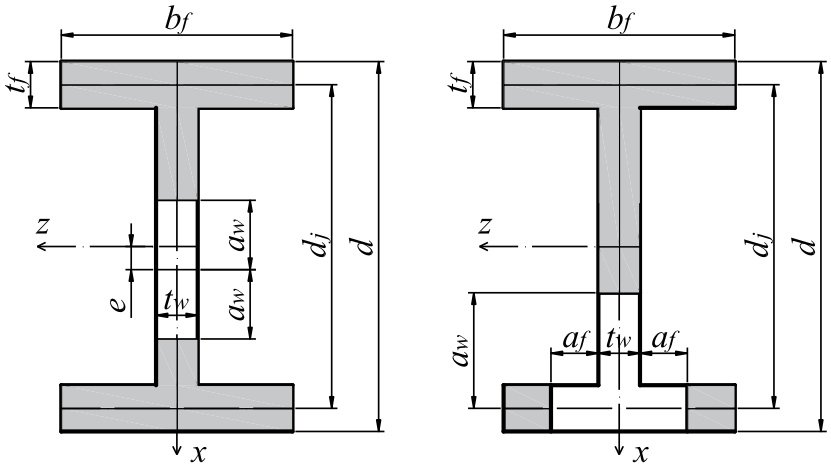

Figure 2.8. Cross-sectional information of cracked I-beams:

(a) Two-tip web crack; (b) symmetric three-tip crack. [23]

The SIF solution for a two-tip web crack subjected to tension or bending was proposed to be

$$K^{A,B} = f^{A,B}(\lambda_w, \varepsilon, \beta)\sigma\sqrt{\pi a_w} \tag{2.14}$$

where a_w : a half of the web crack length, mm

σ : tensile or bending stress at the junction of the web and flange, MPa

The SIF solution for a symmetric three-tip crack subjected to tension or bending was proposed to be

$$K^{w,f} = f^{w,f}(\lambda_w, \lambda_f, \beta)\sigma\sqrt{\pi a_{w,f}} \tag{2.15}$$

where

a_w and a_f : Web crack length and flange crack length, respectively, mm

The normalized parameters in Equations (2.14) and (2.15) are defined as follows:

- The normalized crack eccentricity: $\varepsilon = e/(d_j/2)$ (two-tip web crack)
- The normalized flange crack length: $\lambda_f = a_f/(b_f/2)$
- The normalized web crack length for two-tip web crack (2.16a) and three-tip crack (2.16b):

$$\lambda_w = \begin{cases} \dfrac{a_w}{d_j/2 - e} & (a) \\ a_w/d_j & (b) \end{cases} \tag{2.16}$$

- The flange-to-web area ratio: $\beta = 2A_f/A_w$

Correction factors of stress intensity factors

- Two-tip web crack

$$f^{A,B}(\lambda_w,\varepsilon,\beta) = a_o + a_1\varepsilon + a_2\beta\varepsilon + a_3\varepsilon^2 + a_4\lambda_w + a_5\beta\lambda_w + a_6\varepsilon\lambda_w + a_7\lambda_w{}^2 + a_8\beta\varepsilon\lambda_w + a_9\beta^2\varepsilon + a_{10}\beta\varepsilon^2 + a_{11}\lambda_w\beta^2 + a_{12}\lambda_w\varepsilon^2 + a_{13}\beta\lambda_w{}^2 + a_{14}\varepsilon\lambda_w{}^2 \quad (2.17)$$

where $a_0 - a_{14}$ are regression coefficients given in Table 2.3.

- Symmetric three-tip crack

$$f^{w,f}(\lambda_w,\lambda_f,\beta) = \frac{(a_1 + a_2\beta + a_3\beta^2 + a_4\lambda_w + a_5\lambda_w^2 + a_6\lambda_w^3 + a_7\lambda_f + a_8\lambda_f^2 + a_9\lambda_f^3 + a_{10}\beta\lambda_w\lambda_f + a_{11}\beta\lambda_w^2\lambda_f + a_{12}\beta\lambda_w\lambda_f^2 + a_{13}\beta\lambda_w^2\lambda_f^2)}{(1 + a_{14}\beta + a_{15}\beta^2 + a_{16}\lambda_w + a_{17}\lambda_w^2 + a_{18}\lambda_w^3 + a_{19}\lambda_f + a_{20}\lambda_f^2 + a_{21}\lambda_f^3 + a_{22}\beta\lambda_w\lambda_f + a_{23}\beta\lambda_w^2\lambda_f + a_{24}\beta\lambda_w\lambda_f^2 + a_{25}\beta\lambda_w^2\lambda_f^2)} \quad (2.18)$$

where $a_1 - a_{25}$ are regression coefficients given in Table 2.4.

It was shown that the flange-to-web area ratio β, which accounts for the constraining effect of the flange on two-tip web cracks and the interaction effect on the three-tip web cracks, can sufficiently characterize W shapes in the calculation of SIF.

2.3. Stress intensity factors for cracked plates with non-overlapping crack surface

The non-overlapping problem was first studied by *Paris and Tada [24]*, which was applied for a central crack in an infinite plate under bending, as shown in Figure 2.9.

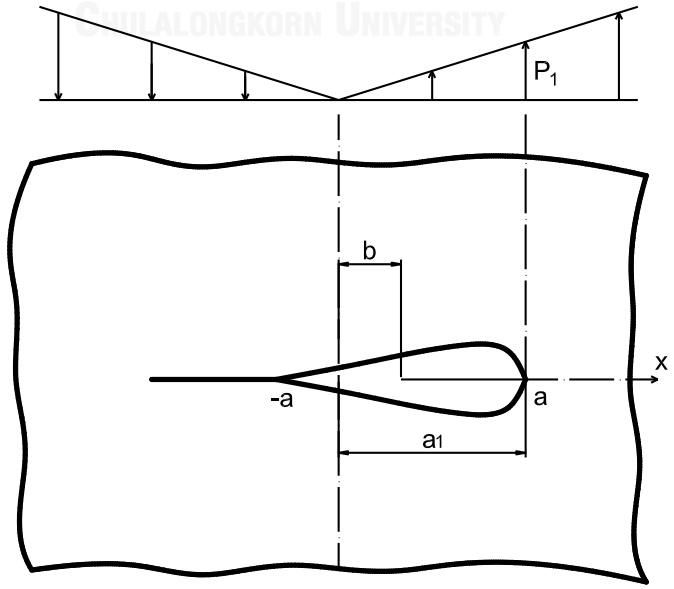

Figure 2.9. Infinite center-cracked plate under bending after crack closure [24]

By superimposing the solutions of bending and uniform tension cases, the analytical solution of SIF, as well as the crack closure length, were determined with assumption that the SIF was zero at the compression-side crack tip.

It was found that $b = a/2$ with zero SIF for the new crack tip at $x = -a$, where b is the eccentricity of the new crack.

The stress intensity factor *K* at the tension-side crack tip was obtained as follow

$$K_{A,eff} = \frac{2}{3}\sqrt{\frac{2}{3}}\sigma_b\sqrt{\pi a} = 0.544\sigma_b\sqrt{\pi a} \quad (2.19)$$

Table 2.3. Coefficients for two-tip web cracks in I-beams [23]

Coefficient	Tension		Bending	
	Upper crack tip	Lower crack tip	Upper crack tip	Lower crack tip
a_0	1	1	0	0
a_1	-0.07184	-0.03591	1.02395	1.02052
a_2	0.05916	0.03257	-0.02824	-0.03142
a_3	0.07266	0.01609	-0.02660	-0.02841
a_4	0.16801	0.17113	-0.51095	0.48403
a_5	-0.15810	-0.17469	-0.00309	-0.02169
a_6	-0.09645	0.00540	0.66587	-0.19538
a_7	0.13248	0.19882	0.02106	0.10116
a_8	0.11124	0.10355	-0.03243	-0.02670
a_9	-0.01464	-0.01573	0.00337	0.00206
a_{10}	-0.03299	0.00399	0.02660	0.03282
a_{11}	0.04288	0.05901	0.00483	0.01704
a_{12}	-0.14373	-0.13149	-0.14302	-0.20652
a_{13}	-0.09648	-0.16125	-0.01281	-0.06069
a_{14}	-0.03380	-0.27916	-0.04610	-0.28079

Table 2.4. Coefficients for symmetric three-tip cracks in I-beams [23]

Coefficient	Tension		Bending	
	Web crack tip	Flange crack tip	Web crack tip	Flange crack tip
a_1	0.82991	1.48266	0.82922	1.39283
a_2	-0.67499	0.29636	-0.58551	0.06970
a_3	0.21031	0.07549	0.16098	0.04610
a_4	5.48154	4.44880	3.18865	3.37633
a_5	-7.24174	2.74806	-1.92470	-2.78526
a_6	6.51764	-8.92438	-5.45652	-1.04763
a_7	-1.22688	-9.01819	-0.87320	-7.16218
a_8	2.27070	10.67798	1.30689	9.95421
a_9	-0.04335	-2.79219	0.75006	-3.94745
a_{10}	-3.53419	39.40912	1.92329	24.63084
a_{11}	5.23305	-33.56530	-1.28348	-20.37830
a_{12}	1.11541	-32.7345	-2.84890	-19.76580
a_{13}	-2.53266	30.52621	3.09458	18.05231
a_{14}	-0.67489	0.31779	-0.67725	0.14847
a_{15}	0.19608	0.08256	0.17624	0.04106
a_{16}	9.15477	2.56783	7.93375	1.27056
a_{17}	-13.48190	-6.28871	-0.68127	-3.72795
a_{18}	10.74853	3.32973	1.25324	2.41420
a_{19}	-2.99836	-6.42741	-2.47185	-5.07106
a_{20}	5.46394	8.44963	4.36222	7.53843
a_{21}	-2.86079	-2.83403	-2.15147	-3.33554
a_{22}	-6.27909	38.11440	-3.59192	23.75073
a_{23}	10.41571	-35.78230	11.11301	-20.20160
a_{24}	3.65483	-38.73570	1.49894	-23.70230
a_{25}	-7.95641	36.97307	-11.80580	20.59509

Bowie and Freese [25] developed an exact solution of SIF for cracks in an infinite plate under bending by modifying the Muskhelishvili method (Figure 2.10). A combination of Modified Mapping Collocation (MMC) and finite element methods was used to determine the non-overlapping SIF solution of cracks in the finite-width plate. It was indicated that the classical solution underestimated the SIFs at crack tip in tension by approximately 9% for both infinite and finite-width plates.

The SIFs at the tension-side crack tip B were shown in the following formulae

$$\begin{aligned} K_{IB} &= (T/2)L^{3/2}\sin^3\alpha \\ K_{IIB} &= -(T/2)L^{3/2}\sin^2\alpha\cos\alpha \end{aligned} \tag{2.20}$$

where K_{IB} and K_{IIB} are stress intensity factors for mode I and mode II, respectively.

The effective crack length *2L/3* after crack closure was then obtained. For the center-cracked infinite plate under bending, the effective SIF was given by

$$\begin{aligned} K_{IB}^{eff} &= T(2L/3)^{3/2}\sin^3\alpha \\ K_{IIB}^{eff} &= -T(2L/3)^{3/2}\sin^2\alpha\cos\alpha \end{aligned} \tag{2.21}$$

It is clearly seen that $K_{IB}/K_{IB}^{eff} = K_{IIB}/K_{IIB}^{eff} = 2(2/3)^{3/2} \approx 1.09$.

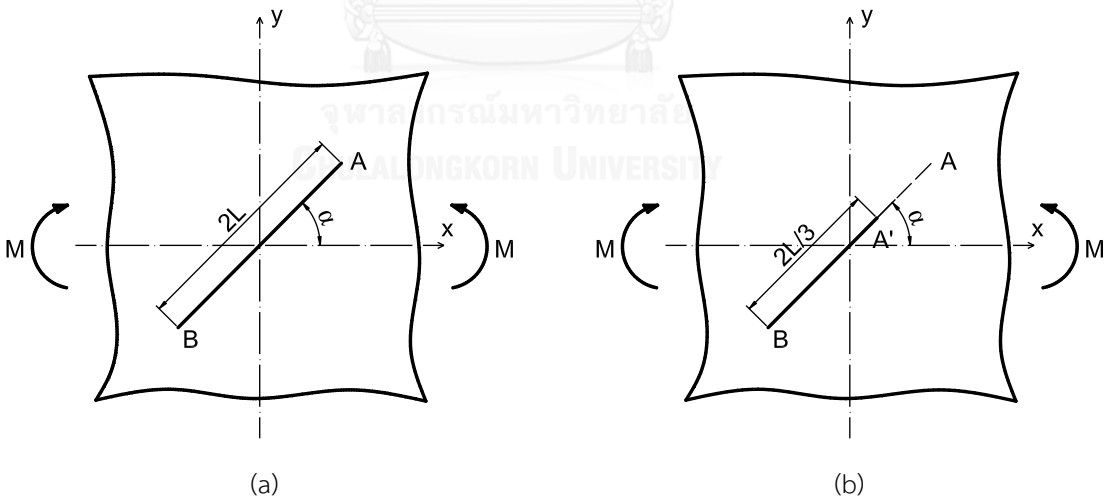

Figure 2.10. Non-overlapping model of center-cracked infinite plate under bending. (a) Original crack; (b) newly formed crack (after closure) [25]

For a crack in the finite-width plate as shown in Figure 2.11, where a closed-form cannot be found, the SIF solution was determined by using the Modified Mapping Collocation (MMC) method combined with the finite elements.

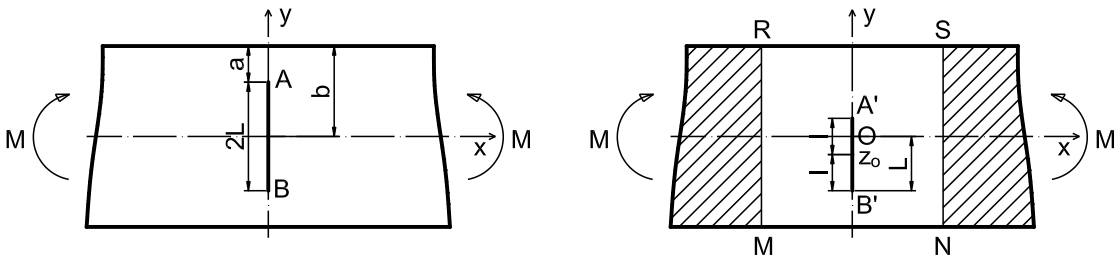

(a) (b)

Figure 2.11. Non-overlapping model of a strip under bending. (a) Original crack; (b) newly formed crack (after closure) [25]

Woo et al. [26] used a collocation method to obtain the SIF solutions of a finite-width plate under bending, as shown in Figure 2.12(a).

For each step of this process, the crack tip in compression that has negative SIF value changed its position closer to tension-side crack tip. If the crack tip in compression reached the zero SIF value, the procedure would be ended. Figures 2.12(b) and 2.12(c) illustrate this process. With the assumption that $K_{IB}^{i+1} = 0$, the approximate crack length a_{i+1} in the $i+1$ step is given by

$$a_{i+1} = \frac{K_{IB}^{i-1} a_i - K_{IB}^{i} a_{i-1}}{K_{IB}^{i-1} - K_{IB}^{i}} \tag{2.22}$$

The actual value of K_{IB}^{i+1} was then calculated. If $K_{IB}^{i+1} \neq 0$, the procedure repeated again until K_{IB} differed from zero by acceptable error.

It was found that the effective length of crack was reduced by 30% and correction factor at tension-side crack tip increased by more than 30% in comparison with classical solutions.

Albrecht and Lenwari [27] proposed a closed-form solution for the infinite plate under linear stress distribution using superposition principle for the overlapping solutions. Figure 2.13 and Figure 2.14 show the non-overlapping model of a center-cracked infinite plate under in-plane bending and linear stress distribution, respectively.

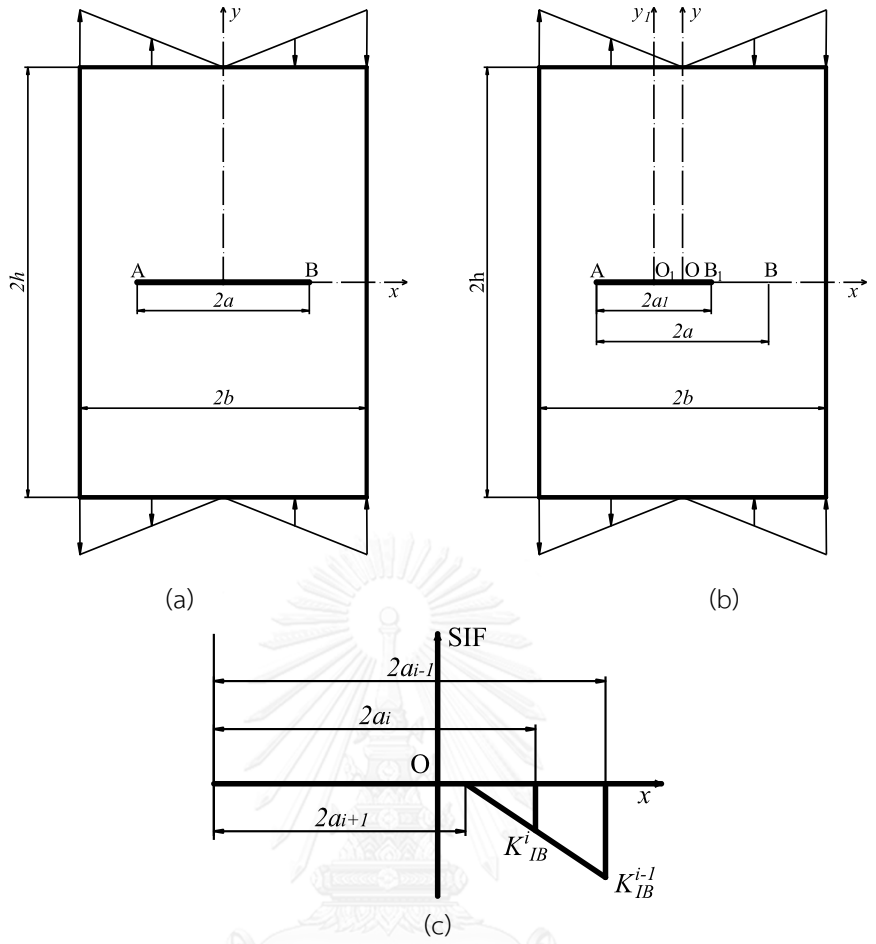

Figure 2.12. A finite-width plate under bending. (a) Original crack; (b) newly formed crack (after closure); (c) Crack length at each step [26]

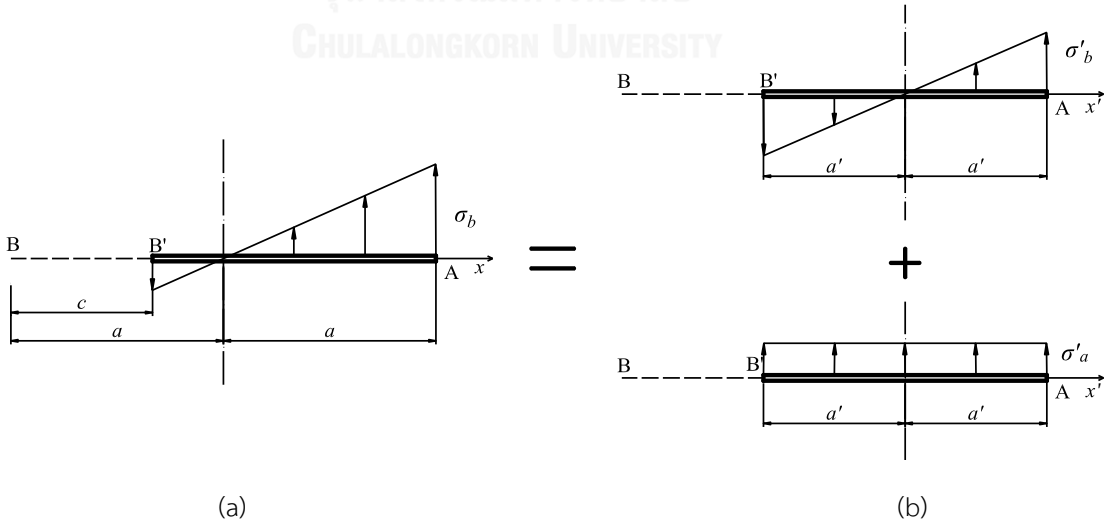

Figure 2.13. Non-overlapping model of center-cracked infinite plate under in-plane bending. (a) Original crack; (b) newly formed crack (after closure) [27]

Based on the superposition principle, the effective SIF at the crack tip A was obtained by applying the necessary condition $K_{B'} = 0$ for a physically acceptable solution.

$$K_{A,eff} = \sigma_a^{'}\sqrt{\pi a'} + \frac{\sigma_b^{'}}{2}\sqrt{\pi a'} = 0.544\sigma_b\sqrt{\pi a'} \tag{2.23}$$

where $a' = 2a/3$, $\sigma_a^{'} = \sigma_b/3$ and $\sigma_b^{'} = 2\sigma_b/3$

The crack closure length $c = 2a/3$ was also determined in this process.

This solution of the effective stress intensity factor at the crack tip A totally coincides with the result given by *Paris and Tada [24]*.

The effective SIF solution at the tension-side crack tip A was given by

$$K_{A,eff} = \left(\sigma_a^{'} + \frac{\sigma_b^{'}}{2}\right)\sqrt{\pi a} = \left[\frac{2}{3}(s+1)\right]^{3/2}\sigma_b\sqrt{\pi a} \tag{2.24}$$

where $a' = \frac{2}{3}(s+1)a$, $\sigma_a^{'} = \frac{1}{3}(s+1)\sigma_b$ and $\sigma_b^{'} = \frac{2}{3}(s+1)\sigma_b$

$s = \sigma_a/\sigma_b$: The axial-to-bending stress ratio.

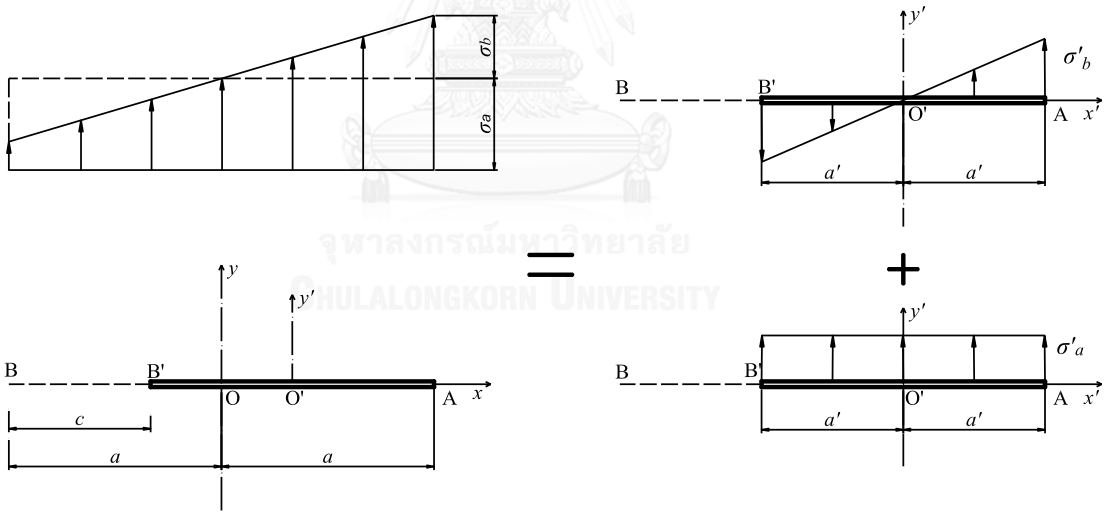

Figure 2.14. Non-overlapping model of center-cracked infinite plate under linear stress distribution. (a) Original crack; (b) newly formed crack (after closure). [27]

A further calculation using the weight function method was conducted to obtain the SIF solution for finite-width plate under polynomial stress distribution. The plate configuration is shown in Figure 2.15.

The m-degree form of polynomial stress distribution was as follow

$$\sigma(x) = \sigma \sum_{0}^{m} D_m (x/W)^m \tag{2.25}$$

The crack tip SIF solution was then represented as

$$K = \left[\sum_{0}^{m} D_m F(\varepsilon, \lambda, m) \right] \sigma \sqrt{\pi a'} \tag{2.26}$$

where $\varepsilon = e/W$: the normalized crack eccentricity

$\lambda = a'/(W-e)$: the normalized crack length

m : the polynomial degree; $m = 0$ for axial, $m = 1$ for bending ...

$F(\varepsilon, \lambda, m)$: correction factor for the SIF

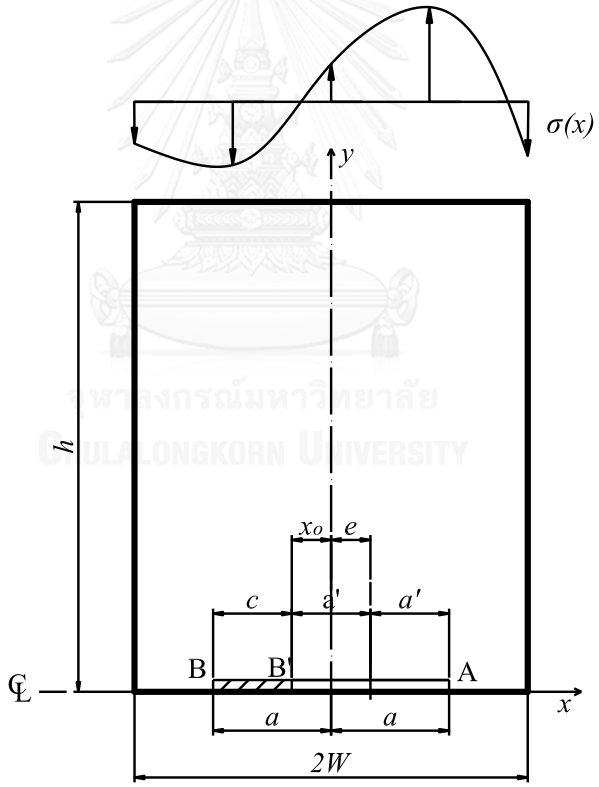

Figure 2.15. Configuration of center-cracked finite-width plate under polynomial stress distribution. [27]

By applying the necessary condition $K_{B'} = 0$ or $\sum_{0}^{m} D_m F(\varepsilon, \lambda, m) = 0$, the effective SIF solution was determined as following expression

$$K_{A,eff} = \sum_{0}^{m} D_m F(\varepsilon, \lambda, \mathrm{m}) \sigma \sqrt{W} \sqrt{\pi (a/W - c/(2W))} \tag{2.27}$$

It was found that the classical solution underestimated the SIF at tension-side crack tip at maximum 15% for the finite-width plate subjected to in-plane bending.

CHAPTER 3
THEORETICAL BACKGROUND

This chapter presents a brief description of theoretical concepts that relate to the research problem. The particular attentions are given on linear-elastic fracture mechanics (especially the stress intensity factor), the J- Integral method and the non-overlapping problem (crack surface interference).

3.1. Linear-elastic fracture mechanics

The fundamental of linear elastic fracture mechanics (LEFM) is one of the most essential concepts in fracture mechanics.

Stress analysis of crack

Considering a linear elastic body subjected to external loading, the closed-form solutions can be derived for the certain crack configurations. Such solutions were first studied by Irwin [1]. In the defined polar coordinate system as shown in Figure 3.1, the stress field for any linear elastic cracked body is represented by

$$\sigma_{ij} = \left(\frac{k}{\sqrt{r}} \right) f_{ij}(\theta) + \sum_{m=0}^{\infty} A_m r^{m/2} g_{ij}^{(m)}(\theta) \tag{3.1}$$

where σ_{ij} : stress tensor;

k : constant value

f_{ij} : non-dimensional function of θ

It is obvious that stress field in the vicinity of the crack tip varies with $1/\sqrt{r}$. The stress singularity is described in Equation (3.1) since stress field approaches infinity when $r \to 0$.

The stress fields near crack-tips can be divided into three basic types, each associated with a local mode of deformation as illustrated in Figure 3.2. The superposition of these three modes is sufficient to describe the most general three-dimensional case of local crack-tip deformation and stress fields. Modes I and mode II can be regarded as two-dimensional plane-extensional problems (opening and in-plane shear). Mode III can be analyzed as the two-dimensional pure shear (or torsion) problem.

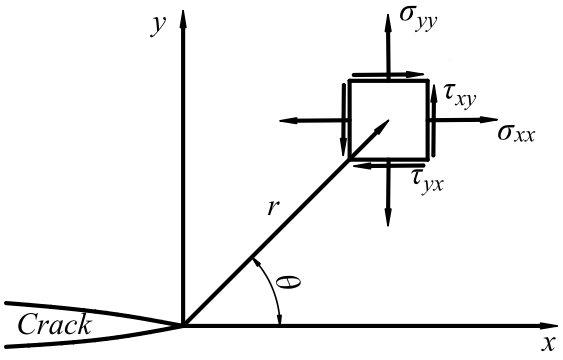

Figure 3.1. The coordinate system at a crack tip. [28]

The stress intensity factor

The constants *k* and f_{ij} depend on the mode of deformation and change proportionally with the level of applied load. For convenience, constant *k* can be replaced by the stress intensity $K = k\sqrt{2\pi}$. Consequently, the stress fields around a crack tip in an isotropic linear elastic body can be expressed as

$$\lim_{r\to 0}\sigma_{ij}^{(I)} = \frac{K_I}{\sqrt{2\pi r}} f_{ij}^{(I)}(\theta) \tag{3.2}$$

$$\lim_{r\to 0}\sigma_{ij}^{(II)} = \frac{K_{II}}{\sqrt{2\pi r}} f_{ij}^{(II)}(\theta) \tag{3.3}$$

$$\lim_{r\to 0}\sigma_{ij}^{(III)} = \frac{K_{III}}{\sqrt{2\pi r}} f_{ij}^{(III)}(\theta) \tag{3.4}$$

for Mode I, II and III, respectively.

The stress intensity factors (K_I , K_{II} and K_{III}) which are not functions of coordinates represent the strength of the stress fields surrounding the crack tip that can be used to predict the failure of a cracked structure. The SIFs depend on the geometries as well as the loading conditions of the body. Consequently, all components of stress, strain and displacement can be determined as a function of *r* and θ when the SIF is known. For this reason, the crack tip SIF is one of the most important concept in fracture mechanics.

The singular stress field expressions for Mode I and Mode II are given in Table 3.1.

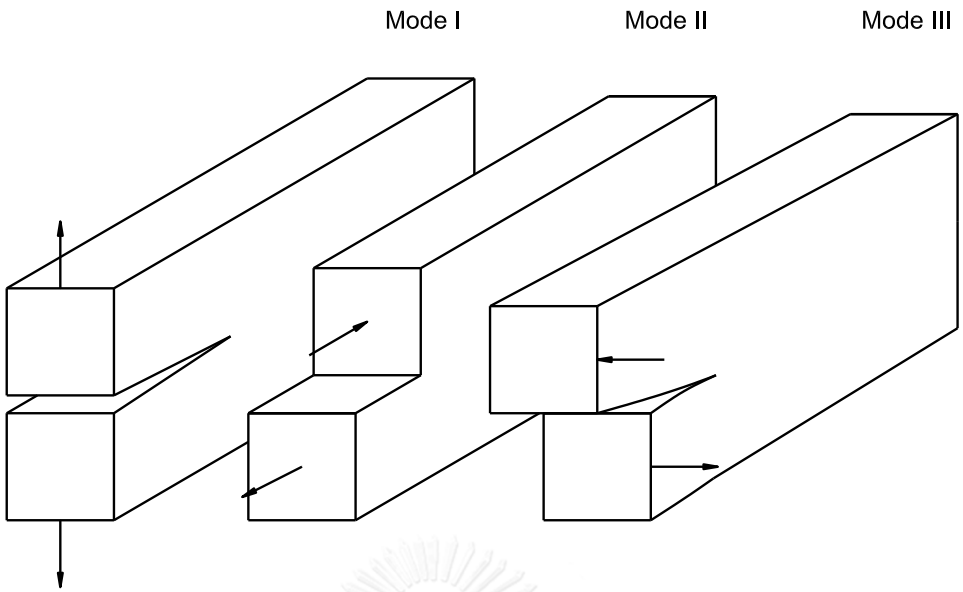

Figure 3.2. The three basic modes of crack extension. [5]

Table 3.1. Linear elastic, isotropic stress fields around the crack tip for Mode I and Mode II [28]

	Mode I	Mode II
σ_{xx}	$\frac{K_I}{\sqrt{2\pi r}}\cos\left(\frac{\theta}{2}\right)\left[1-\sin\left(\frac{\theta}{2}\right)\sin\left(\frac{3\theta}{2}\right)\right]$	$-\frac{K_{II}}{\sqrt{2\pi r}}\sin\left(\frac{\theta}{2}\right)\left[2+\cos\left(\frac{\theta}{2}\right)\cos\left(\frac{3\theta}{2}\right)\right]$
σ_{yy}	$\frac{K_I}{\sqrt{2\pi r}}\cos\left(\frac{\theta}{2}\right)\left[1+\sin\left(\frac{\theta}{2}\right)\sin\left(\frac{3\theta}{2}\right)\right]$	$\frac{K_{II}}{\sqrt{2\pi r}}\sin\left(\frac{\theta}{2}\right)\cos\left(\frac{\theta}{2}\right)\cos\left(\frac{3\theta}{2}\right)$
τ_{xy}	$\frac{K_I}{\sqrt{2\pi r}}\cos\left(\frac{\theta}{2}\right)\sin\left(\frac{\theta}{2}\right)\cos\left(\frac{3\theta}{2}\right)$	$\frac{K_{II}}{\sqrt{2\pi r}}\cos\left(\frac{\theta}{2}\right)\left[1-\sin\left(\frac{\theta}{2}\right)\sin\left(\frac{3\theta}{2}\right)\right]$
σ_{zz}	0 (Plane stress) $\nu(\sigma_{xx}+\sigma_{yy})$ (Plane strain)	0 (Plane stress) $\nu(\sigma_{xx}+\sigma_{yy})$ (Plane strain)
τ_{xz}, τ_{yz}	0	0
Note: ν is Poisson's ratio.		

Displacement field expressions for Mode I and Mode II are represented in Table 3.2.

Table 3.2. Linear elastic, isotropic displacement fields for Mode I and Mode II [28]

	Mode I	Mode II
u_x	$\frac{K_I}{2\mu}\sqrt{\frac{r}{2\pi}}\cos\left(\frac{\theta}{2}\right)\left[\kappa-1+2\sin^2\left(\frac{\theta}{2}\right)\right]$	$\frac{K_{II}}{2\mu}\sqrt{\frac{r}{2\pi}}\sin\left(\frac{\theta}{2}\right)\left[\kappa+1-2\cos^2\left(\frac{\theta}{2}\right)\right]$
u_y	$\frac{K_I}{2\mu}\sqrt{\frac{r}{2\pi}}\sin\left(\frac{\theta}{2}\right)\left[\kappa+1-2\cos^2\left(\frac{\theta}{2}\right)\right]$	$-\frac{K_{II}}{2\mu}\sqrt{\frac{r}{2\pi}}\cos\left(\frac{\theta}{2}\right)\left[\kappa-1+2\sin^2\left(\frac{\theta}{2}\right)\right]$
Note: μ is the shear modulus, $\kappa = 3-4\nu$ (plane strain) and $\kappa = (3-\nu)(1+\nu)$ (plane stress)		

Table 3.3 lists the out-of-plane stress and displacement components for Mode III.

Table 3.3. Out-of-plane components of linear elastic, isotropic stress and displacement in Mode III [28]

$\tau_{xz} = -\frac{K_{III}}{\sqrt{2\pi r}}\sin\left(\frac{\theta}{2}\right)$
$\tau_{yz} = \frac{K_{III}}{\sqrt{2\pi r}}\cos\left(\frac{\theta}{2}\right)$
$u_z = \frac{2K_{III}}{\mu}\sqrt{\frac{r}{2\pi}}\sin\left(\frac{\theta}{2}\right)$

The J contour integral

Rice [29] proposed a path-independent contour integral, J contour integral, for the analysis of cracks. It was shown that the value of J - integral is path-independent of integration around the crack tip. Consider an arbitrary counter-clockwise path (Γ) around the crack tip, as illustrated in Figure 3.3. The - integral is given by

$$J = \int_{\Gamma}\left(wdy - T_i\frac{\partial u_i}{\partial x}ds \right) \tag{3.5}$$

where

$w = \int_0^{\varepsilon_{ij}} \sigma_{ij} d\varepsilon_{ij}$: strain energy density, N/mm^2

$T_i = \sigma_{ij} n_j$: the components of the traction vector, N

σ_{ij} and ε_{ij} : the stress and strain tensors, respectively, MPa

n_j : the components of the unit vector normal to Γ

u_i : displacement vector components, mm

ds : the length increment along the contour Γ, mm

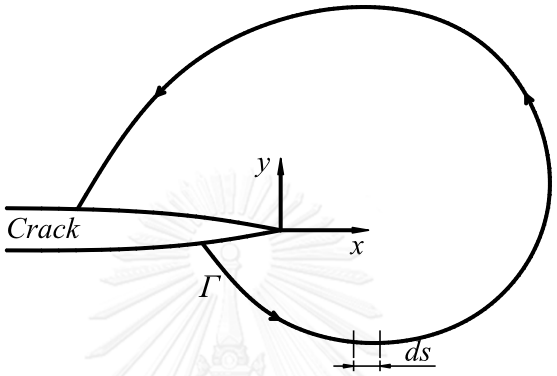

Figure 3.3. Arbitrary contour around the tip of a crack. [28]

The relationship between stress intensity factor K and J - integral is represented as follows

$$J = \frac{K_I^2}{E'} + \frac{K_{II}^2}{E'} + \frac{K_{III}^2}{2\mu} \tag{3.6}$$

where

K_I, K_{II} and K_{III} : stress intensity factors for mode I, II and III, respectively, N/mm$^{3/2}$

$E' = E$ for plane stress, MPa

$E' = \frac{E}{1-\nu^2}$ for plane strain, MPa

E : Young's modulus, MPa

ν : Poisson's ratio

μ : shear modulus

3.2. Non-overlapping crack (crack surface interference)

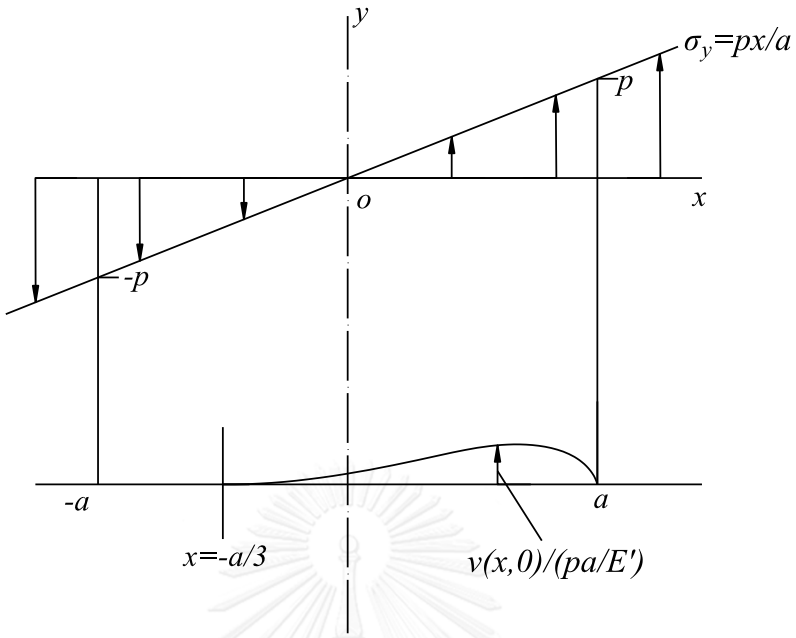

Figure 3.4. The center-cracked infinite plate subjected to in-plane bending. [5]

Table 3.4. Summarized solutions of the infinite plate under in-plane bending. [5]

	Overlapping behavior	Non-overlapping behavior
Mode I SIF	$K_{I\pm a} = \pm\frac{1}{2} p\sqrt{\pi a}$	$K_{I,x=-a/3} = 0$ $K_{I,x=a} = \left(\frac{2}{3}\right)^{3/2} p\sqrt{\pi a} = 0.5443 p\sqrt{\pi a}$
Stress variation near the crack tip	$\underset{\lvert x\rvert>a}{\sigma_y(x,0)} = p\frac{\lvert x\rvert}{x}\frac{\left(\frac{x}{a}\right)^2 - \frac{1}{2}}{\sqrt{\left(\frac{x}{a}\right)^2 - 1}}$	$\underset{x<-a/3, x>a}{\sigma_y(x,0)} = \frac{p}{a}\left(x - \frac{2a}{3}\right)\sqrt{\frac{x+a/3}{x-a}}$
COD profile	$\underset{\lvert x\rvert\le a}{2v(x,0)} = \frac{2pa}{E'}.\left(\frac{x}{a}\right)\sqrt{1-\left(\frac{x}{a}\right)^2}$	$\underset{-a/3\le x\le a}{2v(x,0)} = \frac{2p}{E'}.\left(x+\frac{a}{3}\right)\sqrt{\left(x+\frac{a}{3}\right)(a-x)}$
Crack opening area	$A_{x>0} = \frac{2pa^2}{3E'}$	$A = \left(\frac{4\pi}{9}\right)\frac{2pa^2}{3E'}$

In linear elastic fracture mechanics (LEFM), the negative values of both the stress intensity factors and the crack opening displacements (COD) at the crack tips were

usually predicted by the classical solutions that allow crack surfaces to overlap. Due to the impenetrability of the continuous material, the overlapping solutions are not acceptable in physical viewpoint and, consequently, solutions involving negative SIF are not valid by themselves. This leads to the assumption of non-overlapping behavior in which prevent the penetration of crack surfaces and accept a part of crack length to close. The SIF at the tension-side crack tip as well as the COD profile are then influenced by such crack closure.

Based on [5], some general traits of non-overlapping crack are given below

- The stress variation on the closed crack near the new compression side crack tip and COD profile of the crack surfaces are in the form of a parabola ($\propto r^2$) and a semi-cubical parabola ($\propto r^{3/2}$), respectively (Table 3.4).
- $K_I = 0$ at the new crack tip in compression is a necessary condition for an acceptable solution in physical viewpoint, that produces the finite stresses and a smooth COD of the surfaces at that tip. (Figure 3.4).
- Once the crack surfaces closed, they became a part of the continuum body and might be negligible in the subsequent analysis of crack.
- The non-overlapping crack surface naturally increased the SIF at the tension-side crack tip as well as the crack opening area. For the center-cracked plate under in-plane bending, K_I and the crack opening area became $2(2/3)^{3/2} = 1.089$ and $4\pi/9 = 1.396$ times, respectively, to the overlapping solutions.
- A compression side crack tip did not necessarily close. In Fig 3.4, it is clearly seen that $K_I > 0$ when the left tip was still in the compression region ($-a/3 < x < 0$) and the crack, thus, remained open.
- Referring to Figure 3.5, it is evident that the final geometry of cracks is unique (i.e., the positions of the cuspidal ends, regardless of the level of the applied load. For the linearly varying σ_y at infinity (in-plane bending), the proportional loading is determined when the position of zero crossing of σ_y (i.e., the axis of moment) is fixed. Figure 3.5a obviously shows that both tips of the crack are in the tensile region and the crack surfaces are always open. In Figure 3.5b, the left crack tip is in compressive region, but the compression side crack length is less than one-third of the tension side crack ($a_c < a_t/3$), and the surfaces of the crack still remain open. When $a_c \geq a_t/3$ (Figure

3.5c), the cuspidal end is always formed at $x = -a_t / 3$. The position of the cuspidal end is uniquely determined by the length on the tension side, regardless of the level of the applied load, or the presence of cracks in $x \le -a_t / 3$. Only the COD profile changes proportionally to the applied load.

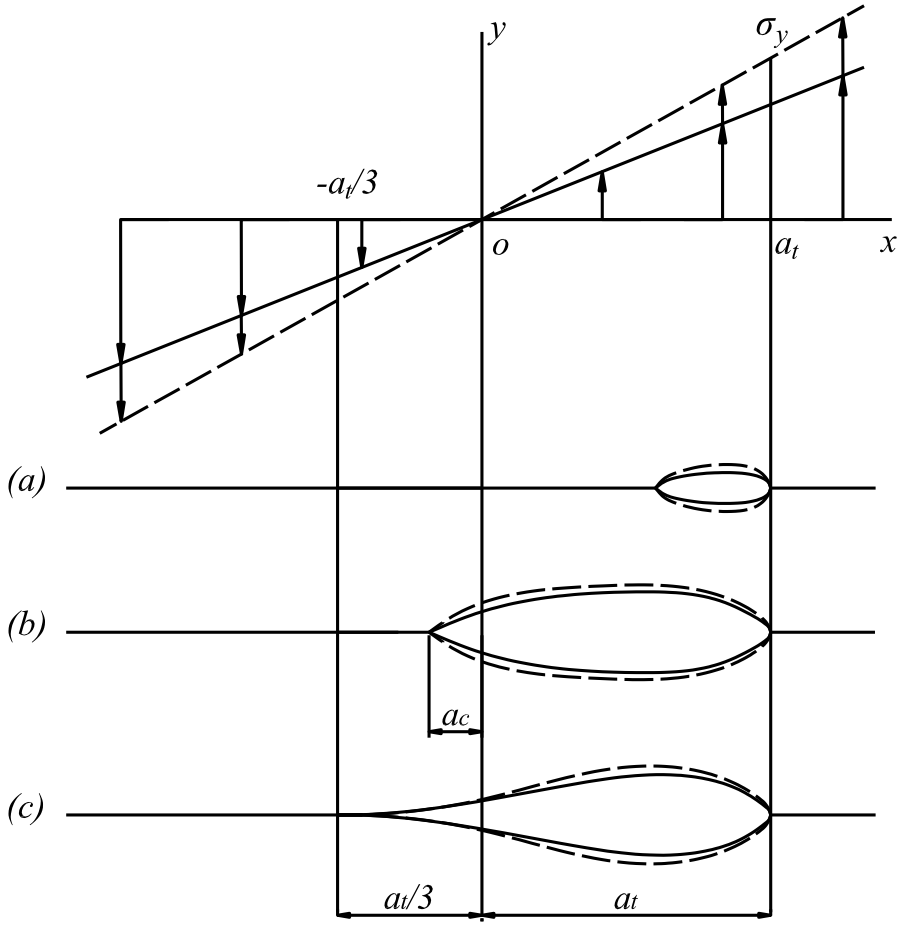

Figure 3.5. The "unique geometry" of cracks under proportional loads. [5]

CHAPTER 4
DEVELOPMENT OF FINITE ELEMENT MODEL

4.1. Finite element model

The commercial finite element program ANSYS was employed to simulate the non-overlapping behavior of steel I-beams containing a crack on the web, as shown in Figure 4.1. The J-integral method was employed to calculate the mode I SIFs of cracked steel I-beams. Eventually, the obtained SIFs were normalized with applied stress and crack length to determine the correction factors. This chapter describes the detailed information of the FEM model such as element type, geometry and boundary conditions of the W-shapes.

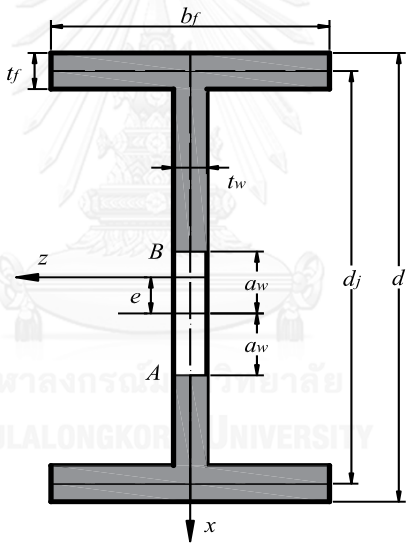

Figure 4.1. Coordinate and symbols for two-tip web crack in I-beam

4.1.1. W-shape details

Table 4.1 lists the W-shapes selected in this research. The W-shapes were chosen from the Manual of Steel Construction [30], with the range of the flange-to-web area ratio ($\beta = 2A_f / A_w$) from 0.83 to 2.11; where A_f and A_w are the cross-sectional areas of the flange and the web, respectively.

The isotropic linear elastic material represented the constitutive behavior of steel was used, including the elastic modulus of 200 GPa and the Poisson's ratio of 0.3.

Table 4.1. W-shapes used in finite element analysis. [30]

Flange-to-web area ratio β	W-shape	Equivalent SI W-shape	Depth-to-width ratio γ	d_j *(mm)*	t_w *(mm)*	b_f *(mm)*	t_f *(mm)*	*Type*
0.83	W40X149[a-c]	W1000X222	3.16	948.9	16	300	21.1	1
0.83	W24X62[b]	W610X92	3.28	587	10.9	179	15	2
1.00	W40X167[c]	W1000X249	3.18	953.8	16.5	300	26.2	-
1.13	W40X294[b]	W1000X438	3.22	981	26.9	305	49	2
1.13	W36X194[b,c]	W920X289	2.92	895	19.4	307	32	1
1.31	W24X94 [b,c]	W610X140	2.59	594.8	13.1	230	22.2	2
1.31	W21X83 [b]	W530X123	2.47	522.8	13.1	212	21.2	1
1.50	W40X324[c]	W1000X483	2.41	974	25.4	404	46	-
1.68	W24X117[b,c]	W610X174	1.83	595.4	14	325	21.6	1
1.68	W30X173[b]	W760X257	1.95	744.8	16.6	381	27.2	2
1.92	W21X122[b,c]	W530X182	1.67	526.6	15.2	315	24.4	1
1.92	W27X281[b]	W690X419	1.9	695	26.9	366	49	2
2.11	W21X201[c]	W530X300	1.7	542.6	23.1	320	41.4	-

[a]W-shapes for validation of the finite element model.

[b]W-shapes for validation of parameter β .

[c]W-shapes for parametric study.

Notes: - $\beta = 2A_f / A_w$ is the flange-to-web area ratio.

- $\gamma = d_j / b_f$ is the depth-to-width ratio.

Flange-to-web area ratio and depth-to-width ratio

The relationship between the flange-to-web area ratio (β) and the depth-to-width ratio (γ) of all 273 W-shapes listed in The Steel Construction Manual [30] is showed in Figure 4.2. Each data point represents one W shape. Almost 60% of the data points are in the range of β values from 1 to 2.

Five pairs of the cracked W-shapes, specified by the footnote b in Table 4.1, were chosen to assess the effect of the parameter depth-to-width ratio γ . Each pair has the

same β value but different γ values. Type 1 denotes the W-shapes with lower depth-to-width ratio in comparison with Type 2 (Figure 4.2).

The overlapping and non-overlapping SIF solutions at the lower crack tip were calculated with the combination of: β = 0.83, 1.13, 1.31, 1.68 and 1.92; λ_w = 0.3 and 0.7; ε = 0. For both overlapping and non-overlapping behaviors, the difference between the shapes in each type was less than 1% (Table 4.2) that is similar to the conclusion of Albrecht et al. [23].

It is apparent that the effect of the depth-to-width ratio was not significant and the flange-to-web area ratio could be sufficient to characterize the W- shapes for both overlapping and non-overlapping behaviors.

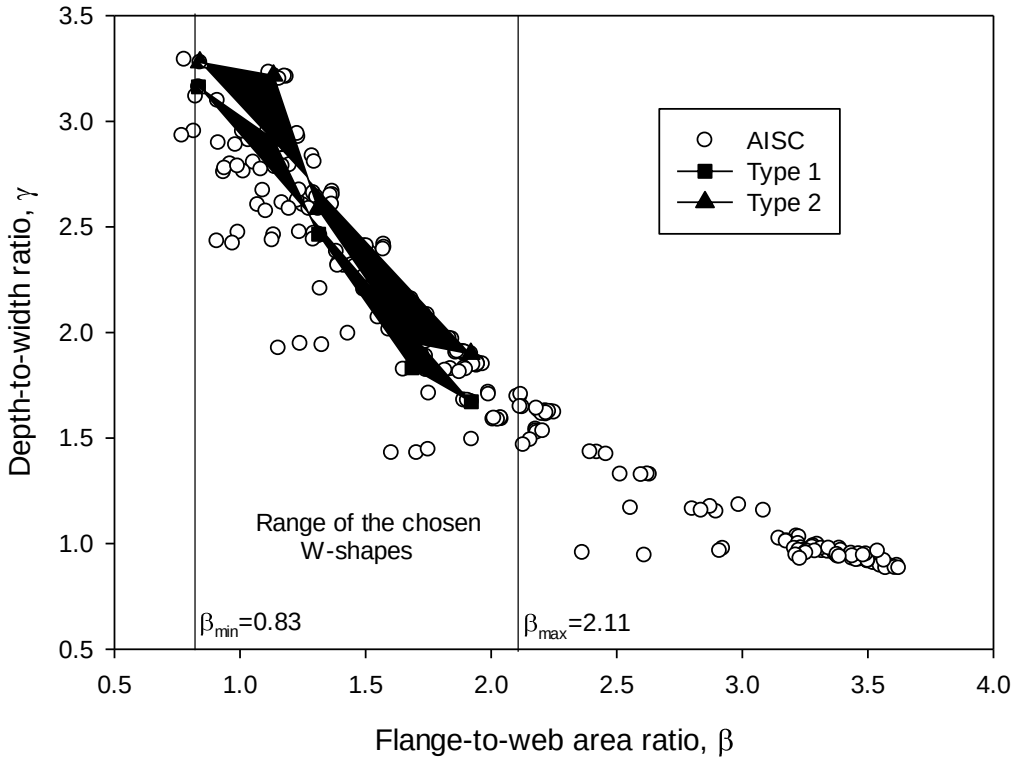

Figure 4.2. Relationship between β and γ of AISC W-shapes. [30]

Table 4.2. Effect of the depth-to-width ratio to the correction factor

Flange-to-web area ratio β	W-shape	Depth-to-width ratio γ	λ_w	Correction factor at lower crack tip			Difference %
				Albrecht et al. [23] F_{LIT} (M)	ANSYS solution Overlapping (N)	ANSYS solution Non-overlapping (O)	(N-M)/M
0.83	W40x149 (A)	3.16	0.3	0.1479	0.1429	0.1989	-3.4
			0.7	0.3593	0.3510	0.4730	-2.3
	W24x62 (B)	3.28	0.3	0.1479	0.1429	0.1989	-3.4
			0.7	0.3593	0.3507	0.4723	-2.4
	Difference % (B-A)/A*100		0.3		**0.0**	**0.0**	
			0.7		**-0.1**	**-0.1**	
1.13	W36x194 (C)	2.92	0.3	0.1473	0.1424	0.1664	-3.3
			0.7	0.3529	0.3466	0.4033	-1.8
	W40x294 (D)	3.22	0.3	0.1473	0.1424	0.1662	-3.4
			0.7	0.3529	0.3459	0.4019	-2.0
	Difference % (D-C)/C*100		0.3		**-0.1**	**-0.1**	
			0.7		**-0.2**	**-0.3**	
1.31	W21x83 (E)	2.47	0.3	0.1474	0.1421	0.1660	-3.6
			0.7	0.3500	0.3447	0.4003	-1.5
	W24x94 (F)	2.59	0.3	0.1474	0.1419	0.1658	-3.7
			0.7	0.3500	0.3474	0.4032	-0.7
	Difference % (F-E)/E*100		0.3		**-0.1**	**-0.2**	
			0.7		**0.8**	**0.7**	
1.68	W24x117 (G)	1.83	0.3	0.1486	0.1408	0.1646	-5.3
			0.7	0.3466	0.3405	0.3948	-1.8
	W30x173 (H)	1.95	0.3	0.1486	0.1411	0.1649	-5.1
			0.7	0.3466	0.3410	0.3952	-1.6
	Difference % (H-G)/G*100		0.3		**0.2**	**0.2**	
			0.7		**0.1**	**0.1**	
1.92	W21x122 (I)	1.67	0.3	0.1502	0.1400	0.1606	-6.8
			0.7	0.3461	0.3378	0.3911	-2.4
	W27x281 (J)	1.90	0.3	0.1502	0.1400	0.1605	-6.8
			0.7	0.3461	0.3368	0.3890	-2.7
	Difference % (J-I)/I*100		0.3		**0.0**	**0.0**	
			0.7		**-0.3**	**-0.5**	

4.1.2. Boundary condition

Due to the symmetry of the I-beam geometry, the definition of symmetry boundary condition supported by ANSYS was utilized to reduce computational expenses, as shown in Figure 4.3. The length of the W-shape was maintained at a constant ratio of two times of the beam height, $L = d_j$. In-plane linear stress was applied directly on the outmost lines of the web and the flange of I-beams. The I-beam was constrained by a simply support along the edge of a flange, i.e. a roller support.

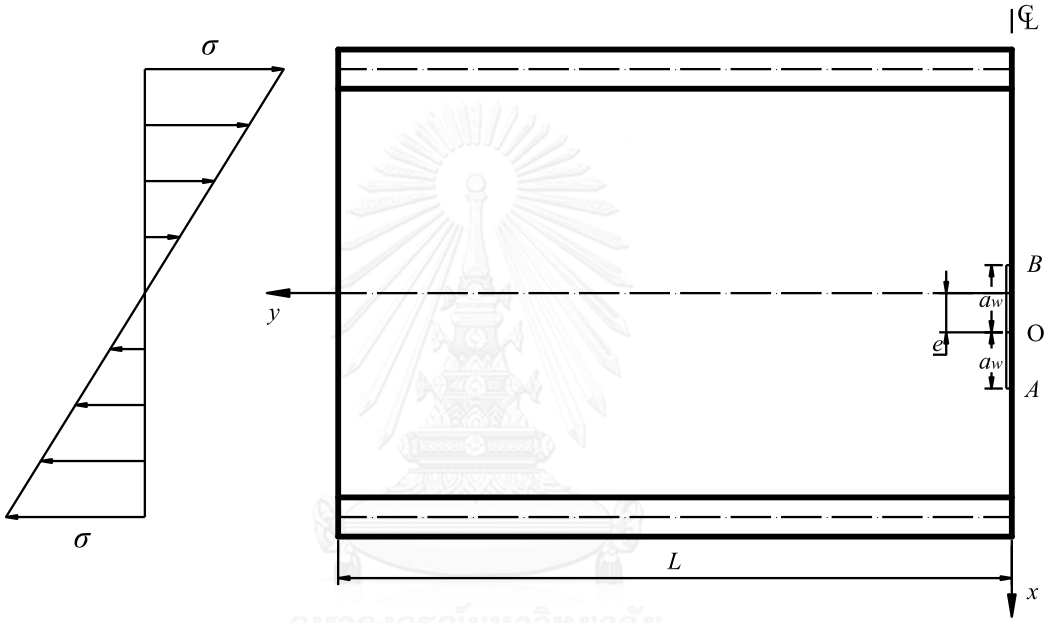

Figure 4.3. Geometry of the W-shapes containing two-tip web crack.

4.1.3. Element type

The eight-node quadrilateral shell elements (SHELL281) were selected for modeling the I-beams. Each node of SHELL281 element has three translational and three rotational degrees of freedom. Typically, this element is used to simulate the thin or moderate shape of structural members for both linear and non-linear behavior (Figure 4.4). The W-shapes were simulated by one web plate combined with two flange plates, supported by the command “AGLUE” in ANSYS program to ensure the strain compatibility of the nodes along the junction lines. The shell element plates were modeled by their mid-plane and thickness, with both membrane and bending characteristics.

To include the non-overlapping behavior, the 3-D contact elements (CONTA177 and TARGE170) were placed between two sides of crack surfaces. These elements prevented the crack surfaces from penetrating each other under compressive loading. Figure 4.5 illustrates a 3-D contact pair consisting of contact surface (CONTA177) and target surface (TARGE170).

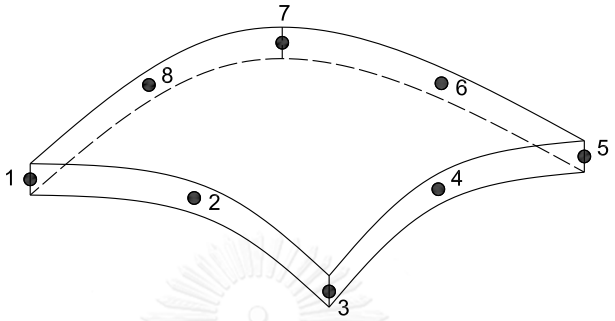

Figure 4.4. Eight-node quadrilateral shell elements (SHELL281) [31]

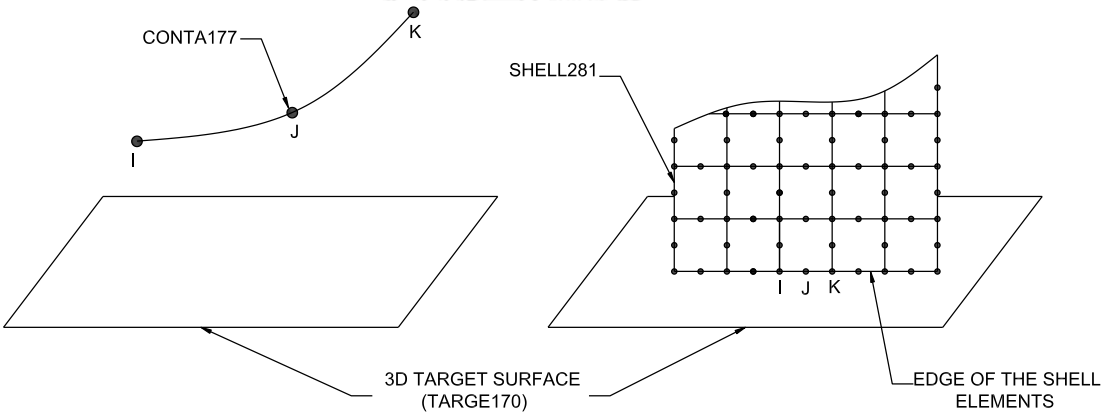

Figure 4.5. 3D Contact elements (TARGE170 and CONTA177) [31]

In finite element program ANSYS, 3D line-to-surface contact element CONTA177 which has two or three nodes is used to simulate flexible-flexible or rigid-flexible (used in the present model) contact between a 3D beam and a surface, or between a shell edge and a surface (with or without mid-side nodes) [31].

To model the target surface for the I-beams, an arbitrary sized zone (length $l = d_j$; width $w = b_f$) which was adequate to capture all necessary contact was created at crack plane (Figure 4.6a). Subsequently, to decrease the computational cost, the ANSYS command "CNCHECK, TRIM" was used to eliminate the contact and target elements which were initially in far field, i.e. open or not near contact (Figure 4.6b).

Normally, the 3D contact and target elements that used for W-shape model were defined with the default properties in ANSYS program, i.e. “Contact algorithm” (KEYOPT(2)) and “Behavior of contact surface” (KEYOPT(12)) were set as “Augmented Lagrange method” and “Standard”, respectively. In “Augmented Lagrange method”, “Normal penalty stiffness” (FKN) and “Penetration tolerance” (FTOLN) were set by default to the values “1” and “0.1”, respectively.

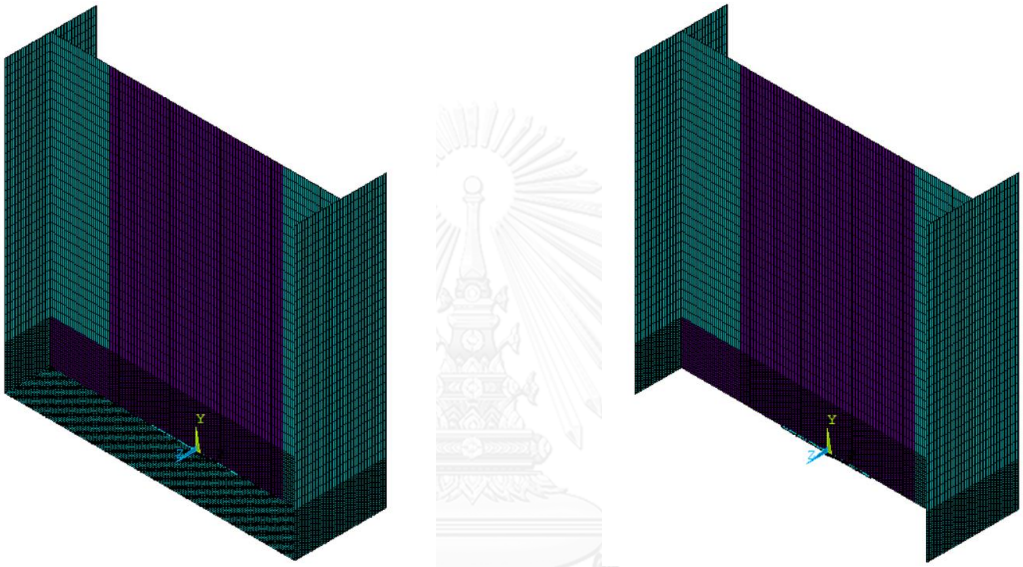

(a) (b)

Figure 4.6. 3D target surface (TARGE170): (a) before and (b) after using “CNCHECK, TRIM”.

However, for some cases especially with short crack ($\lambda_w \leq 0.2$), the penetration of the crack surfaces in compression side after contact were still too large that might lead to an un-satisfied SIF solution (Figure 4.7). The x-axis and y-axis of Figure 4.7 illustrate the crack length and deformation of the crack surface, respectively. The negative value of deformation represented the overlap of crack surface. To avoid those situations, the “Normal penalty stiffness” property have to be adjusted to a larger value, i.e. FKN = 10. On the other hand, the global convergence difficulty would occur due to the high stiffness value. So, before the analysis was solved, the nonlinear convergence criteria of solution controls had to be set as “based on Displacement U” instead of default options “based on Force F and Moment M”.

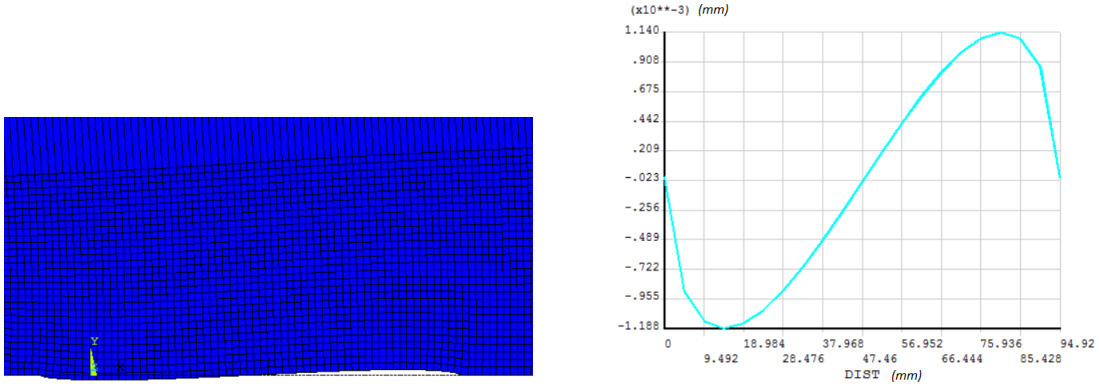

(a)

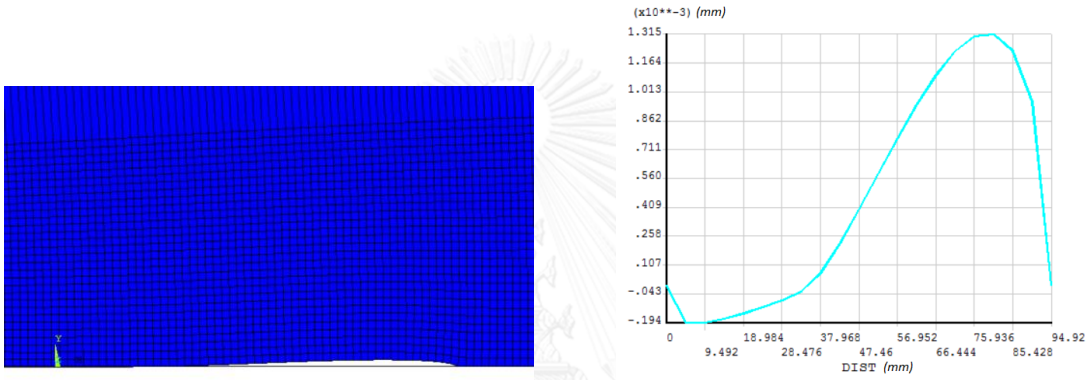

(b)

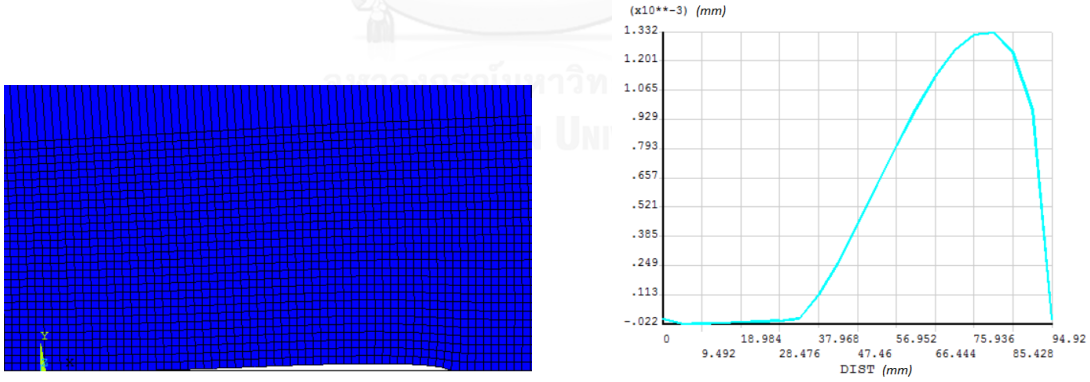

(c)

Figure 4.7. Deformations of the web cracks of shape W40x149 under bending ($\sigma = 100\,MPa$, $\lambda_w = 0.1$) for: (a) Model without contact elements;
(b) and (c): Models including contact elements with FKN = 1 and FKN =10, respectively.

4.1.4. Mesh design

For the web of the W- shapes, a mesh refinement zone (shaded area) was defined depending on the crack length around the crack-tip region, as illustrated in Figure 4.8.

The mesh pattern of the refinement zone is shown in Figure 4.9. Parameter m defines the number of elements along the short edge of rectangular refine-mesh area. The effect of mesh density around the crack tip was evaluated by conducting a sensitivity analysis on the center-cracked steel plate (plate A, table 4.3) under tensile loading (Figure 4.10).

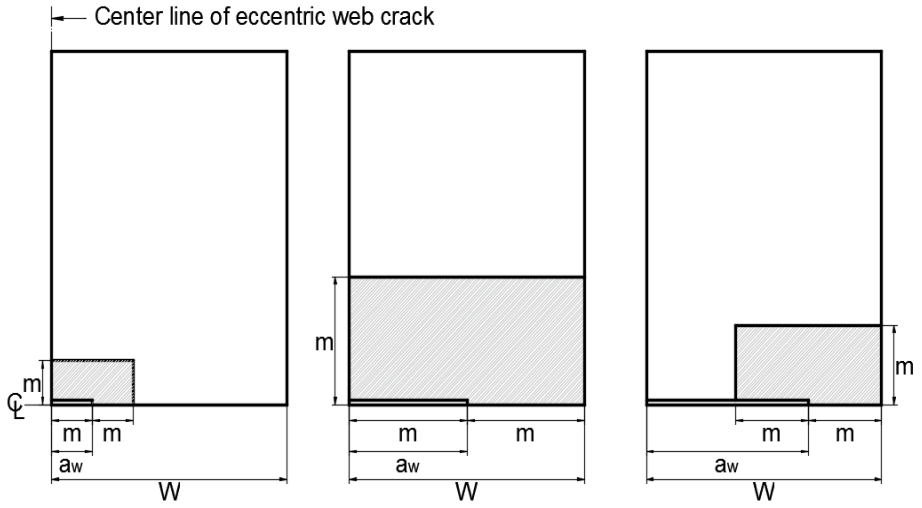

Figure 4.8. Mesh scheme for different crack length

Table 4.3. Plates used in finite element analysis

Plate	Thickness b (mm)	Width W (mm)	Height h (mm)	Remote loading σ (MPa)	Element type	Young's modulus (GPa)	Poisson's ratio
Plate A[a]	10	50	150	100	SHELL281	200	0.3
Plate B[b]	16	100	300	100	SHELL281	200	0.3
Plate C[b,c]	16	474.45	948.9	100	SHELL281	200	0.3

[a]For sensitivity analysis [b]For validation of model [c]For parametric study

The SIFs of centered cracks (K_{FEM}) were compared with the solutions of Tada et al. [4] (K_{LIT}) for two cases of the crack length (a/W = 0.2 and 0.8), as shown in Table 4.4. The J- Integral values in Table 4.4 were obtained by only a half of the model. Therefore, the SIF of full plate in plane stress condition can be represented as:

$$K = \sqrt{JE} = \sqrt{2 \times J_{half} \times E} \tag{4.1}$$

According to [5], the SIF of finite-width plate under tension is expressed as

$$K_{LIT} = \left[1 - 0.0025\left(\frac{a}{W}\right)^2 + 0.06\left(\frac{a}{W}\right)^4\right]\sqrt{\sec\frac{\pi a}{2W}} \tag{4.2}$$

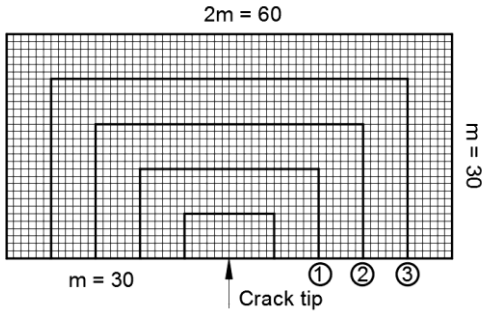

Figure 4.9. Mesh pattern of the refinement zone around crack tip

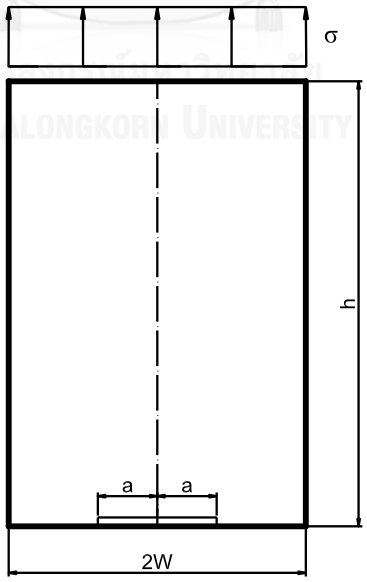

Figure 4.10. Center-cracked plate under tension [5]

The path-independence of the SIF values was also examined. For $a/W = 0.2$ and $m = 45$, the SIFs obtained by the counterclockwise paths 1, 2 and 3 (Figure 4.9) were

574.83, 574.61 and 574.37 $N / mm^{3/2}$, respectively (Table 4.4). In this study, the paths along the edge of the refinement mesh area were used to calculate the J- Integral values around the web crack tips of I-beams.

It was apparent that the mesh with $m = 30$ was fine enough to capture the singularity in the vicinity of the crack tip (Figure 4.11). The maximum difference for both a / W = 0.2 and 0.8 was within 2%. Figure 4.12 shows the typical mesh pattern of two-tip web crack in the ANSYS program.

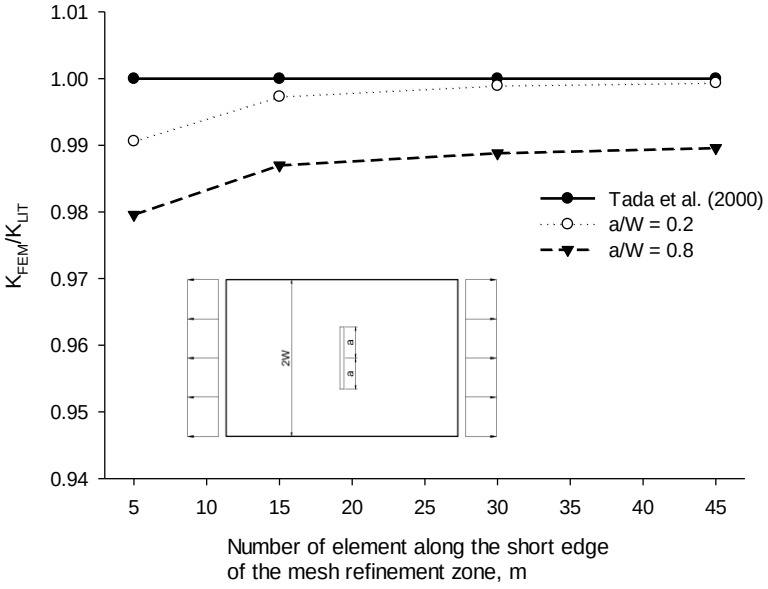

Figure 4.11. Sensitivity analysis of mesh density to SIFs

Table 4.4. Sensitivity analysis of the mesh density around crack tip region to SIFs

a/W	Number of element division along crack length m	PATH	J- Integral for a half model	K_{FEM} ($N/mm^{3/2}$)	K_{LIT} Equation (4.2) [5] ($N/mm^{3/2}$)	Difference %
0.2	5	1	0.81306	570.28	574.74	-0.77
		2	0.81142	569.71		-0.88
		3	0.81040	569.35		-0.94
	15	1	0.82270	573.65		-0.19
		2	0.82223	573.49		-0.22
		3	0.82137	573.19		-0.27
	30	1	0.82530	574.56		-0.03
		2	0.82467	574.34		-0.07
		3	0.82406	574.13		-0.11
	45	1	0.82608	574.83		0.02
		2	0.82544	574.61		-0.02
		3	0.82476	574.37		-0.06
0.8	5	1	10.194	2019.31	2062.90	-2.11
		2	10.176	2017.52		-2.20
		3	10.209	2020.79		-2.04
	15	1	10.339	2033.62		-1.42
		2	10.347	2034.40		-1.38
		3	10.364	2036.08		-1.30
	30	1	10.377	2037.35		-1.24
		2	10.384	2038.04		-1.21
		3	10.402	2039.80		-1.12
	45	1	10.388	2038.43		-1.19
		2	10.397	2039.31		-1.14
		3	10.413	2040.88		-1.07

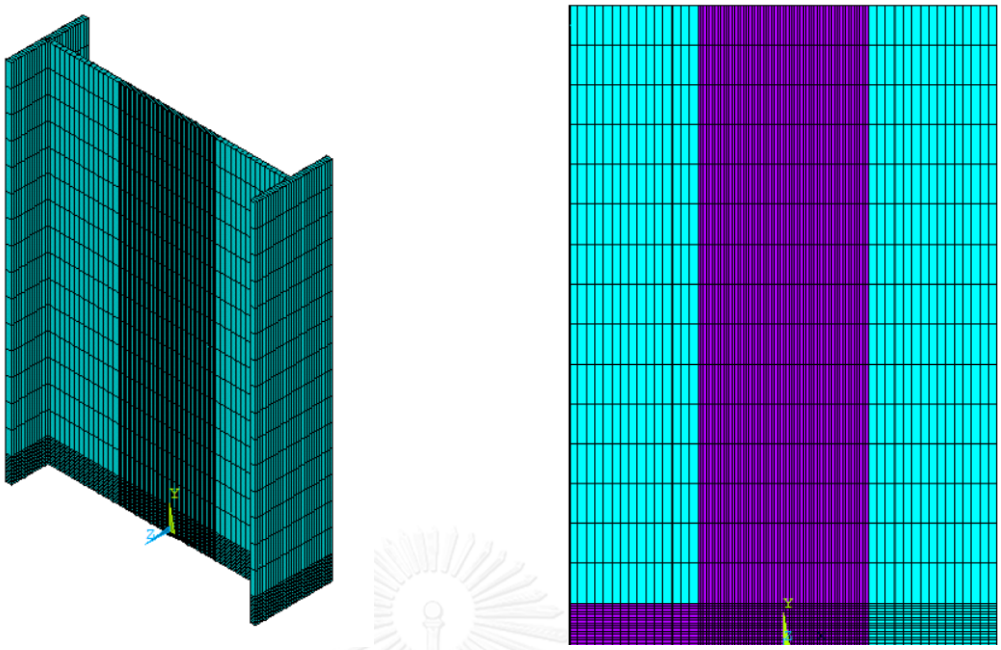

(a) (b)

Figure 4.12. Typical mesh for two-tip web crack: (a) Entire beam; (b) web only.

4.2. Development of SIF solution for W-shapes subjected to polynomial stress distribution

The steel I-beam subjected to polynomial stress distribution was examined in this section. The configuration of the newly formed web crack is illustrated in Figure 4.13.

The m-degree form of polynomial stress distribution in I-beam was as follow

$$\sigma(x) = \sigma \sum_{0}^{m} D_m \left[x / (d_j / 2) \right]^m \tag{4.3}$$

The SIFs solution after crack closure were then represented as

$$K^{A,B'} = \left[\sum_{0}^{m} D_m f^{A,B'}(\varepsilon', \lambda'_w, \beta, m) \right] \sigma \sqrt{\pi a'_w} \tag{4.4}$$

where $\varepsilon' = e' / (d_j / 2)$: the new normalized crack eccentricity

$\lambda'_w = a'_w / (d_j / 2 - e')$: the new normalized crack length

m : the polynomial degree; $m = 0$ for tension, $m = 1$ for bending (Albrecht et al., [23]).

e' : the new eccentricity

$f^{A,B'}(\varepsilon', \lambda'_w, \beta, m)$: correction factors for the SIF at crack tip A and B'.

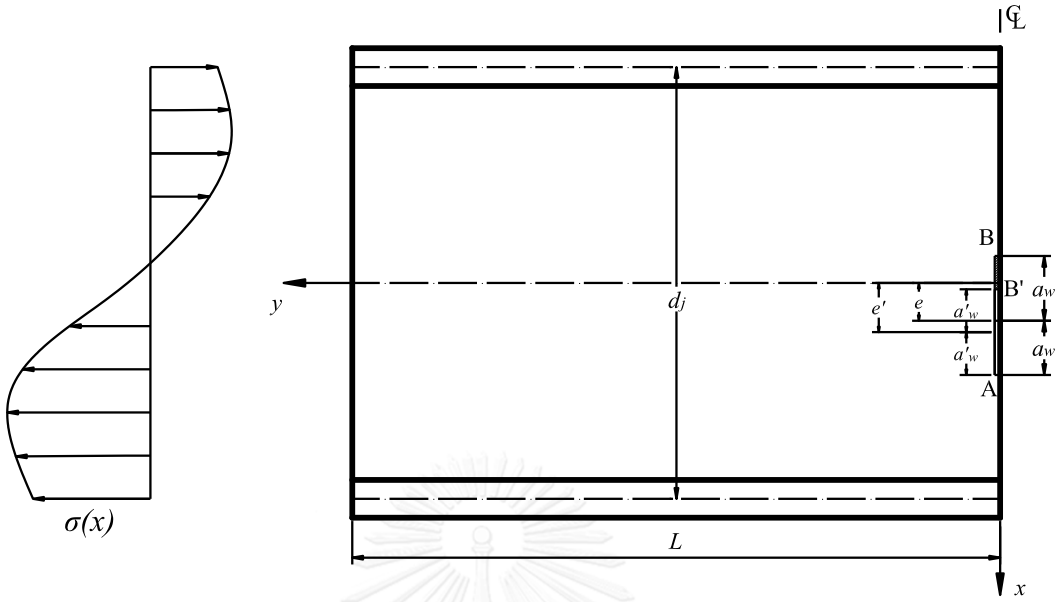

Figure 4.13. Newly formed web crack after crack closure

After crack closure, the crack became more eccentric, and the parameters of the new web crack was determined as follow

$$a'_w = a_w - (e' - e) \tag{4.5}$$

$$\varepsilon' = \varepsilon + (e' - e)/(d_j/2) \tag{4.6}$$

$$\lambda'_w = \frac{a'_w - (e' - e)}{d_j/2 - e'} = \frac{\lambda_w \times (1-\varepsilon) - (e' - e)/(d_j/2)}{1 - \varepsilon - (e' - e)/(d_j/2)} \tag{4.7}$$

where $\varepsilon = e/(d_j/2)$: the original normalized eccentricity

e : the original eccentricity

$\lambda_w = \frac{a_w}{d_j/2 - e}$: the original normalized crack length

By applying the necessary condition

$$K_{B'} = 0 \text{ or } \sum_0^m D_m f^{B'}(\varepsilon', \lambda'_w, \beta, m) = 0 \tag{4.8}$$

The effective SIF solution was determined as following expression

$$K_{eff}^{A} = \sum_{0}^{m} D_m f^{A}(\varepsilon', \lambda'_w, \beta, m)\sigma\sqrt{\pi a'_w}$$
$$= \sum_{0}^{m} D_m f^{A}(\varepsilon', \lambda'_w, \beta, m)\sigma\sqrt{\pi\left[a_w - (e' - e)\right]} \quad (4.9)$$

CHAPTER 5
VALIDATION OF MODEL

5.1. Plate subjected to bending

A simple model of center-cracked finite-width plate under bending (Plate B, Table 4.2) was performed to verify the non-overlapping behavior in crack.

The SIF results from this model agreed very well with the previously conducted numerical study (*Albrecht and Lenwari, [27]*). The differences were within 4% for both overlapping and non-overlapping models (Figure 5.1).

Besides, an additional model of eccentric-cracked finite width plate under bending was simulated for plate B to validate the overlapping crack.

The correction factors of eccentric cracks ($\varepsilon = e/W = 0.1$) were compared with the solution of *Chen and Albrecht [32]* for the range of $\lambda = a/(W-e)$ from 0.1 to 0.9, as shown in Figure 5.2. The maximum difference was less than 4% for both lower and upper crack tip.

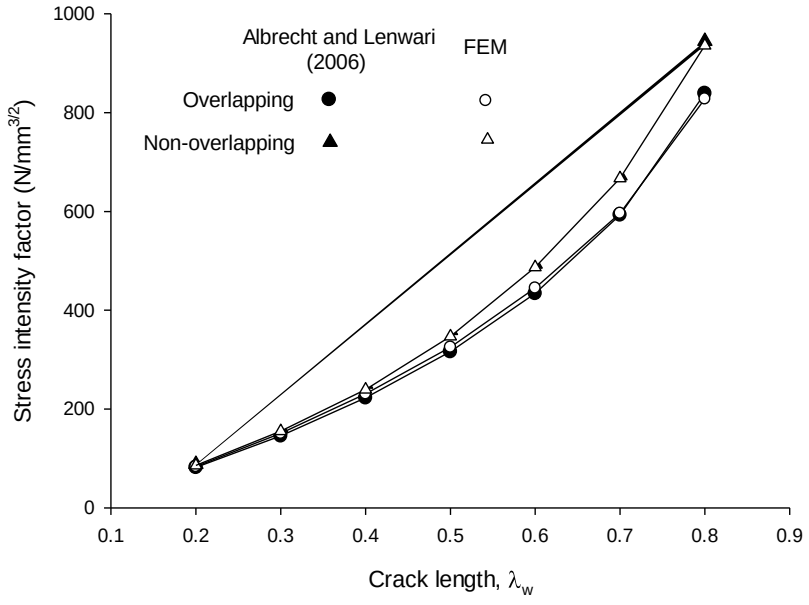

Figure 5.1. SIF solution of center-cracked plate under bending (Plate B, Table 4.2)

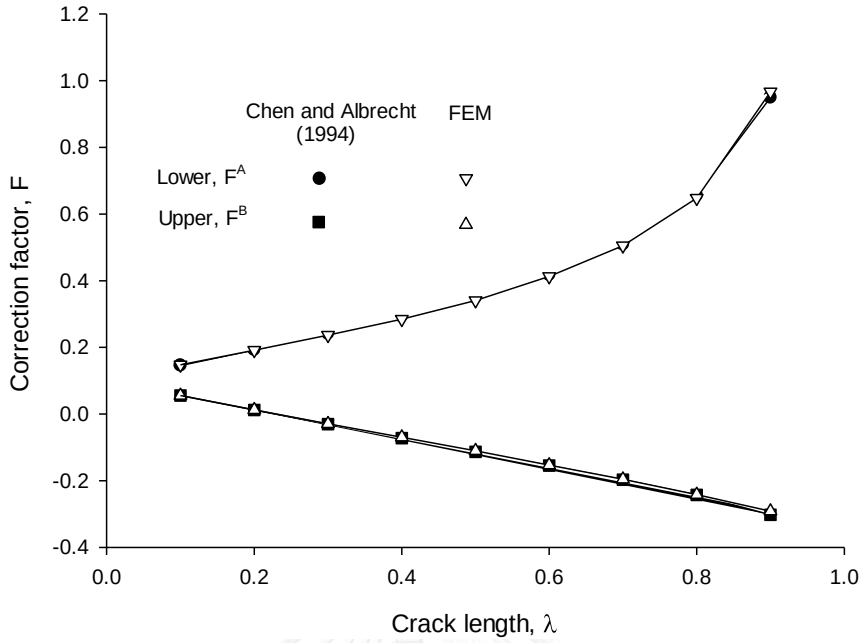

Figure 5.2. SIF solution of eccentric-cracked plate under bending (Plate B, Table 4.2, ε =0.1)

From the above solution, it was obvious that the singularity around the crack tip region in the overlapping and non-overlapping conditions could be captured by the proposed model.

5.2. W-shape subjected to bending without contact elements

A finite element model of shape W40x149 ($\beta = 0.83$) subjected to both tension and bending was performed in overlapping condition for the range of web crack length λ_w from 0.2 to 0.8.

Figure 5.3 and Figure 5.4 show the comparison of correction factors between the overlapping finite element models and solution of Albrecht et al. [23], for both upper and lower crack tips under tension and bending, respectively.

It was apparent that the finite element model under bending agreed well with the results in [23]. For the model subjected to tension, although the form of the straight line was not totally fitted with the literature line, the maximum difference was still within 2%.

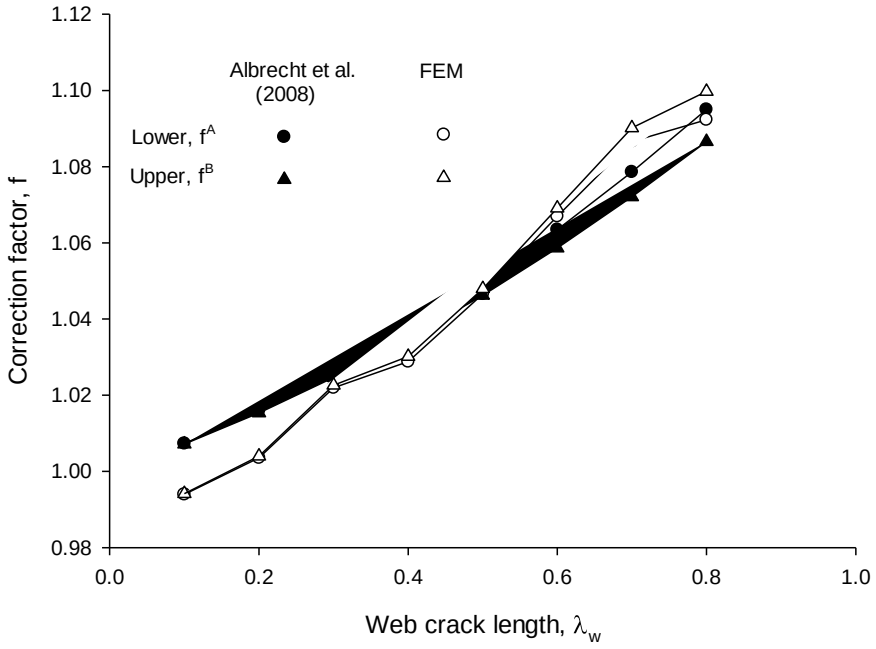

Figure 5.3. Correction factors for both lower and upper crack tips in overlapping I-beam under tension (W40x149, ε = 0)

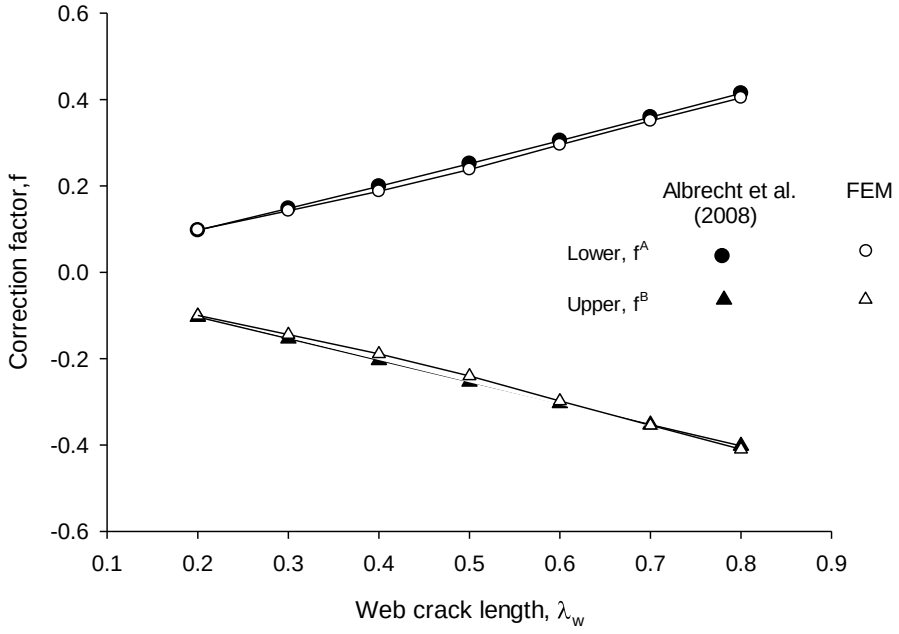

Figure 5.4. Correction factors for both lower and upper crack tips in overlapping I-beam under bending (W40x149, ε = 0)

5.3. W-shape subjected to bending with contact elements.

Superposition solution – Section 4.2

The form of bending stress in I-beam was as follow

$$\sigma(x) = \sigma\left[x/(d_j/2) \right]$$

where σ is the stress at the junction lines of the W-shapes.

According to Equation (2.14), the overlapping SIF for central web crack of shape W40x149 ($\beta = 0.83$) was

$$K^{A,B} = f^{A,B}(0, \lambda_w, 0.83, 1)\sigma\sqrt{\pi a_w} \tag{5.1}$$

The coefficients of the correction factor for bending case ($m = 1$) were shown in Table 2.3. [23]

According to Equation (4.4), the non-overlapping SIF for central web crack of shape W40x149 was

$$K^{A} = f^{A}(\varepsilon', \lambda'_w, 0.83, 1)\sigma\sqrt{\pi a'_w} \tag{5.2}$$

$$K^{B'} = f^{B'}(\varepsilon', \lambda'_w, 0.83, 1)\sigma\sqrt{\pi a'_w} \tag{5.3}$$

where $e = 0$, $\varepsilon' = \varepsilon + (e' - e)/(d_j/2) = e'/(d_j/2)$ (5.4)

$$\lambda'_w = \frac{\lambda_w - e'/(d_j/2)}{1 - e'/(d_j/2)} \tag{5.5}$$

By applying the necessary condition

$$K^{B'} = 0 \text{ or } f^{B'}(\varepsilon', \lambda'_w, 0.83, 1) = 0 \tag{5.6}$$

The effective SIF solution was determined as following expression

$$\begin{aligned} K^{A}_{eff} &= f^{A}_{eff}(\varepsilon', \lambda'_w, 0.83, 1)\sigma\sqrt{\pi a'_w} \\ &= f^{A}_{eff}(\varepsilon', \lambda'_w, 0.83, 1)\sigma\sqrt{\pi\left(a_w - e'\right)} \end{aligned} \tag{5.7}$$

By using Secant method to determine the root of Equation (5.6) in Matlab program, the values of e' were calculated for the range of λ_w from 0.1 to 0.9, as shown in Table 5.1.

Table 5.1. Correction factors for central web crack in shape W40x149 under bending with λ_w from 0.1 to 0.9.

λ_w	e' (mm)	ε'	Crack closure length (mm)	λ'_w	Correction factor, f^A		f^A_{eff} / f^A
					Overlapping	Non-overlapping	
0.1	15.90	0.034	31.80	0.0688	0.0483	0.0659	1.365
0.2	31.61	0.067	63.22	0.1429	0.0976	0.1331	1.363
0.3	47.14	0.099	94.28	0.2228	0.1479	0.2012	1.360
0.4	62.50	0.132	125.01	0.3090	0.1992	0.2701	1.356
0.5	77.73	0.164	155.47	0.4021	0.2516	0.3394	1.349
0.6	92.85	0.196	185.71	0.5027	0.3049	0.4085	1.340
0.7	107.90	0.227	215.81	0.6117	0.3593	0.4769	1.327
0.8	122.93	0.259	245.87	0.7301	0.4147	0.5437	1.311
0.9	138.01	0.291	276.02	0.8590	0.4711	0.6078	1.290

Finite element solution

A non-overlapping finite element model of shape W40x149 ($\beta = 0.83$) subjected to bending was performed for the range of central web crack length λ_w from 0.1 to 0.9. The correction factors of the non-overlapping web crack were compared with the result in Table 5.1, as shown in Figure 5.5.

Figure 5.6 shows the crack closure length of non-overlapping central web crack in shape W40x149.

The non-overlapping correction factor of the lower crack tip and the crack closure length in the finite element model of shape W40x149 agreed well with the superposition result in section 4.2 for most of the data points.

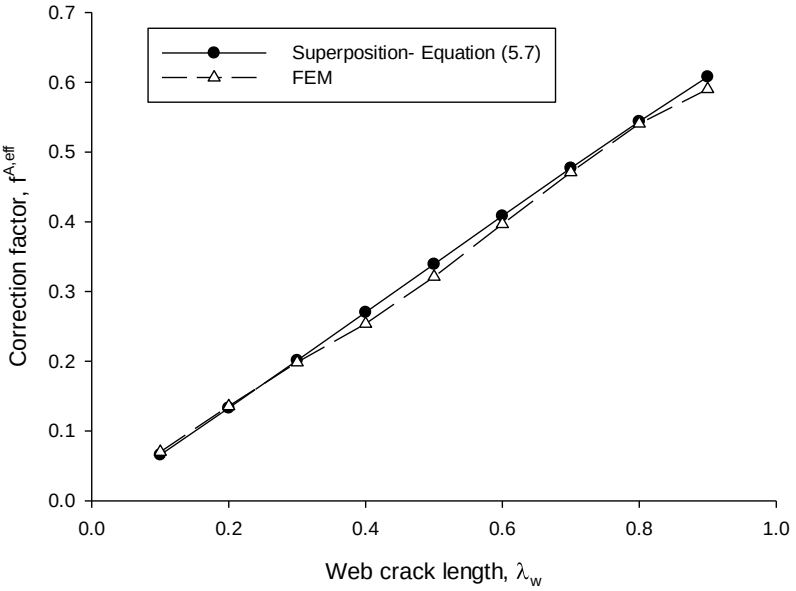

Figure 5.5. Correction factors for the lower crack tip in non-overlapping I-beam under bending (W40x149, ε = 0)

The numerical solution in section 4.2 can be further developed for the higher-order polynomial stress distribution if the forms of correction factor equations are determined (i.e. $f(\varepsilon, \lambda_w, \beta, m)$ with $m \geq 2$).

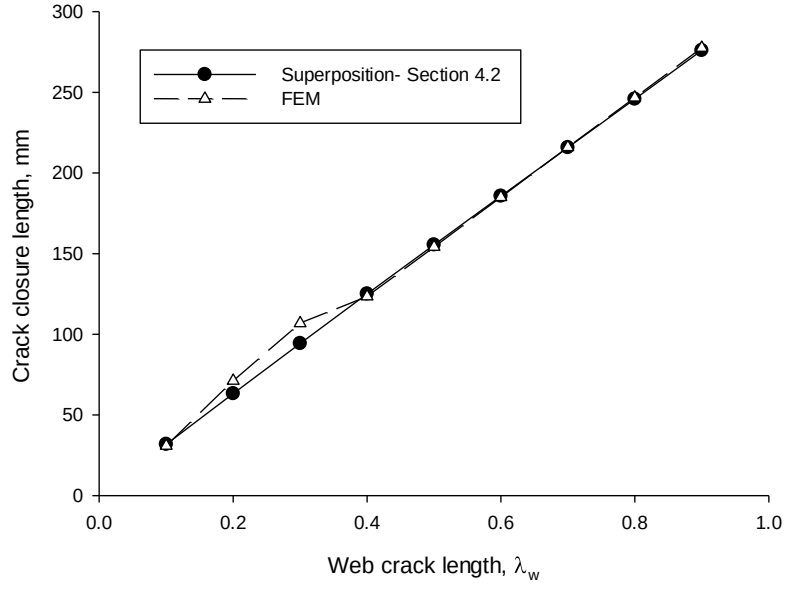

Figure 5.6. Crack closure length of non-overlapping I-beam under bending (W40x149, ε = 0)

5.4. W-shape subjected to linear stress distribution with contact elements.

Superposition solution – Section 4.2

The form of linear stress distribution in I-beam was as follow

$$\sigma(x)=\sigma\sum_{0}^{m=1}D_m\left[x/(d_j/2)\right]^m=\sigma\left\{D_0+D_1\times\left[x/(d_j/2)\right]\right\}$$

where m: the polynomial degree ($m=0$ for tension, $m=1$ for bending)

According to Equation (2.14), the overlapping SIF for central web crack of shape W40x149 ($\beta=0.83$) under linear stress distribution was

$$\begin{aligned}K^{A,B}&=\left[\sum_{0}^{m=1}D_m f^{A,B}(0,\lambda_w,0.83,m)\right]\sigma\sqrt{\pi a_w}\\&=\left[D_0\times f^{A,B}(0,\lambda_w,0.83,0)+D_1\times f^{A,B}(0,\lambda_w,0.83,1)\right]\sigma\sqrt{\pi a_w}\end{aligned}\tag{5.8}$$

The coefficients of the correction factor for tension and bending cases were shown in Table 2.3. [23]

According to Equation (4.4), the non-overlapping SIF for central web crack of shape W40x149 was

$$\begin{aligned}K^{A}&=\left[\sum_{0}^{m=1}D_m f^{A}(\varepsilon',\lambda'_w,0.83,m)\right]\sigma\sqrt{\pi a'_w}\\&=\left[D_0\times f^{A}(\varepsilon',\lambda'_w,0.83,0)+D_1\times f^{A}(\varepsilon',\lambda'_w,0.83,1)\right]\sigma\sqrt{\pi a'_w}\end{aligned}\tag{5.9}$$

$$\begin{aligned}K^{B'}&=\left[\sum_{0}^{m=1}D_m f^{B'}(\varepsilon',\lambda'_w,0.83,m)\right]\sigma\sqrt{\pi a'_w}\\&=\left[D_0\times f^{B'}(\varepsilon',\lambda'_w,0.83,0)+D_1\times f^{B'}(\varepsilon',\lambda'_w,0.83,1)\right]\sigma\sqrt{\pi a'_w}\end{aligned}\tag{5.10}$$

where $e=0$, $\varepsilon'=\varepsilon+(e'-e)/(d_j/2)=e'/(d_j/2)$ (5.11)

$$\lambda'_w=\frac{\lambda_w-e'/(d_j/2)}{1-e'/(d_j/2)}\tag{5.12}$$

By applying the necessary condition

$$K^{B'}=0 \text{ or } D_0\times f^{B'}(\varepsilon',\lambda'_w,0.83,0)+D_1\times f^{B'}(\varepsilon',\lambda'_w,0.83,1)=0\tag{5.13}$$

The effective SIF solution was determined as following expression

$$K_{eff}^{A} = \left[\sum_{0}^{m=1} D_m f_{eff}^{A}(\varepsilon', \lambda'_w, 0.83, m)\right]\sigma\sqrt{\pi a'_w}$$
$$= \left[D_0 \times f_{eff}^{A}(\varepsilon', \lambda'_w, 0.83, 0) + D_1 \times f_{eff}^{A}(\varepsilon', \lambda'_w, 0.83, 1)\right]\sigma\sqrt{\pi(a_w - e')} \quad (5.14)$$

By using Secant method to determine the root of Equation (5.13) in Matlab program, the values of e' were calculated for the range of λ_w from 0.1 to 0.9 with $D_o = 0.25$ and $D_1 = 1$, as shown in Table 5.2.

Table 5.2. Correction factors for central web crack in shape W40x149 under linear stress distribution with λ_w from 0.1 to 0.9 ($D_o = 0.25$ and $D_1 = 1$)

λ_w	e' (mm)	ε'	Crack closure length (mm)	λ'_w	Correction factor, $F^A = \sum_{0}^{m=1} D_m f^A$		F_{eff}^{A} / F^{A}
					Overlapping	Non-overlapping	
0.1	0.000	0.000	0.00	0.100	0.3001	0.3001	1.00
0.2	0.000	0.000	0.00	0.200	0.3516	0.3516	1.00
0.3	0.000	0.000	0.00	0.300	0.4044	0.4044	1.00
0.4	0.000	0.000	0.00	0.400	0.4585	0.4585	1.00
0.5	0.000	0.000	0.00	0.500	0.5140	0.5140	1.00
0.6	11.613	0.024	23.23	0.590	0.5708	0.5834	1.02
0.7	25.806	0.054	51.61	0.683	0.6290	0.6561	1.04
0.8	39.792	0.084	79.58	0.782	0.6885	0.7286	1.06
0.9	53.592	0.113	107.18	0.887	0.7493	0.8001	1.07

Finite element solution

The overlapping and non-overlapping finite element models of shape W40x149 ($\beta = 0.83$) subjected to the linear stress distribution in form of $\sigma(x) = \sigma\sum_{0}^{m=1} D_m\left[x/(d_j/2)\right]^m = \sigma\left\{0.25 + 1\times\left[x/(d_j/2)\right]\right\}$ were performed for the range of central web crack length λ_w from 0.1 to 0.9. The correction factors of the overlapping and non-overlapping web cracks were compared with the result in Table 5.2, as shown in Figure 5.7.

Figure 5.8 shows the crack closure length of non-overlapping central web crack in shape W40x149.

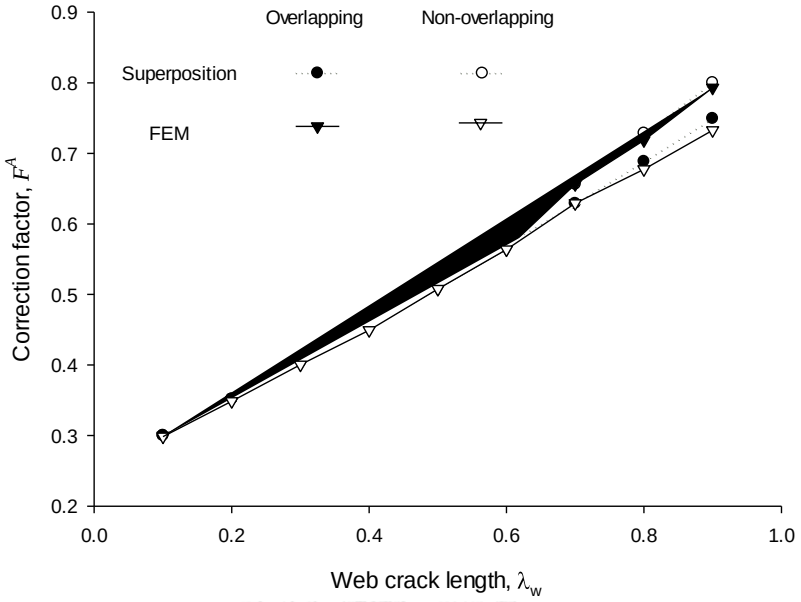

Figure 5.7. Correction factors for the lower crack tip in non-overlapping I-beam under linear stress distribution (W40x149, ε = 0)

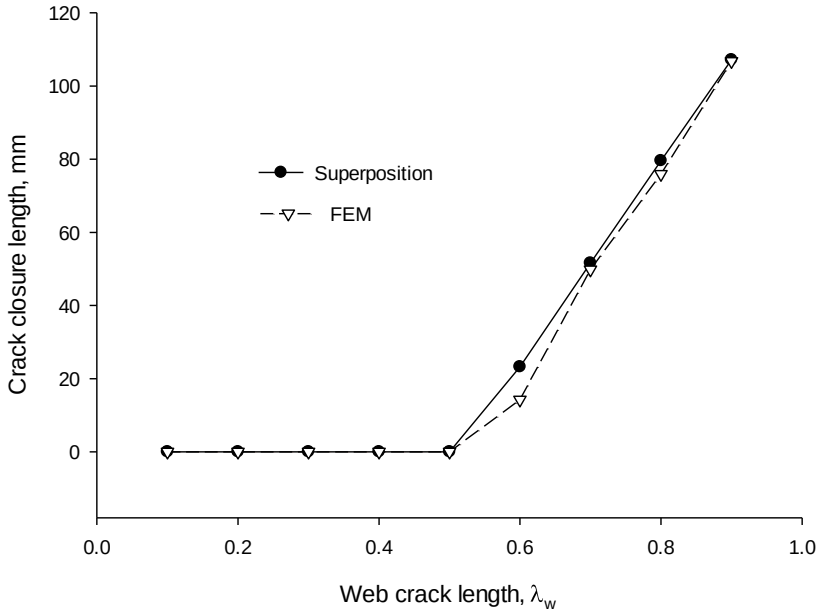

Figure 5.8. Crack closure length of non-overlapping I-beam under linear stress distribution (W40x149, ε = 0)

CHAPTER 6
PARAMETRIC STUDY

6.1. Effect of the length of the W-shape

In this section, the effect of the length to the I-beam (W40x149) which contains central web crack (ε =0) was examined for a combination of five values of the half-beam length (L / d_j = 0.25, 0.5, 1, 1.5 and 2); two values of the normalized crack length (λ_w =0.2 and 0.7) and two types of loading (tension and bending) (Tables 6.1 and 6.2).

Table 6.1. Effect of the length on the SIF of center-cracked W40x149 under tension

λ_w	L / d_j	Albrecht et al. [23] $K_{Albrecht}$		Overlapping K_{FEM}		Differences % $(K_{FEM} - K_{Albrecht}) / K_{Albrecht}$	
		Upper crack tip	Lower crack tip	Upper crack tip	Lower crack tip	Upper crack tip	Lower crack tip
0.2	0.25	1753.37	1754.40	2016.23	2017.32	15.0	15.0
	0.5			1817.53	1816.98	3.7	3.6
	1			1740.10	1739.36	-0.8	-0.9
	1.5			1733.76	1733.02	-1.1	-1.2
	2			1732.84	1732.10	-1.2	-1.3
0.7	0.25	3463.58	3484.54	9219.98	9216.94	166.2	164.5
	0.5			5065.49	5055.57	46.3	45.1
	1			3595.44	3583.80	3.8	2.8
	1.5			3521.99	3510.33	1.7	0.7
	2			3519.03	3507.36	1.6	0.7

Table 6.2. Effect of the length on the SIF of center-cracked W40x149 under bending

λ_w	L/d_j	Albrecht et al. [23] $K_{Albrecht}$		Overlapping K_{FEM}		Differences % $(K_{FEM}-K_{Albrecht})/K_{Albrecht}$	
		Upper crack tip	Lower crack tip	Upper crack tip	Lower crack tip	Upper crack tip	Lower crack tip
0.2	0.25	-175.48	168.51	-172.55	176.53	-1.7	4.8
	0.5			-172.17	172.30	-1.9	2.2
	1			-172.47	169.88	-1.7	0.8
	1.5			-172.38	169.53	-1.8	0.6
	2			-172.13	169.26	-1.9	0.4
0.7	0.25	-1137.25	1160.84	-1615.51	1625.34	42.1	40.0
	0.5			-1186.22	1179.80	4.3	1.6
	1			-1145.22	1134.07	0.7	-2.3
	1.5			-1144.97	1133.65	0.7	-2.3
	2			-1144.80	1133.45	0.7	-2.4

For both lower and upper crack tips, the values of $K_{FEM}/K_{Albrecht}$ approached the reference line ($K_{FEM}/K_{Albrecht}=1$) when the half-length of beam L increased (Figures 6.1a and 6.1b).

From the Figure 6.1, it is also obvious that the value of $L=d_j$ is adequate for an acceptable SIF solution of I-beam in this study.

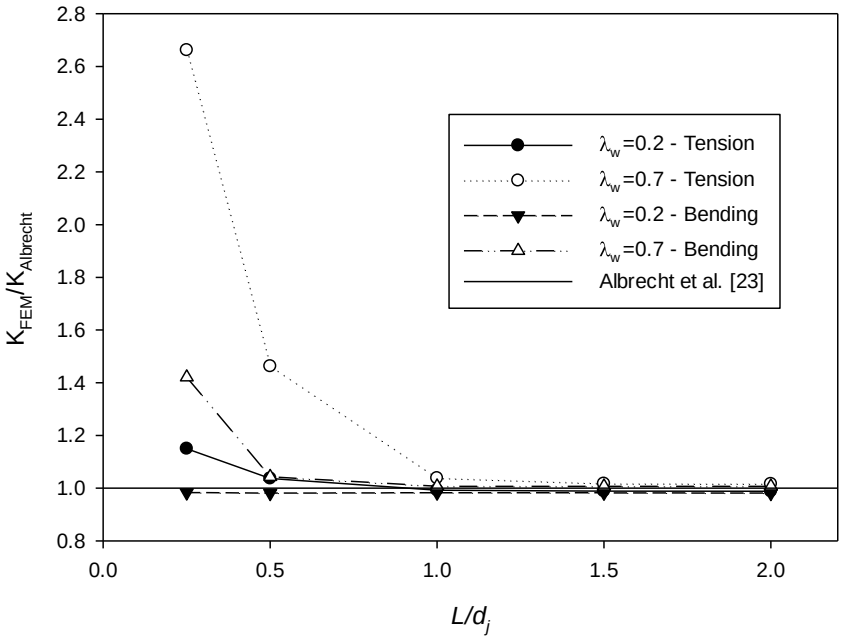

(a)

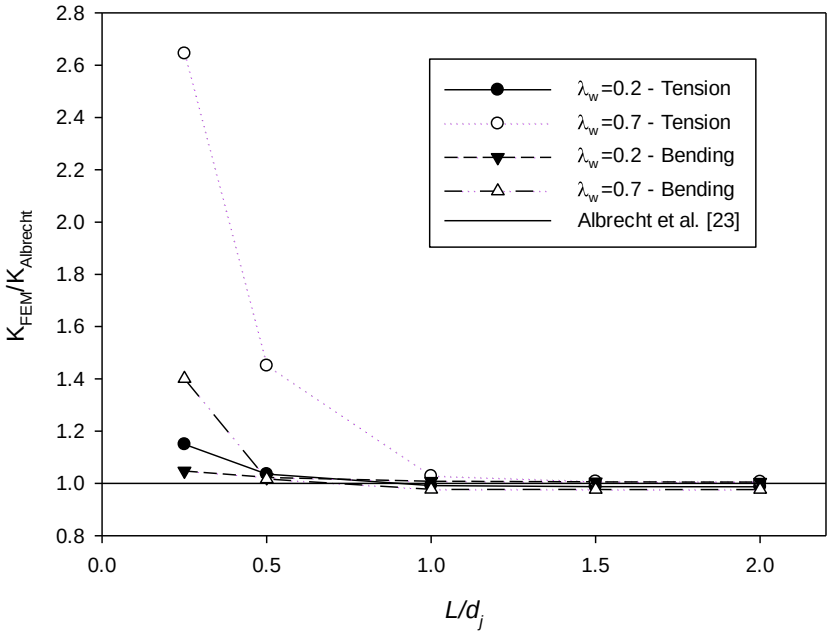

(b)

Figure 6.1 Effect of the length to center-cracked SIF of shape W40x149 under tension and bending for: (a) Upper crack tip; (b) Lower crack tip.

6.2. Effect of the magnitude of applied load on the crack opening displacement (COD)

The effect of the magnitude of the applied load on the COD profile for shape W40x149 ($\varepsilon = 0$) under bending was investigated with a combination of two values of the normalized crack length (λ_w =0.2 and 0.7) and three levels of the bending magnitude (σ =100, 150 and 200 MPa), as shown in Figures 6.2 and 6.3. The x-axis and y-axis of the Figures show the crack length and deformation of the crack surface, respectively.

Table 6.3. COD profile of shape W40x149 containing center-cracked web.

λ_w	σ (MPa)	Stress intensity factor (N/mm$^{3/2}$)		Crack opening displacement U_{max} (mm)		U_{max}/σ (mm^3/N)		Crack closure length (Non-overlapping) (mm)
		Overlapping	Non-overlapping	Overlapping	Non-overlapping	Overlapping	Non-overlapping	
0.2	100	169.53	184.51	0.004637	0.005351	4.637x10^{-5}	5.351x10^{-5}	71.19
	150	254.29	276.76	0.006956	0.008027	4.637x10^{-5}	5.351x10^{-5}	
	200	339.05	369.01	0.009275	0.010704	4.638x10^{-5}	5.352x10^{-5}	
0.7	100	1134.07	1255.26	0.05848	0.06905	5.848x10^{-4}	6.905x10^{-4}	216.01
	150	1701.12	1882.88	0.08772	0.10358	5.848x10^{-4}	6.905x10^{-4}	
	200	2268.13	2510.54	0.11697	0.13811	5.849x10^{-4}	6.906x10^{-4}	

From the Table 6.3, the crack closure lengths for both λ_w =0.2 and λ_w =0.7 were constant (71.19 mm and 216.01 mm, respectively). It means that the position of the newly formed crack tip in compression are unique, regardless of the level of the bending load. On contrary, the SIFs and the crack opening displacements varied proportionally to the applied loads: U_{max}/σ maintained constant for both overlapping and non-overlapping models (with λ_w =0.2, U_{max}/σ were equal to 4.637x10^{-5} and 5.351x10^{-5}, respectively).

This phenomenon is also observed by Tada et al. [5] for the non-overlapping crack in plate (Section 3.2).

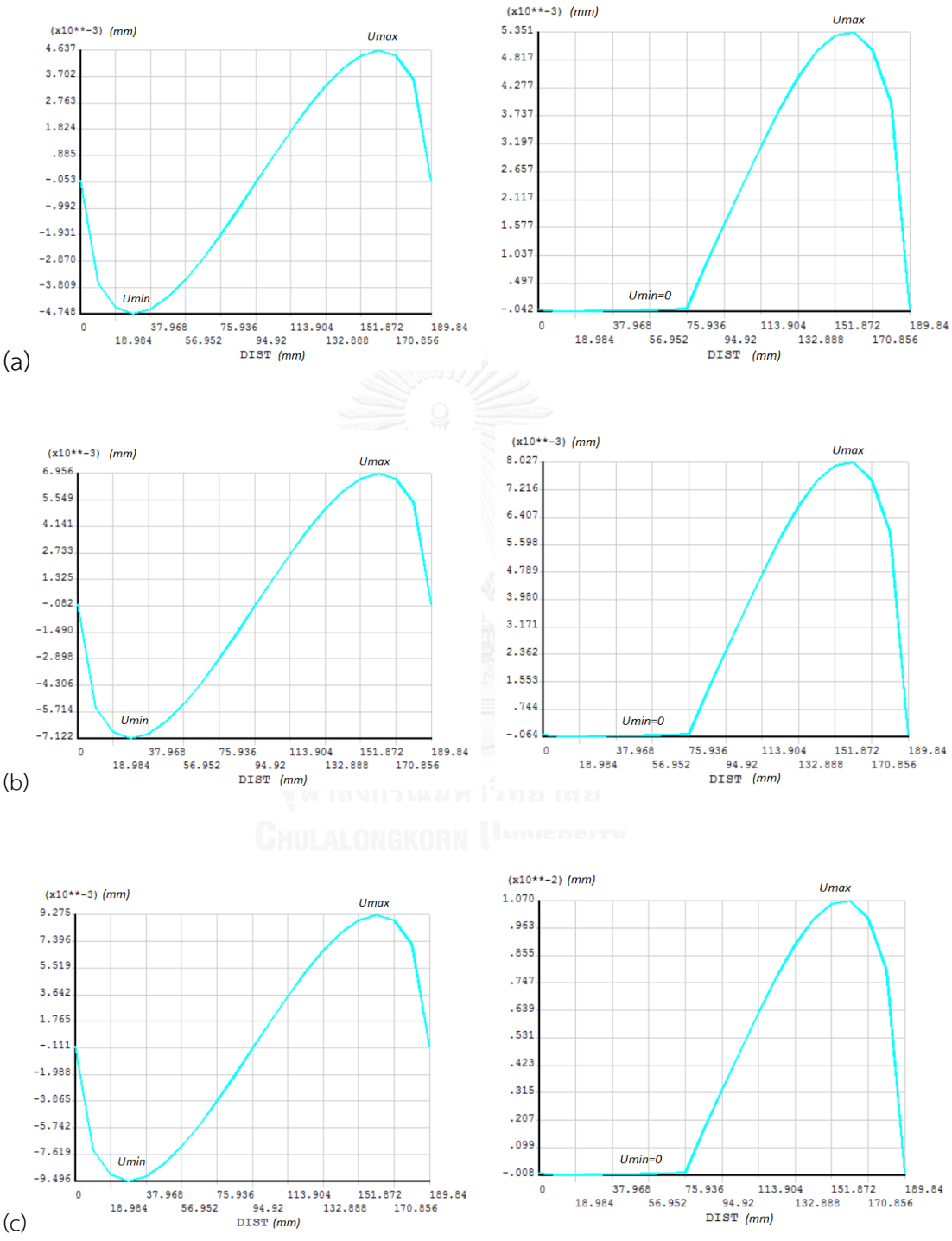

Figure 6.2. COD profile of shape W40x149 (λ_w = 0.2, ε =0) with: (a) σ =100 MPa, (b) σ =150 MPa and (c) σ =200 MPa for both overlapping and non-overlapping cracks.

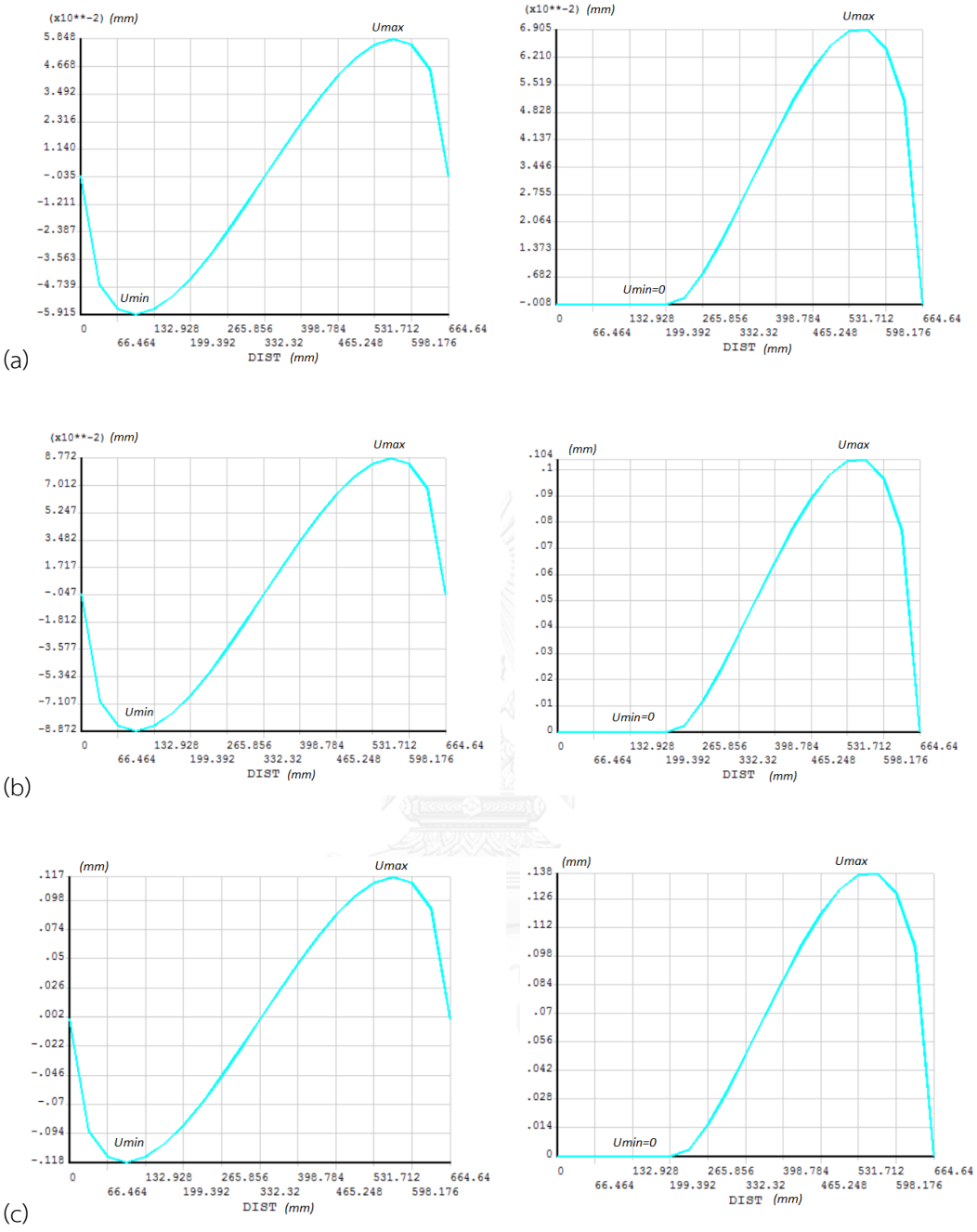

Figure 6.3. COD profile of shape W40x149 (λ_w = 0.7, ε =0) with: (a) σ =100 MPa, (b) σ =150 MPa and (c) σ =200 MPa for both overlapping and non-overlapping cracks.

6.3. Effects of parameters on correction factor (β , λ_w and ε)

To investigate the effect of the parameters including the web crack length λ_w, the normalized eccentricity ε and the flange-to-web area ratio β, a total of 400 finite element analyses under in-plane bending were performed with a combination of eight W-shapes (β values from 0.83 to 2.11, as listed in Table 4.1), five values of the eccentricity (ε = 0, 0.1 – 0.7 in steps of 0.2), five values of crack length (λ_w =0.1 – 0.9 in steps of 0.2) and two types of models (with and without contact elements). The lengths of W-shapes were maintained at a constant ratio of two times of the beam height, $L = d_j$.

Figure 6.4 shows the comparison of the correction factors at the lower crack tip in models using contact elements between shape W40x149 and plate C (equivalent to the web of shape W40x149). Due to the constraining effect of the flange on the web crack which is characterized by the flange-to-web area ratio β, the SIFs in plate were always larger than I-beam solutions. When β increased, the correction factors decreased because of the increase in constraining effect (Figures 6.6). The effect of β on correction factor became more explicit with the large values of crack eccentricity (ε ≥ 0.5), when the lower crack tip was closed to the flange. In Figure 6.5 (ε = 0),

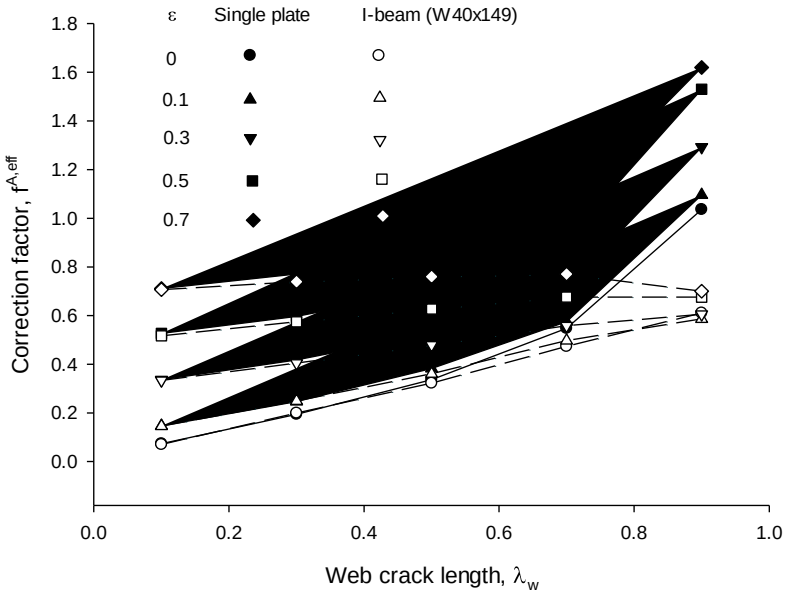

Figure 6.4. Comparison between W-shape (W40x149, β =0.83) and single plate (plate C, Table 4.3) solutions of the lower crack tip for models with contact elements under bending

the parameter β almost had no effect on the correction factor for each value of λ_w because the crack tip was relatively far from the junction line of the web and flange.

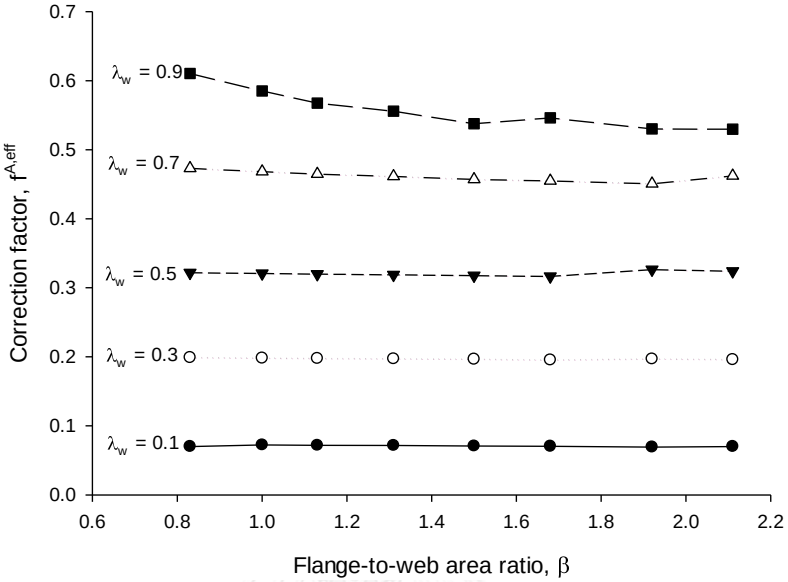

Figure 6.5. Effects of β and λ_w on the correction factor (ε =0)

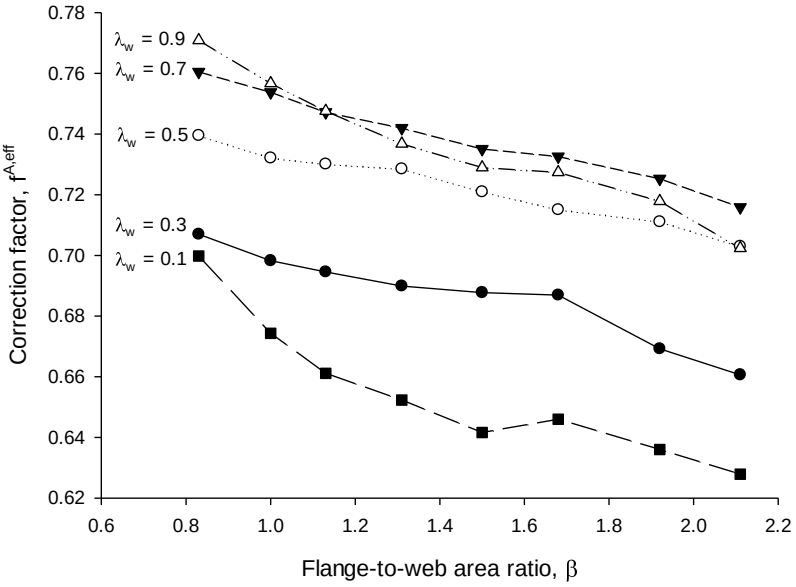

Figure 6.6. Effects of β and λ_w on the correction factor (ε =0.7)

For the lower crack tip in W-shape, the stress intensity factor and correction factor typically increased with the crack length for both models with and without contact

elements. However, they decreased when the crack tip propagated close to the lower flange (λ_w = 0.9 and ε ≥ 0.5), as shown in Figures 6.7 and 6.8.

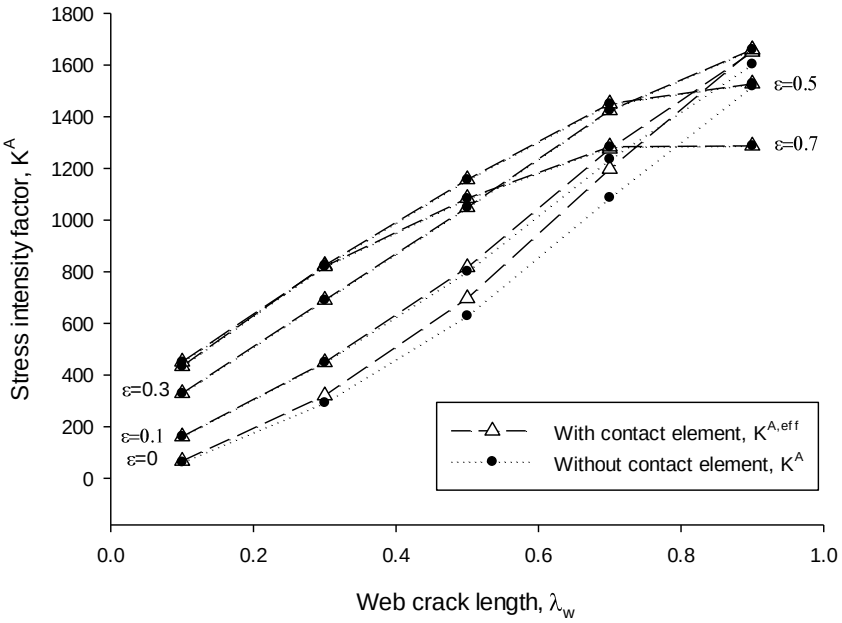

Figure 6.7. Effects of λ_w and ε on the correction factor (W36x194, β = 1.13)

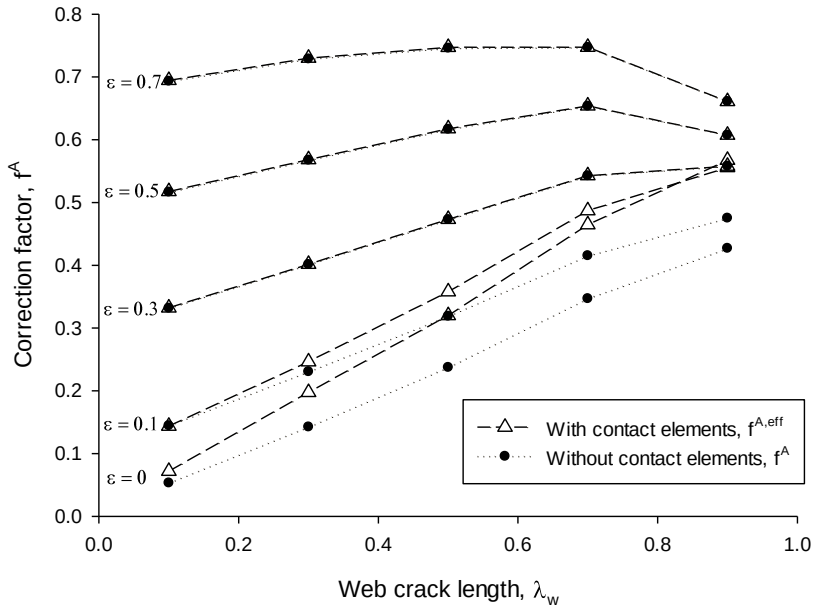

Figure 6.8. Effects of λ_w and ε on the correction factor (W36x194, β = 1.13)

Figures 6.10 and 6.9 show the correction factors of the W-shape models with and without contact elements, respectively. Each value of crack eccentricity was

represented by a surface. It is obvious that the correction factors always increase as the eccentricity ε increases.

For $\varepsilon \geq 0.3$, the crack closure of the W-shapes did not occur and the crack remained open for all combinations despite the fact that the upper crack tip still lie in compressive region (similar to the crack of infinite plate in Figure 3.5b). This can be attributed to the influence of the crack in tension side. When most of crack length was under tension, the opening trend turned into dominant and controlled the closing trend of the crack in compression. As shown in Table 6.4, the effect of non-overlapping behavior ($f^{A,eff} / f^{A}$) became pronounced when ε decreased. Figures 6.11 and 6.12 represent the effect of the crack eccentricity on correction factor in the models using contact elements of shapes W40x147 and W21x201, respectively. Each line corresponded to one crack length. As ε increased, the correction factor of each λ_w also rose (except for λ_w = 0.9, the non-overlapping solutions at ε =0 and 0.1 were higher than correction factor at ε = 0.3 which was not influenced by non-overlapping crack).

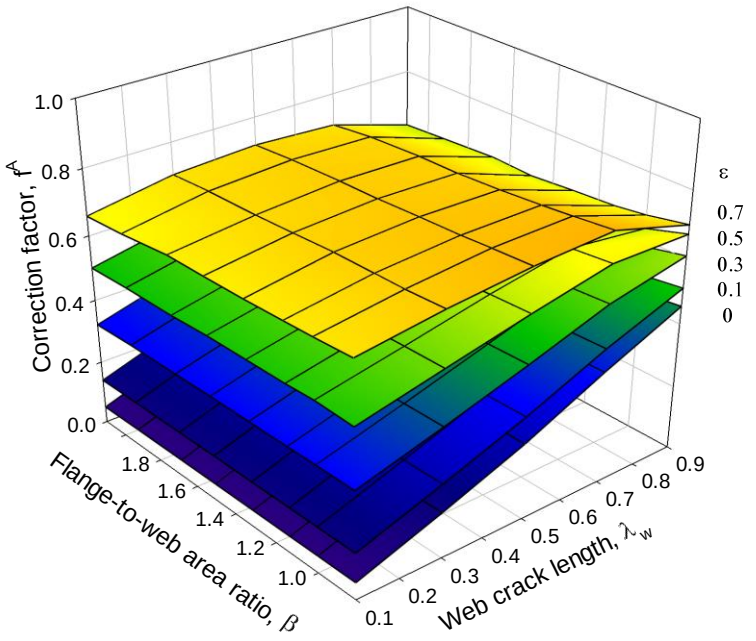

Figure 6.9. Correction factors for the lower crack tip of the W-shape model without contact elements (200 analyses)

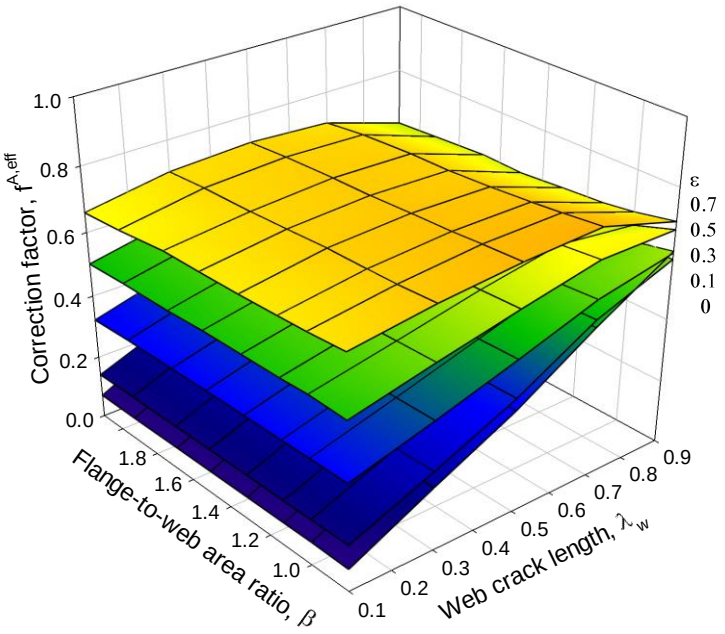

Figure 6.10. Correction factors for the lower crack tip of the W-shape model with contact elements (200 analyses)

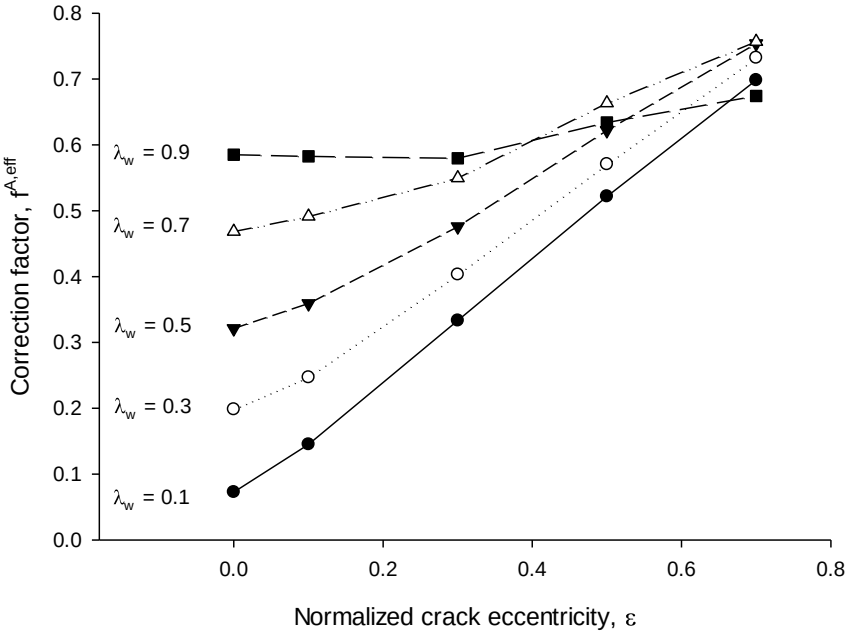

Figure 6.11. Effects of ε and λ_w on the correction factor (W40x167, β = 1.00)

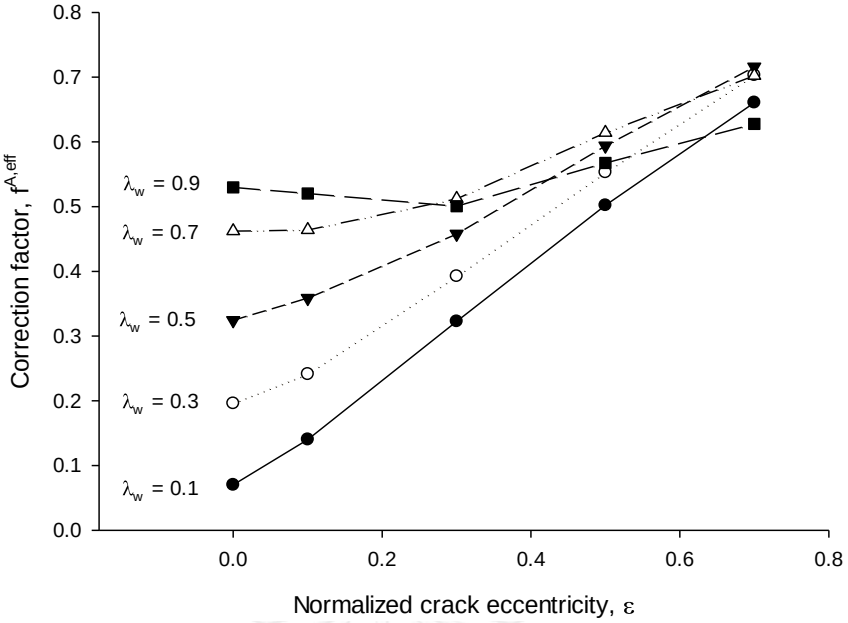

Figure 6.12. Effects of ε and λ_w on the correction factor (W21x201, β = 2.11)

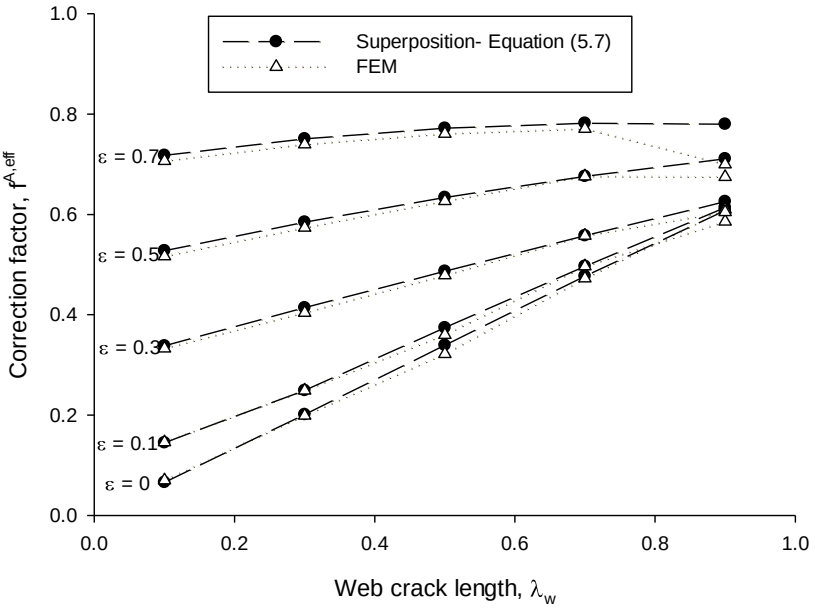

Figure 6.13. Correction factor at lower crack tip in model using contact element (W40x149)

The correction factor at lower crack tip and the crack closure length in comparison between finite element and superposition solutions (as represented in Section 5.3) of shape W40x149 (β = 0.83) under bending were plotted in Figures 6.13 and 6.14, respectively.

Table 6.4. Correction factor of lower crack tip in shape W40x149

ε	λ_w	Albrecht et al. [23]			Closure length (mm)	FEM			Closure length (mm)
		f^A	$f^{A,eff}$	$f^{A,eff}/f^A$		f^A	$f^{A,eff}$	$f^{A,eff}/f^A$	
0	0.1	0.048	0.066	1.37	31.80	0.054	0.070	1.31	30.85
	0.3	0.148	0.201	1.36	94.28	0.143	0.199	1.39	106.78
	0.5	0.252	0.339	1.35	155.47	0.238	0.322	1.35	154.25
	0.7	0.359	0.477	1.33	215.81	0.351	0.473	1.35	216.01
	0.9	0.471	0.608	1.29	276.02	0.455	0.610	1.34	277.64
0.1	0.1	0.145	0.145	1.00	0.00	0.145	0.146	1.00	0.00
	0.3	0.238	0.249	1.05	20.90	0.231	0.249	1.08	32.04
	0.5	0.332	0.374	1.13	75.69	0.321	0.360	1.12	74.75
	0.7	0.428	0.497	1.16	129.91	0.423	0.497	1.17	134.55
	0.9	0.527	0.614	1.17	184.12	0.510	0.586	1.15	172.99
0.3	0.1	0.338	0.338	1.00	0.00	0.333	0.333	1.00	0.00
	0.3	0.414	0.414	1.00	0.00	0.404	0.404	1.00	0.00
	0.5	0.487	0.487	1.00	0.00	0.478	0.479	1.00	0.00
	0.7	0.558	0.558	1.00	0.00	0.558	0.558	1.00	0.00
	0.9	0.626	0.626	1.00	0.35	0.608	0.605	1.00	0.00
0.5	0.1	0.528	0.528	1.00	0.00	0.516	0.517	1.00	0.00
	0.3	0.585	0.585	1.00	0.00	0.572	0.574	1.00	0.00
	0.5	0.634	0.634	1.00	0.00	0.626	0.627	1.00	0.00
	0.7	0.676	0.676	1.00	0.00	0.675	0.676	1.00	0.00
	0.9	0.711	0.711	1.00	0.00	0.672	0.675	1.00	0.00
0.7	0.1	0.718	0.718	1.00	0.00	0.704	0.707	1.00	0.00
	0.3	0.751	0.751	1.00	0.00	0.736	0.740	1.00	0.00
	0.5	0.772	0.772	1.00	0.00	0.759	0.761	1.00	0.00
	0.7	0.782	0.782	1.00	0.00	0.770	0.771	1.00	0.00
	0.9	0.780	0.780	1.00	0.00	0.700	0.700	1.00	0.00

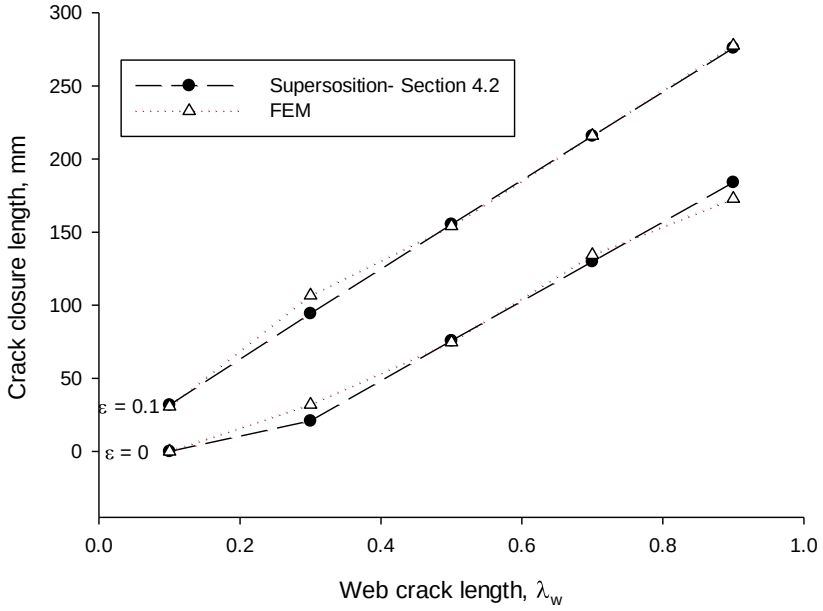

Figure 6.14. Closure length of web crack in model using contact element (W40x149)

It is apparent that the FEM and superposition solutions agreed well with each other, except for $\varepsilon \geq 0.5$ and $\lambda_w = 0.9$ because this crack length was not included in the regression equation (2.17) from the finite element analyses of Albrecht et al. [23]. The present finite element solution became more different in comparison with result in [23] due to the increase in the constraining effect when the crack tip approached the web-to-flange junction line. In practice, some cases with large eccentricity cannot be applicable because the lower crack tip were propagated across the flange, i.e. the W-shapes with ε =0.7, λ_w =0.9 and $\beta \geq 1.13$.

Figures 6.15 and 6.16 plot the correction factors for W-shape models with and without contact elements for $\varepsilon = 0$ and $\varepsilon = 0.1$, respectively. As ε decreased, the difference in correction factor between models with and without element increased.

It was found that the overlapping finite element solutions underestimated the SIFs at lower crack tip up to 11% (at $\varepsilon = 0$ and $\lambda_w = 0.5$). This number for the single plate (plate C, Table 4.3) were 14%. For the correction factor, the maximum values of enhancement were 39% and 37% for I-beam and plate, respectively (as shown in Table 6.4).

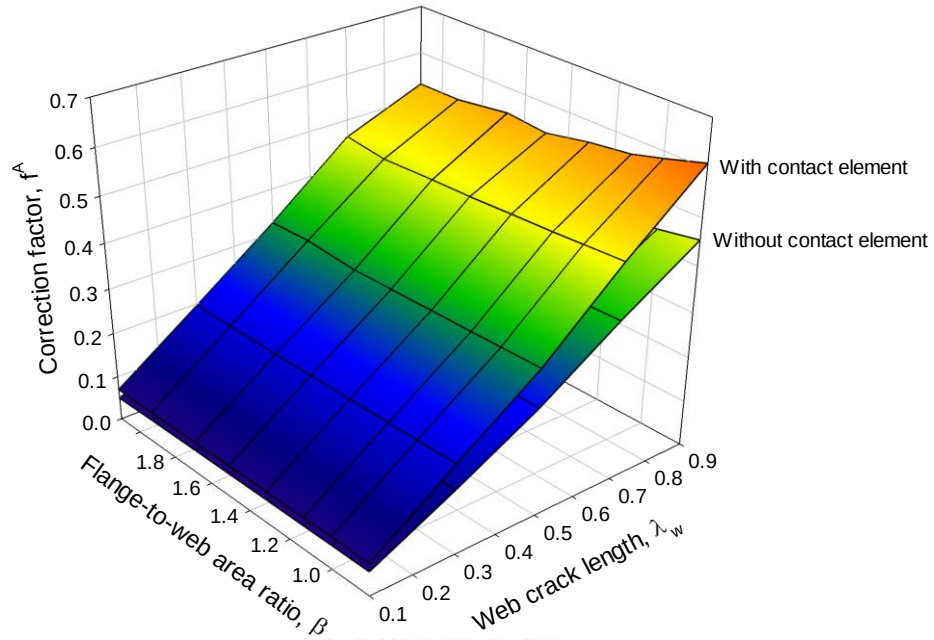

Figure 6.15. Correction factors of the W-shape models with and without contact elements ($\varepsilon = 0$)

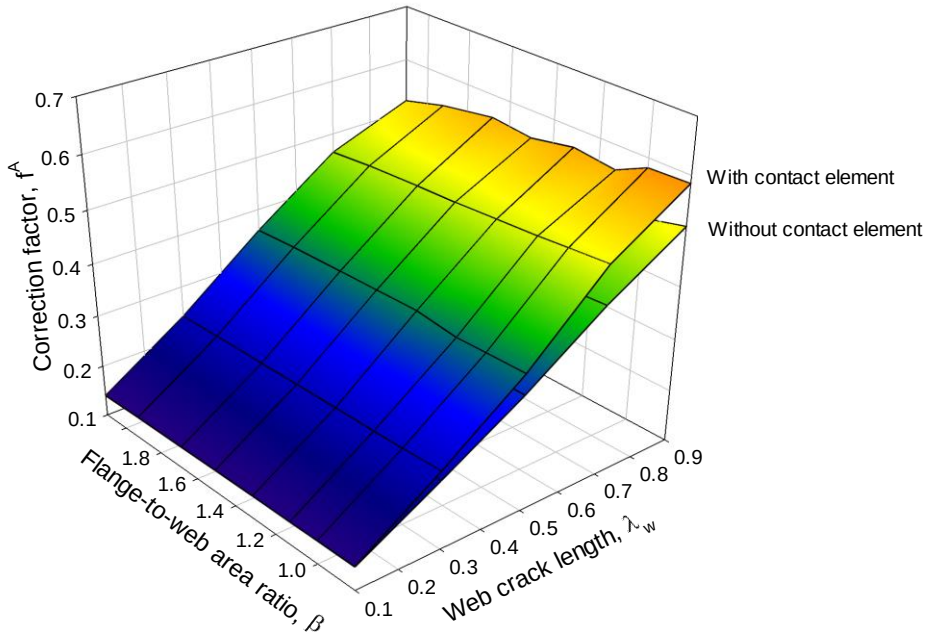

Figure 6.16. Correction factors of the W-shape model with and without contact elements ($\varepsilon = 0.1$)

CHAPTER 7
CONCLUSIONS

Summary

The physically acceptable analysis of stress intensity factors (SIFs) for cracked steel I-beams under bending was presented in this study. Based on the linear elastic fracture mechanics (LEFM), a three-dimensional finite element analysis of the stress intensity factor for a two-tip web crack in W-shape (AISC 2010) was performed considering the non-overlapping crack surfaces. The W-shapes were selected with the range of flange-to-web area ratio from 0.83 to 2.11 because almost 60% of the AISC W- shapes are within this range. Besides, a numerical solution based on the superposition of previous finite element result of Albrecht et al. [23] was subsequently developed to verify with the non-overlapping finite element model. The effects of beam length, magnitude of applied load, crack length, crack eccentricity and flange-to-web area ratio on the correction factor of the non-overlapping model were also discussed. The main conclusions in this research are as follows

a. The overlapping solutions were not conservative due to the underestimation of SIF at the tension side crack tip, especially in case of small eccentricities ($\varepsilon \leq 0.1$). The maximum difference of the SIF between overlapping and non-overlapping solutions was up to 11%. For $\varepsilon \geq 0.3$, the overlapping crack surfaces did not occur. Therefore, the SIF equation proposed by Albrecht et al. [23] still can be applicable for W-shapes in practice with a minor modification: a safety factor of 1.1 should be considered in SIF equation for $\varepsilon \leq 0.1$ in cracked beam under bending.

b. It was found that the position of the new crack tip in compression are unique, regardless of the magnitude of the bending load in I-beam. On contrary, the crack tip opening displacement (CTOD) varied proportionally to the applied load for the model with contact elements. Similar phenomenon on cracked plate under bending was observed by Tada et al. [5], as mentioned in section 3.2.

c. For the case of tension and bending, the SIF values approached the solution of Albrecht et al. [23] as the length of I-beam increased. It was point out that the half-beam length of $L = d_j$ was adequate for an acceptable solution in this study.

d. Due to the constraining effect which is characterized by the flange-to-web area ratio β, the non-overlapping SIF values and the percentage of the SIF underestimation in a single plate were always larger than the I-beam solutions. When β increased, the correction factors decreased because of the increase in constraining effect. The effect of β became pronounced with the large values of λ_w and ε, when the crack tip propagated close to the junction line of the web to the flange.

e. The correction factor typically increased with the crack length for both models with and without contact elements. However, it decreased when the crack tip approached the flange (λ_w = 0.9 and ε ≥ 0.5).

f. The correction factors always rose as the eccentricity ε increased. In contrast, the effect of non-overlapping behavior ($f^{A,eff}$ / f^{A}) became prominent when ε decreased.

Extension of the research for the future work

The numerical solution in Section 4.2 can be further developed for the two-tip web crack and symmetric three-tip crack of the W-shape subjected to polynomial stress distribution if the forms of the overlapping SIF equations are determined in the following researches (for $m \geq 2$). More combinations of the stress distribution can give a more clearly behavior of the non-overlapping crack surfaces through the SIFs at the tension side crack tip as well as the COD profile in the opened portion.

REFERENCES

1. Irwin, G.R., *Analysis of stresses and strains near the end of a crack traversing a plate.* Spie Milestone series MS, 1997. **137**(167-170): p. 16.
2. Koiter, W., *Note on the stress intensity factors for sheet strips with cracks under tensile loads.* Delft Technical University, Department of Mechanical Engineering Report, 1965(314).
3. Brown, W. and J. Srawley, *Plane strain crack toughness testing of high strength metallic materials*, in *Plane Strain Crack Toughness Testing of High Strength Metallic Materials*. 1966, ASTM International.
4. Feddersen, C., *Discussion to plane strain crack toughness testing.* ASTM STP, 1966. **410**: p. 77.
5. Tada, H., P.C. Paris, and G.R. Irwin, *The Stress Analysis of Cracks Handbook*. 3 ed. 2000: Wiley.
6. SANDERS JR, J., *The effect of a stringer on the stress in a cracked sheet.* Journal of Applied Mechanics, 1965.
7. Isida, M., *Analysis of stress intensity factors for the tension of a centrally cracked strip with stiffened edges.* Engineering Fracture Mechanics, 1973. **5**(3): p. 647-665.
8. Kienzler, R.H., G, *An elementary theory of detective beams.* Acta Mechanica, 1986. **62**: p. 37-46.
9. Herrmann, G. and H. Sosa, *On bars with cracks.* Engineering fracture mechanics, 1986. **24**(6): p. 889-894.
10. Huajian, G. and G. Herrmann, *On estimates of stress intensity factors for cracked beams and pipes.* Engineering Fracture Mechanics, 1992. **41**(5): p. 695-706.
11. Dunn, M.L., W. Suwito, and B. Hunter, *Stress intensity factors for cracked I-beams.* Engineering fracture mechanics, 1997. **57**(6): p. 609-615.
12. Müller, W., G. Herrmann, and H. Gao, *Elementary strength theory of cracked beams.* Theoretical and Applied Fracture Mechanics, 1993. **18**(2): p. 163-177.

13. Ricci, P. and E. Viola, *Stress intensity factors for cracked T-sections and dynamic behaviour of T-beams.* Engineering fracture mechanics, 2006. **73**(1): p. 91-111.
14. Ghafoori, E. and M. Motavalli, *Analytical calculation of stress intensity factor of cracked steel I-beams with experimental analysis and 3D digital image correlation measurements.* Engineering Fracture Mechanics, 2011. **78**(18): p. 3226-3242.
15. Xie, Y., H. Xu, and P. Li, *Crack mouth widening energy-release rate and its application.* Theoretical and applied fracture mechanics, 1998. **29**(3): p. 195-203.
16. Xie, Y. and X. Wang, *Application of G*-integral on cracked structural beams.* Journal of constructional steel research, 2004. **60**(9): p. 1271-1290.
17. Xie, Y., X. Wang, and Y. Lin, *Stress intensity factors for cracked rectangular cross-section thin-walled tubes.* Engineering fracture mechanics, 2004. **71**(11): p. 1501-1513.
18. Tian, L., et al., *Mixed-mode fracture & non-planar fatigue analyses of cracked I-beams, using a 3D SGBEM–FEM Alternating Method.* Theoretical and Applied Fracture Mechanics, 2014. **74**: p. 188-199.
19. Hmidan, A., Y.J. Kim, and S. Yazdani, *Correction factors for stress intensity of CFRP-strengthened wide-flange steel beams with various crack configurations.* Construction and Building Materials, 2014. **70**: p. 522-530.
20. Hmidan, A., Y.J. Kim, and S. Yazdani, *Stress intensity factors for cracked steel girders strengthened with CFRP sheets.* Journal of Composites for Construction, 2014. **19**(5): p. 04014085.
21. Fisher, J.W., *Effect of weldments on the fatigue strength of steel beams.* NCHRP report, 1970.
22. Fisher, J.W., et al., *Fatigue strength of steel beams with welded stiffeners and attachments.* NCHRP report, 1974(147).
23. Albrecht, P., A. Lenwari, and D. Feng, *Stress intensity factors for structural steel I-beams.* Journal of structural engineering, 2008. **134**(3): p. 421-429.

24. Paris, P.C. and H. Tada, *The stress intensity factors for cyclic reversed bending of a single edge cracked strip including crack surface interference.* International Journal of Fracture, 1975. **11**(6): p. 1070-1072.
25. Bowie, O. and C. Freese, *On the "overlapping" problem in crack analysis.* Engineering Fracture Mechanics, 1976. **8**(2): p. 373-379.
26. Woo, C., et al., *A simple model for the contact problem of a finite cracked plate in bending.* Engineering fracture mechanics, 1988. **29**(2): p. 227-231.
27. Albrecht, P. and A. Lenwari, *Stress intensity factor for center-cracked plate with crack surface interference.* Engineering fracture mechanics, 2006. **73**(8): p. 1035-1045.
28. Anderson, T.L. and T. Anderson, *Fracture mechanics: fundamentals and applications*. 2005: CRC press.
29. Rice, J.R., *A path independent integral and the approximate analysis of strain concentration by notches and cracks.* Journal of Applied Mechanics, 1968.
30. AISC, *Steel Construction Manual*. 14 ed. 2011, CHICAGO: American Institute of Steel Construction. 2192.
31. *User's guide*. ANSYS 15.0: Canonsburg, PA.
32. Chen, X. and P. Albrecht, *Weight functions for eccentric cracks*, in *Fracture mechanics: Twenty-fourth volume*. 1994, ASTM International.

APPENDIX

THE FINITE ELEMENT MODEL OF STEEL I-BEAMS

WITH NON-OVERLAPPING CRACK SURFACE

IN ANSYS MECHANICAL APDL

1. Description of the problem

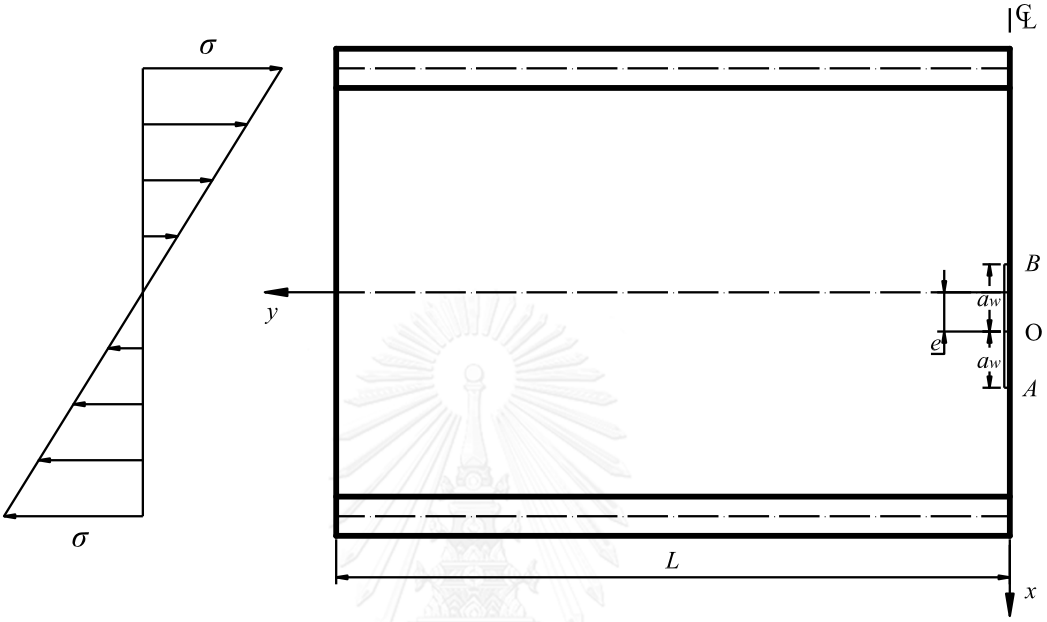

W-shape details: W40x167 (β =1.0, d_j = 953.8 mm, t_w = 16.5 mm, b_f = 300 mm, t_f = 26.2 mm)

- A half of the web crack length: a_w = 143.07 mm (λ_w = 0.3).
- Bending stress at the junction of the web and flange: σ = 100 MPa
- The crack eccentricity: e = 0 mm
- Half length of the I-beam: L = 953.8 mm

2. Analysis of the problem

- STEP 1 : Choose the discipline to show in the GUI

GUI: Main menu > Preferences

Click on “Structural”.

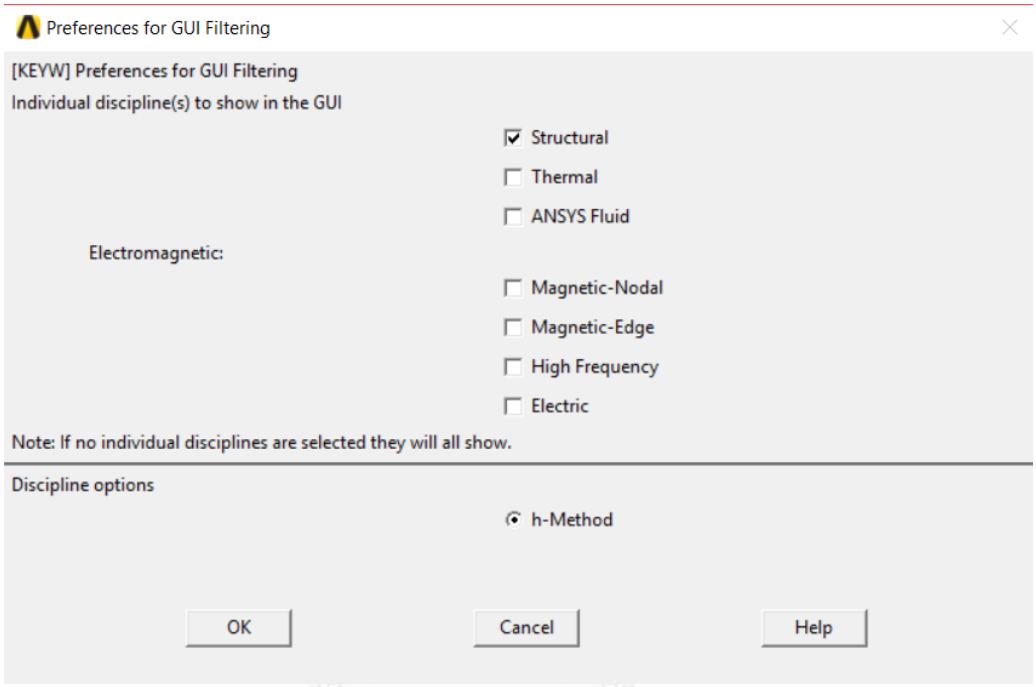

Batch text:

```
/NOPR
KEYW,PR_SET,1
KEYW,PR_STRUC,1
KEYW,PR_THERM,0
KEYW,PR_FLUID,0
KEYW,PR_ELMAG,0
KEYW,MAGNOD,0
KEYW,MAGEDG,0
KEYW,MAGHFE,0
KEYW,MAGELC,0
KEYW,PR_MULTI,0
/GO
```

➢ STEP 2 : Define element types

GUI: Main menu > Preprocessor > Element Type > Add/Edit/Delete

Element types 1, 2 and are defined as “8 node 281 shell element”, “3D Target element TARGE170” and “3D line-surface contact element CONTA177”, respectively.

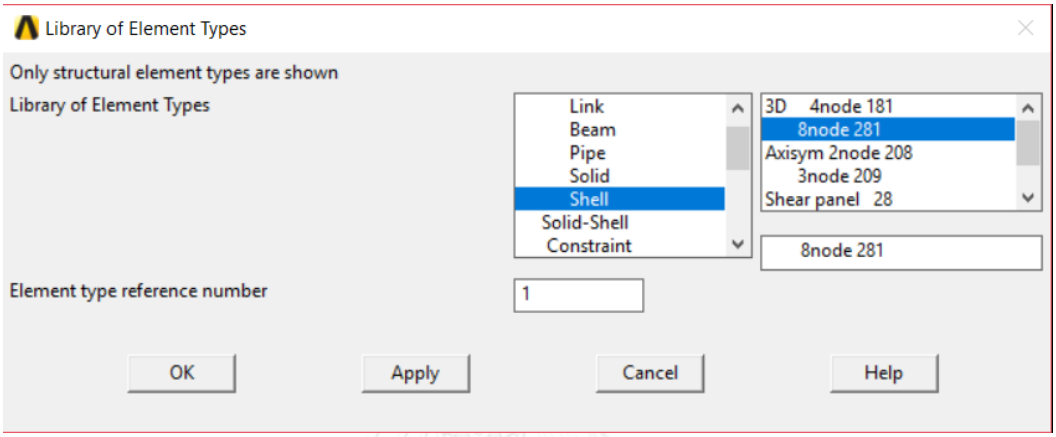

Batch text:

ET,1,SHELL281

ET,2,TARGE170

ET,3,CONTA177

➢ STEP 3 : Define material properties

GUI: Main Menu > Preprocessor > Material Props > Material Models

The material is linear elastic isotropic with E = 200 GPa, ν = 0.3.

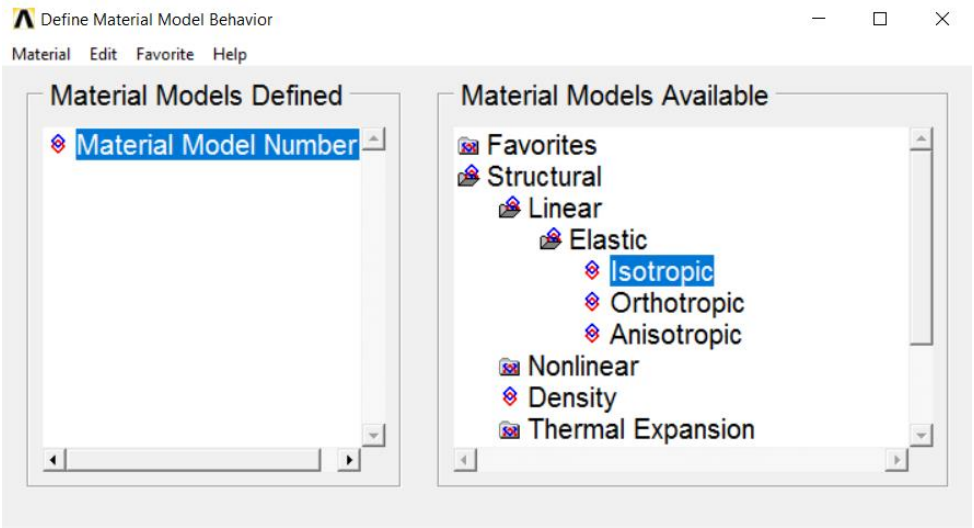

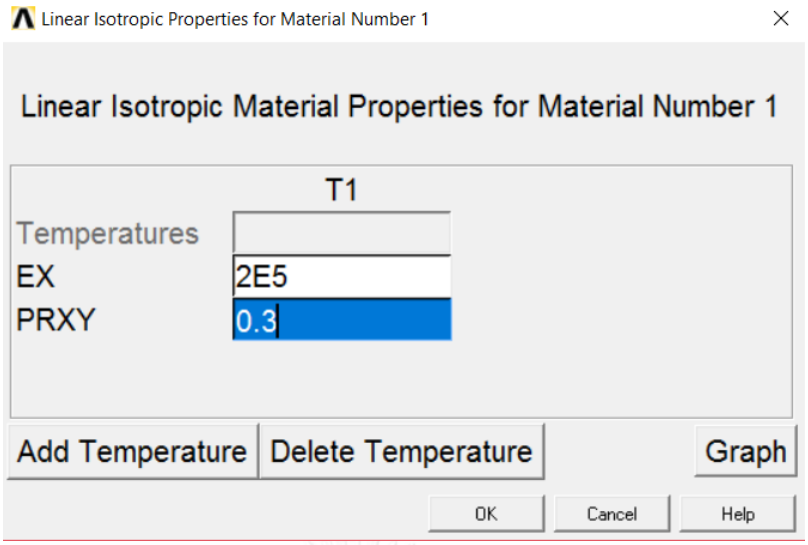

Batch text:

MPTEMP,,,,,,,,

MPTEMP,1,0

MPDATA,EX,1,,2E5

MPDATA,PRXY,1,,0.3

➢ STEP 4 : Define shell sections

GUI: Main Menu > Preprocessor > Sections > Shell > Lay-up > Add/Edit

The thickness of the web and the flange are 16.5 and 26.2 mm, respectively.

Choose “Mid-Plane” for “Section Offset”.

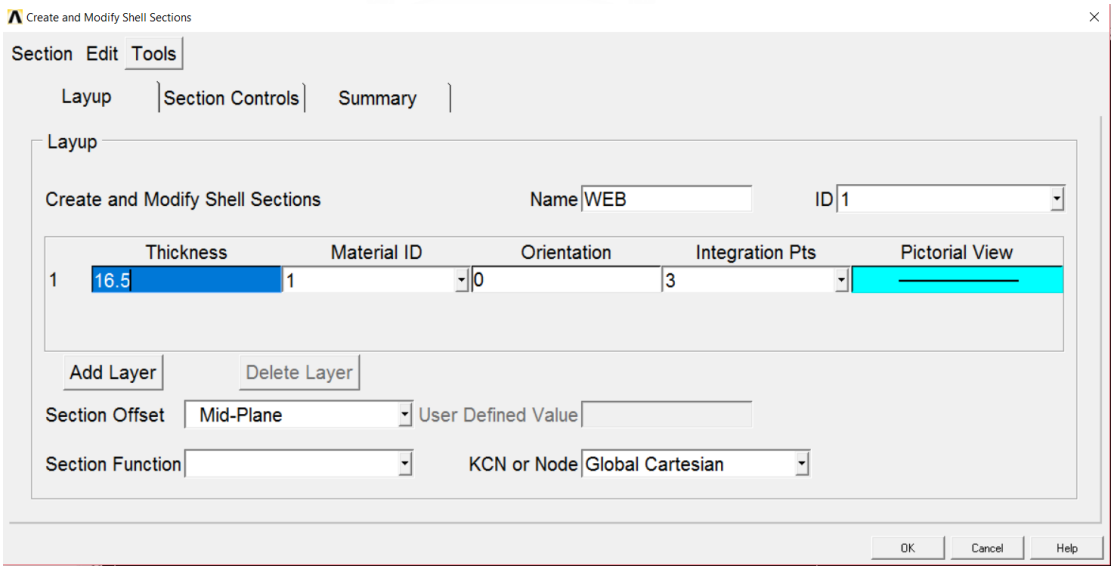

Batch text:

sect,1,shell,,W

secdata, 16.5,1,0.0,3

secoffset,MID

seccontrol,,,, , , ,

sect,2,shell,,F

secdata, 26.2,1,0,3

secoffset,MID

seccontrol,0,0,0, 0, 1, 1,

➢ STEP 5 : Create the I-beam geometry

GUIs: Main Menu > Preprocessor > Modeling > Create > Keypoints > In Active CS

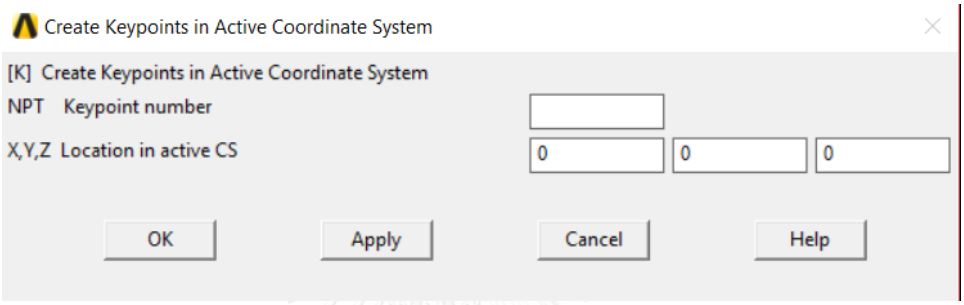

Main Menu > Preprocessor > Modeling > Create > Lines > Lines > In Active Coord

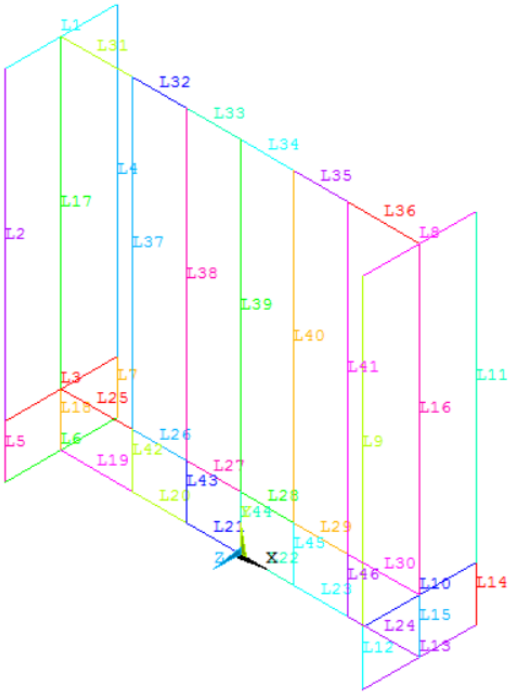

Main Menu > Preprocessor > Modeling > Create > Areas > Arbitrary > By Lines

Main Menu > Preprocessor > Modeling > Operate > Booleans > Glue > Areas

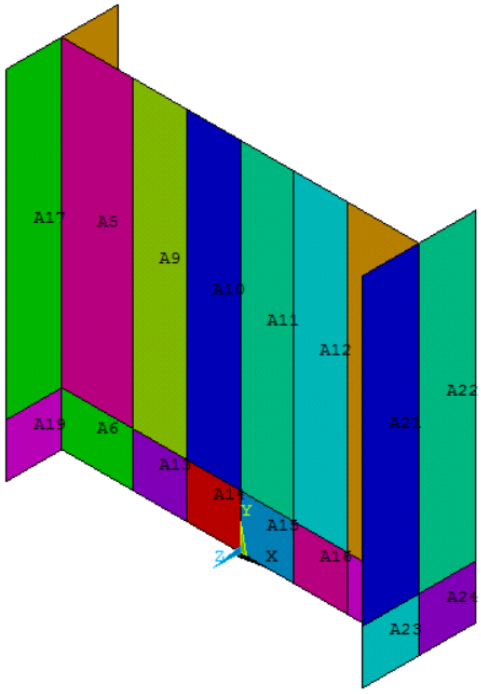

Batch text:

K, ,0,0,,

K, ,143.07,0,,

K, ,-143.07,0,,

K, ,286.14,0,,

K, ,-286.14,0,,

K, ,476.9,0,,

K, ,-476.9,0,,

FLST,3,7,3,ORDE,2

FITEM,3,1

FITEM,3,-7

K, ,-476.9,0,150,

K, ,-476.9,0,-150,

K, ,476.9,0,-150,

K, ,476.9,0,150,

FLST,3,11,3,ORDE,2

FITEM,3,1

FITEM,3,-11

KGEN,2,P51X, , , ,143.07, , ,0

FLST,3,11,3,ORDE,2

```
FITEM,3,1
FITEM,3,-11
KGEN,2,P51X, , , ,953.8, , ,0
L,      30,      31
L,      30,      19
L,      19,      20
L,      20,      31
L,      19,       8
L,       8,       9
L,       9,      20
L,      33,      32
L,      33,      22
L,      22,      21
L,      21,      32
L,      22,      11
L,      11,      10
L,      10,      21
L,       6,      17
L,      17,      28
L,      29,      18
L,      18,       7
L,       7,       5
L,       5,       3
L,       3,       1
L,       1,       2
L,       2,       4
L,       4,       6
L,      18,      16
L,      16,      14
L,      14,      12
L,      12,      13
L,      13,      15
L,      15,      17
L,      29,      27
L,      27,      25
```

```
L,      25,     23
L,      23,     24
L,      24,     26
L,      26,     28
L,      27,     16
L,      25,     14
L,      23,     12
L,      24,     13
L,      26,     15
L,      16,      5
L,      14,      3
L,      12,      1
L,      13,      2
L,      15,      4
FLST,2,4,4
FITEM,2,2
FITEM,2,1
FITEM,2,4
FITEM,2,3
AL,P51X
FLST,2,4,4
FITEM,2,5
FITEM,2,6
FITEM,2,7
FITEM,2,3
AL,P51X
FLST,2,4,4
FITEM,2,12
FITEM,2,10
FITEM,2,14
FITEM,2,13
AL,P51X
FLST,2,4,4
FITEM,2,10
FITEM,2,11
```

FITEM,2,8
FITEM,2,9
AL,P51X
FLST,2,4,4
FITEM,2,17
FITEM,2,31
FITEM,2,37
FITEM,2,25
AL,P51X
FLST,2,4,4
FITEM,2,25
FITEM,2,18
FITEM,2,19
FITEM,2,42
AL,P51X
FLST,2,4,4
FITEM,2,16
FITEM,2,36
FITEM,2,41
FITEM,2,30
AL,P51X
FLST,2,4,4
FITEM,2,15
FITEM,2,24
FITEM,2,46
FITEM,2,30
AL,P51X
FLST,2,4,4
FITEM,2,32
FITEM,2,37
FITEM,2,38
FITEM,2,26
AL,P51X
FLST,2,4,4
FITEM,2,33

FITEM,2,38
FITEM,2,39
FITEM,2,27
AL,P51X
FLST,2,4,4
FITEM,2,34
FITEM,2,39
FITEM,2,40
FITEM,2,28
AL,P51X
FLST,2,4,4
FITEM,2,35
FITEM,2,40
FITEM,2,41
FITEM,2,29
AL,P51X
FLST,2,4,4
FITEM,2,26
FITEM,2,42
FITEM,2,43
FITEM,2,20
AL,P51X
FLST,2,4,4
FITEM,2,27
FITEM,2,43
FITEM,2,44
FITEM,2,21
AL,P51X
FLST,2,4,4
FITEM,2,28
FITEM,2,44
FITEM,2,45
FITEM,2,22
AL,P51X
FLST,2,4,4

FITEM,2,29

FITEM,2,45

FITEM,2,46

FITEM,2,23

AL,P51X

FLST,2,16,5,ORDE,2

FITEM,2,1

FITEM,2,-16

AGLUE,P51X

- STEP 6 : Mesh the geometry

GUIs: Main Menu > Preprocessor > Meshing > Mesh Attributes > Pick Areas

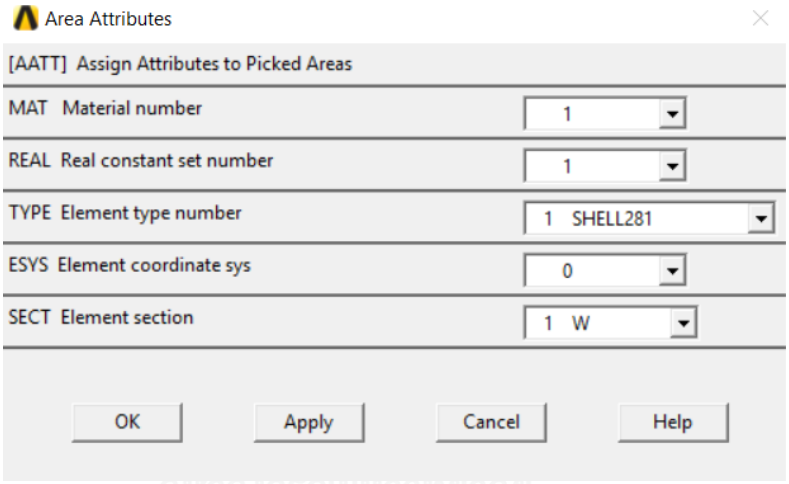

Main Menu > Preprocessor > Meshing > Size Cntrls > ManualSize > Lines > Picked Lines

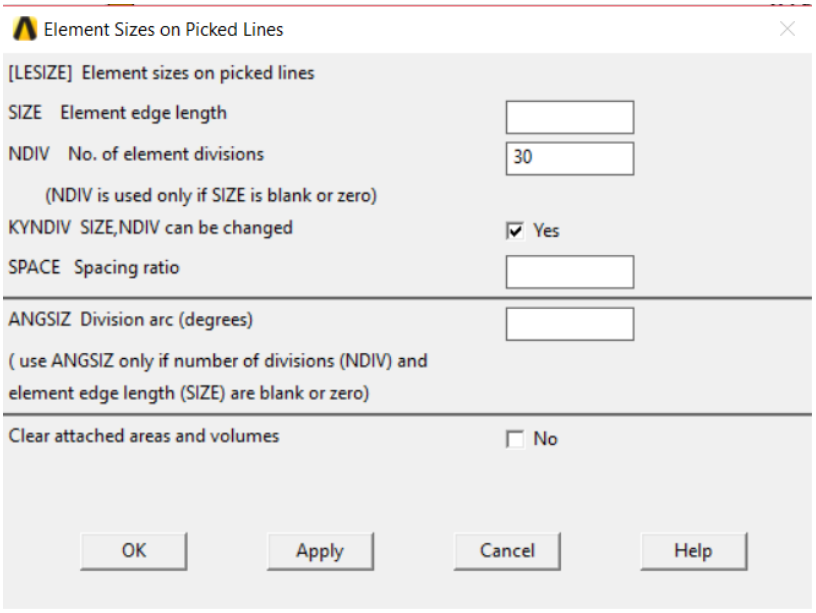

Main Menu > Preprocessor > Meshing > Mesh > Areas > Free

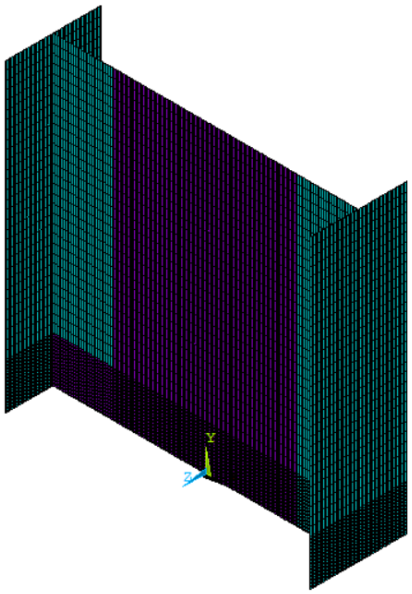

Batch text:

```
FLST,5,4,5,ORDE,2
FITEM,5,17
FITEM,5,-20
CM,_Y,AREA
ASEL, , , ,P51X
CM,_Y1,AREA
CMSEL,S,_Y
CMSEL,S,_Y1
AATT,       1, ,    1,       0,    2
CMSEL,S,_Y
CMDELE,_Y
CMDELE,_Y1
FLST,5,4,5,ORDE,2
FITEM,5,21
FITEM,5,-24
CM,_Y,AREA
ASEL, , , ,P51X
CM,_Y1,AREA
CMSEL,S,_Y
CMSEL,S,_Y1
```

```
AATT,       1, ,   1,       0,   2
CMSEL,S,_Y
CMDELE,_Y
CMDELE,_Y1
FLST,5,12,5,ORDE,2
FITEM,5,5
FITEM,5,-16
CM,_Y,AREA
ASEL, , , ,P51X
CM,_Y1,AREA
CMSEL,S,_Y
CMSEL,S,_Y1
AATT,       1, ,   1,       0,   1
CMSEL,S,_Y
CMDELE,_Y
CMDELE,_Y1
FLST,5,52,4,ORDE,9
FITEM,5,2
FITEM,5,4
FITEM,5,-5
FITEM,5,7
FITEM,5,9
FITEM,5,11
FITEM,5,-12
FITEM,5,14
FITEM,5,-58
CM,_Y,LINE
LSEL, , , ,P51X
CM,_Y1,LINE
CMSEL,,_Y
LESIZE,_Y1, , ,30, , , , ,1
MSHKEY,0
FLST,5,20,5,ORDE,2
FITEM,5,5
FITEM,5,-24
```

CM,_Y,AREA

ASEL, , , ,P51X

CM,_Y1,AREA

CHKMSH,'AREA'

CMSEL,S,_Y

AMESH,_Y1

CMDELE,_Y

CMDELE,_Y1

CMDELE,_Y2

➢ STEP 7 : Apply the displacement boundary condition

GUIs: Main Menu > Preprocessor > Loads > Define Loads > Apply > Structural > Displacement > On Lines

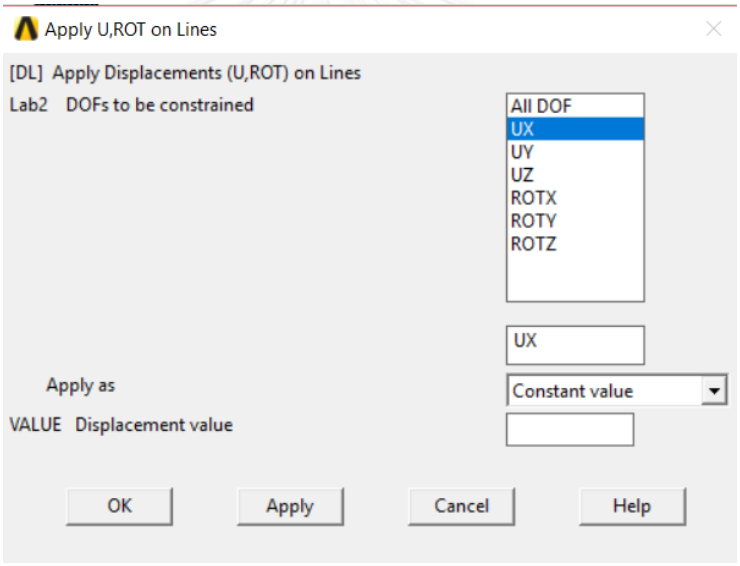

Main Menu > Preprocessor > Loads > Define Loads > Apply > Structural > Displacement > Symmetry B.C. > On Lines

Batch text:

FLST,2,2,4,ORDE,2

FITEM,2,57

FITEM,2,-58

/GO

DL,P51X, ,UX,

FLST,2,2,4,ORDE,2

FITEM,2,57

FITEM,2,-58
/GO
DL,P51X, ,UZ,
FLST,2,2,4,ORDE,2
FITEM,2,57
FITEM,2,-58
/GO
DL,P51X, ,ROTX,
FLST,2,2,4,ORDE,2
FITEM,2,57
FITEM,2,-58
/GO
DL,P51X, ,ROTY,
FLST,2,8,4,ORDE,8
FITEM,2,19
FITEM,2,-20
FITEM,2,23
FITEM,2,-24
FITEM,2,51
FITEM,2,-52
FITEM,2,57
FITEM,2,-58
DL,P51X, ,SYMM

- STEP 8 : Apply the pressure

GUIs: Main Menu > Preprocessor > Loads > Define Loads > Apply > Functions > Define/Edit

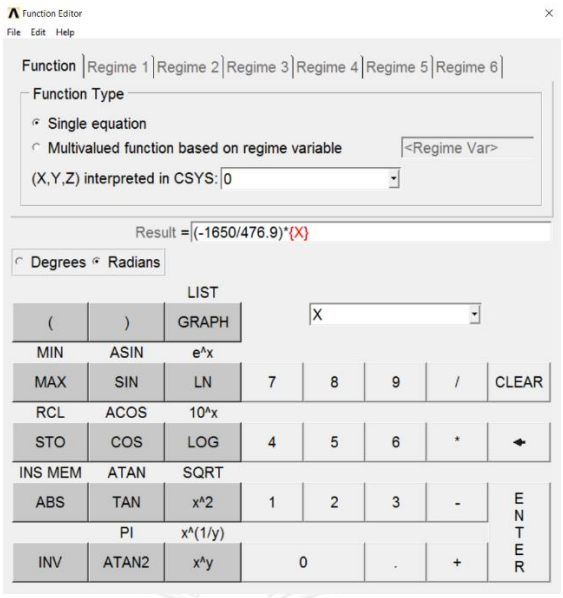

Main Menu > Preprocessor > Loads > Define Loads > Apply > Functions > Read File

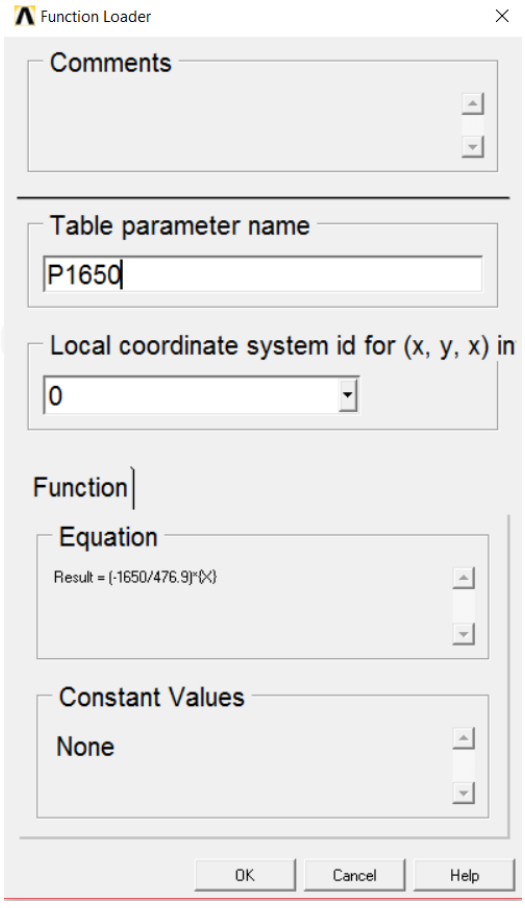

Main Menu > Preprocessor > Loads > Define Loads > Apply > Structural > Pressure > On Lines

On flange > Constant value

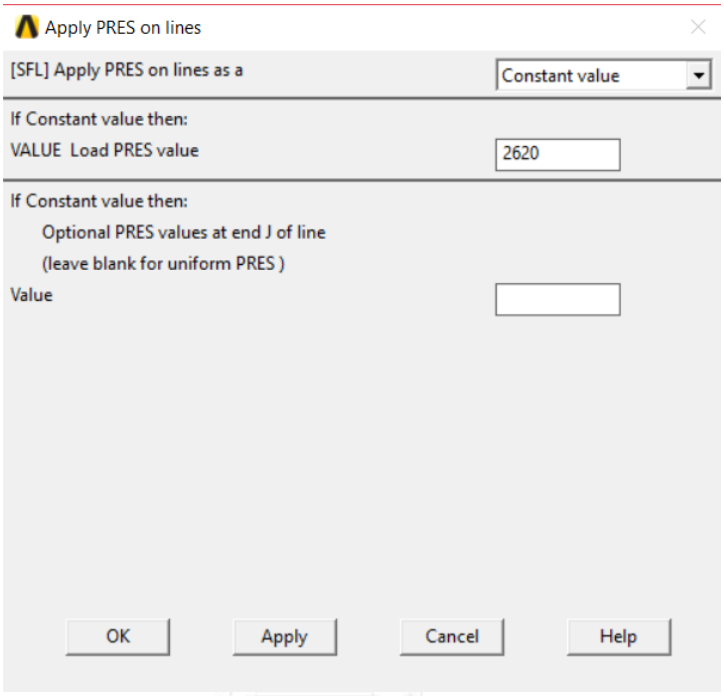

On web > Existing table

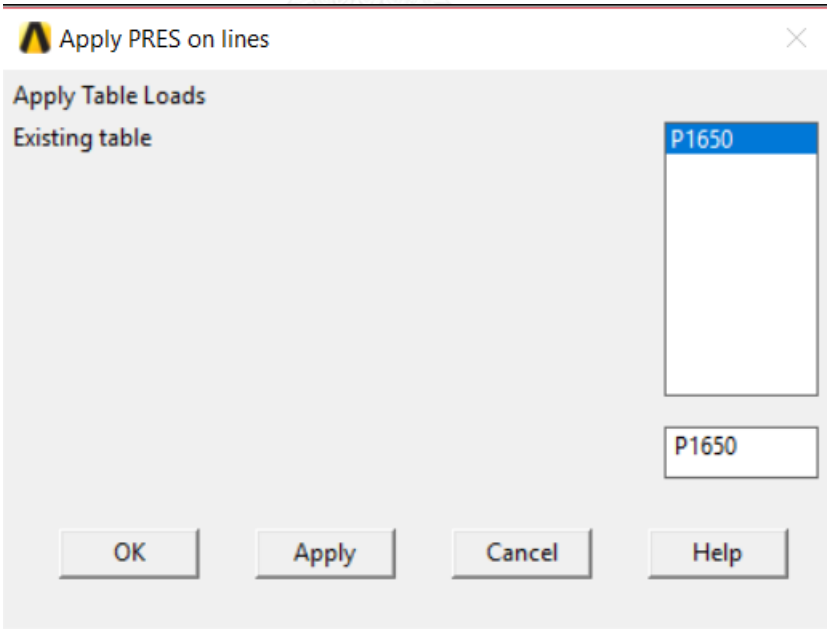

Batch text:

FLST,2,2,4,ORDE,2

FITEM,2,48

FITEM,2,50

```
/GO
SFL,P51X,PRES,2620,
FLST,2,2,4,ORDE,2
FITEM,2,54
FITEM,2,56
/GO
SFL,P51X,PRES,-2620,
*DEL,_FNCNAME
*DEL,_FNCMTID
*DEL,_FNCCSYS
*SET,_FNCNAME,'P1650'
*SET,_FNCCSYS,0
! /INPUT,.\Desktop\THESIS\ANSYS Load\p1650.func,,,1
*DIM,%_FNCNAME%,TABLE,6,9,1,,,,%_FNCCSYS%
!
! Begin of equation: (-1650/476.9)*{X}
*SET,%_FNCNAME%(0,0,1), 0.0, -999
*SET,%_FNCNAME%(2,0,1), 0.0
*SET,%_FNCNAME%(3,0,1), 0.0
*SET,%_FNCNAME%(4,0,1), 0.0
*SET,%_FNCNAME%(5,0,1), 0.0
*SET,%_FNCNAME%(6,0,1), 0.0
*SET,%_FNCNAME%(0,1,1), 1.0, -1, 0, 0, 0, 0, 0
*SET,%_FNCNAME%(0,2,1), 0.0, -2, 0, 1, 0, 0, -1
*SET,%_FNCNAME%(0,3,1),    0, -3, 0, 1, -1, 2, -2
*SET,%_FNCNAME%(0,4,1), 0.0, -1, 0, 1650, 0, 0, -3
*SET,%_FNCNAME%(0,5,1), 0.0, -2, 0, 1, -3, 3, -1
*SET,%_FNCNAME%(0,6,1), 0.0, -1, 0, 476.9, 0, 0, -2
*SET,%_FNCNAME%(0,7,1), 0.0, -3, 0, 1, -2, 4, -1
*SET,%_FNCNAME%(0,8,1), 0.0, -1, 0, 1, -3, 3, 2
*SET,%_FNCNAME%(0,9,1), 0.0, 99, 0, 1, -1, 0, 0
! End of equation: (-1650/476.9)*{X
!-->
FLST,2,6,4,ORDE,2
FITEM,2,31
```

FITEM,2,-36

/GO

SFL,P51X,PRES, %P1650%

➢ STEP 9 : Create and mesh the target plane

GUIs: Main Menu > Preprocessor > Modeling > Create > Areas > Arbitrary > Through KPs

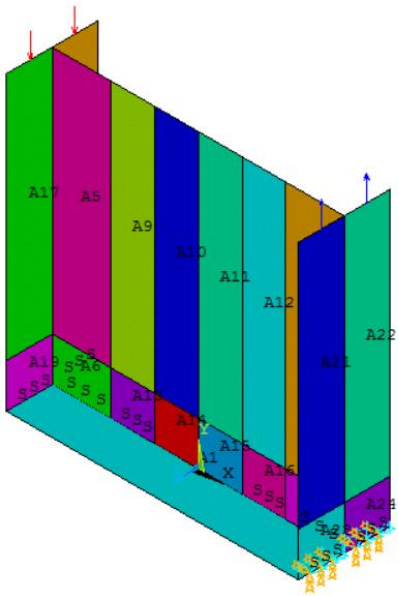

Main Menu > Preprocessor > Meshing > Mesh Attributes > Pick Areas

Pick area #1.

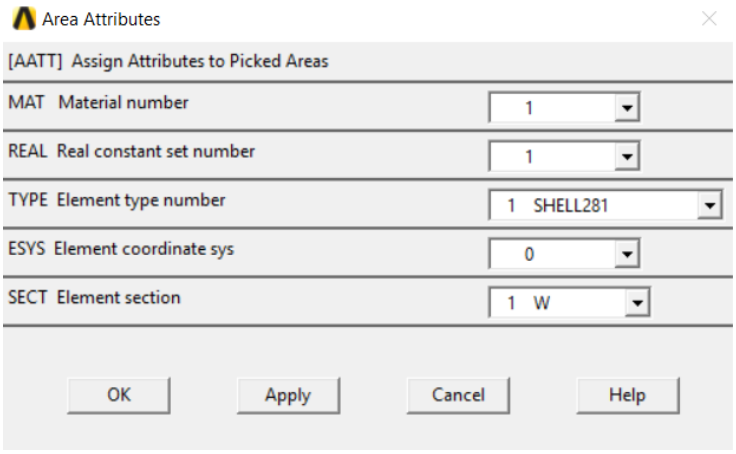

Main Menu > Preprocessor > Meshing > Size Cntrls > ManualSize > Areas > Picked Areas

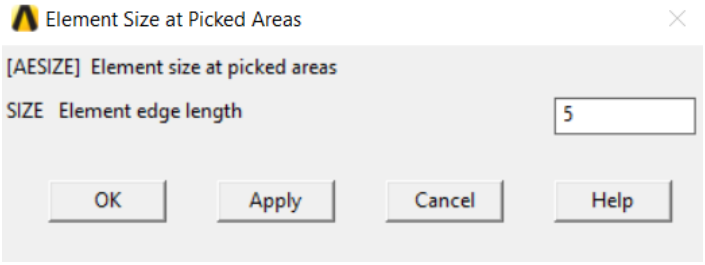

Main Menu > Preprocessor > Meshing > Mesh > Areas > Free

Batch text:

```
FLST,2,4,3
FITEM,2,8
FITEM,2,11
FITEM,2,10
FITEM,2,9
A,P51X
CM,_Y,AREA
ASEL, , , ,       1
CM,_Y1,AREA
CMSEL,S,_Y
CMSEL,S,_Y1
AATT,      1,      1,   1,      0,   1
CMSEL,S,_Y
CMDELE,_Y
CMDELE,_Y1
FLST,2,1,5,ORDE,1
FITEM,2,1
AESIZE,P51X,5,
MSHKEY,0
CM,_Y,AREA
ASEL, , , ,       1
CM,_Y1,AREA
CHKMSH,'AREA'
CMSEL,S,_Y
AMESH,_Y1
CMDELE,_Y
```

CMDELE,_Y1

CMDELE,_Y2

MSHKEY,0

➢ STEP 10 : Assign the target and contact elements

GUIs: Main Menu > Preprocessor > Modeling > Create > Elements > Elem Attributes

For contact element CONTA177 along the shell edge of the web

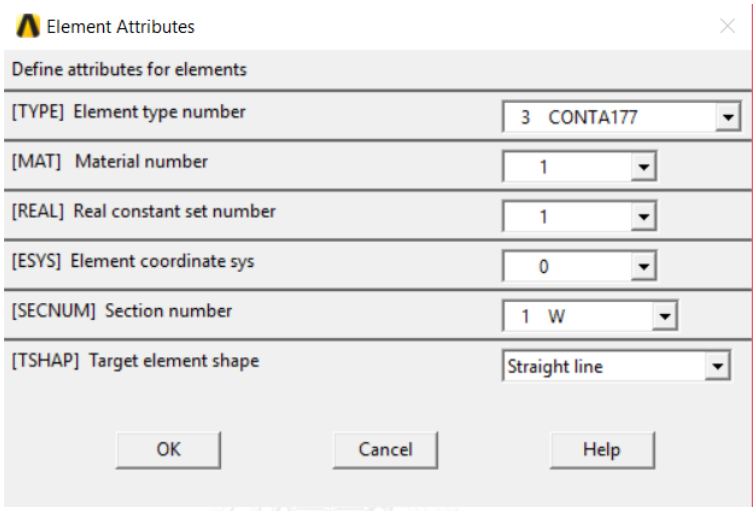

For the target surface TARGE170

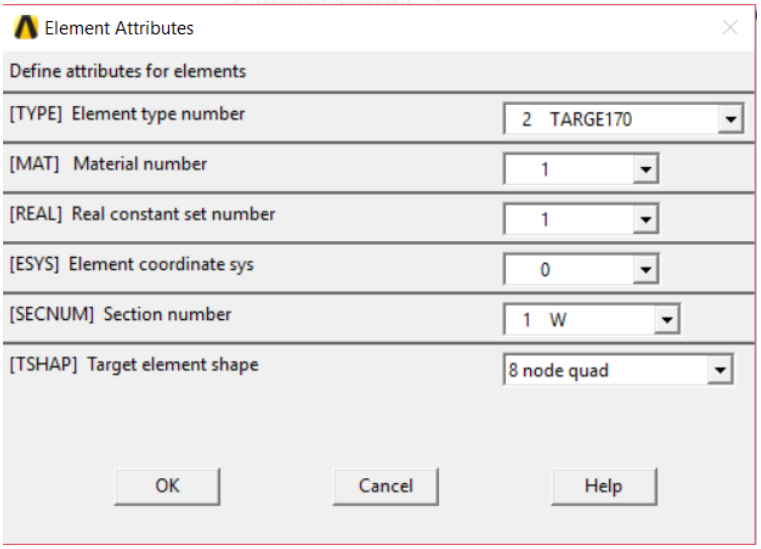

Main Menu > Preprocessor > Modeling > Create > Elements > Surf/Contact > Surf to Surf

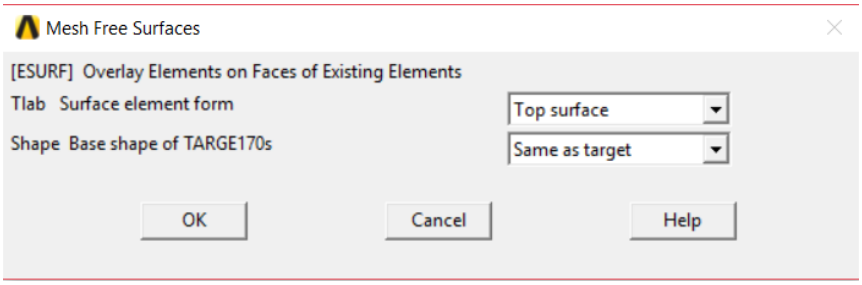

Main Menu > Preprocessor > Meshing > Clear > Areas

Main Menu > Preprocessor > Modeling > Delete > Areas Only

Pick area #1.

“CNCHECK, TRIM” to eliminate the unnecessary contact and target elements.

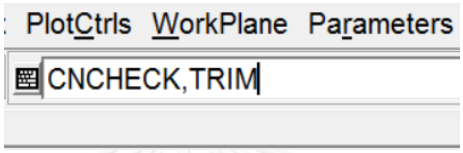

Batch text:

FLST,5,2,4,ORDE,2

FITEM,5,21

FITEM,5,-22

LSEL,S, , ,P51X

NSLL,S,1

NPLOT

TYPE, 3

MAT, 1

REAL, 1

ESYS, 0

SECNUM, 1

TSHAP,LINE

FLST,5,121,1,ORDE,7

FITEM,5,22142

FITEM,5,24842

FITEM,5,24902

FITEM,5,-24960

FITEM,5,27542

FITEM,5,27602

FITEM,5,-27660

CM,_Y,NODE

```
NSEL, , , ,P51X
CM,_Y1,NODE
CMSEL,S,_Y
CMSEL,,_Y1
ESURF, ,TOP,
CMSEL,,_Y
CMDELE,_Y
CMDELE,_Y1
ASEL,S, , ,       1
NSLA,S,1
NPLOT
TYPE,   2
MAT,       1
REAL,       1
ESYS,       0
SECNUM,   1
TSHAP,QUA8
FLST,5,34883,1,ORDE,6
FITEM,5,38402
FITEM,5,41102
FITEM,5,49322
FITEM,5,52022
FITEM,5,54722
FITEM,5,-89600
CM,_Y,NODE
NSEL, , , ,P51X
CM,_Y1,NODE
CMSEL,S,_Y
CMSEL,,_Y1
ESURF, ,TOP,
CMSEL,,_Y
CMDELE,_Y
CMDELE,_Y1
ACLEAR,       1
ADELE,       1
```

EPLOT

ALLSEL,ALL

CNCHECK,TRIM

➢ STEP 11 : Solve the problem

GUIs: Main Menu > Solution > Analysis Type > Sol'n Controls

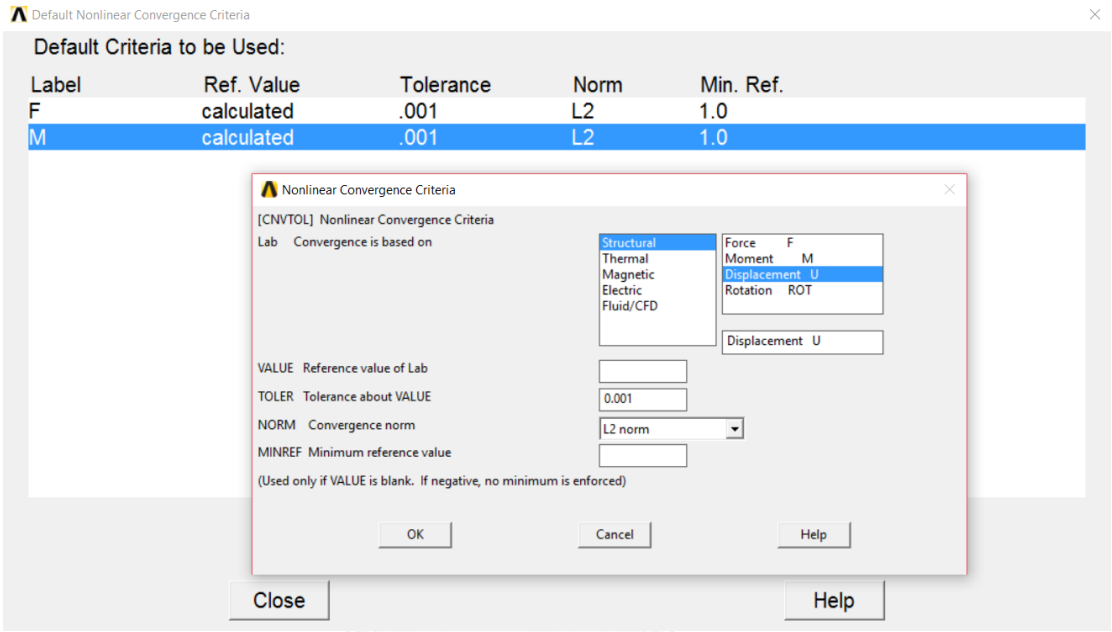

Main Menu > Solution > Solve > Current LS

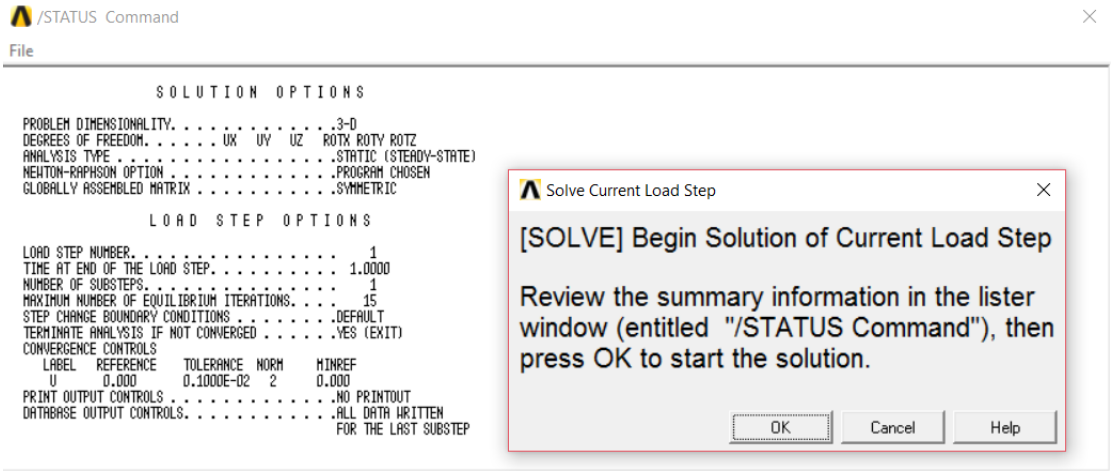

Batch text:

/SOL

CNVTOL,U, ,0.001,2, ,

/STATUS,SOLU

SOLVE

➢ STEP 12 : Define a path around crack tip

GUIs: Main Menu > General Postproc > Path Operations > Define Path > By Nodes

Define the path along the edge of the refinement mesh area around the tension side crack tip.

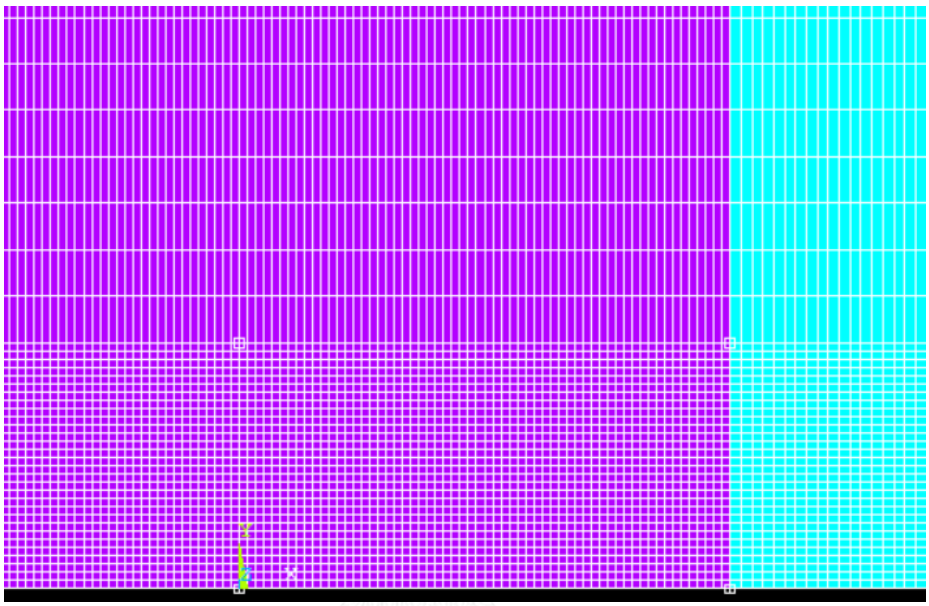

Batch text:

```
/POST1
FLST,2,4,1
FITEM,2,8463
FITEM,2,5703
FITEM,2,13983
FITEM,2,24842
PATH,s,4,30,20,
PPATH,P51X,1
PATH,STAT
```


➢ STEP 13 : Calculate the J- Integral value

Batch text:

```
AVPRIN,0, ,
ETABLE, ,SENE,
AVPRIN,0, ,
```

```
ETABLE, ,VOLU,
SEXP,sexp,SENE,VOLU,1,-1,
AVPRIN,0, ,
PDEF, ,ETAB,SEXP,AVG
/PBC,PATH, ,0
PCALC,INTG,WDY,ETABSEXP,YG,1,
AVPRIN,0, ,
PDEF, ,S,X,AVG
/PBC,PATH, ,0
AVPRIN,0, ,
PDEF, ,S,Y,AVG
/PBC,PATH, ,0
AVPRIN,0, ,
PDEF, ,S,XY,AVG
/PBC,PATH, ,0
PVECT,NORM,NX,NY,NZ
PCALC,MULT,SXNX,SX,NX,1,
PCALC,MULT,SXYNY,SXY,NY,1,
PCALC,MULT,SYNY,SY,NY,1,
PCALC,MULT,SXYNX,SXY,NX,1,
PCALC,ADD,TX,SXNX,SXYNY,1,1, ,
PCALC,ADD,TY,SYNY,SXYNX,1,1, ,
*GET,DX,PATH,,LAST,S
*SET,DX,DX/100
PCAL,ADD,XG,XG,,,,-DX/2
PDEF,UX1,U,X
PDEF,UY1,U,Y
PCAL,ADD,XG,XG,,,,DX
PDEF,UX2,U,X
PDEF,UY2,U,Y
PCAL,ADD,XG,XG,,,,-DX/2
*SET,C,1/DX
PCAL,ADD,C1,UX2,UX1,C,-C
PCAL,ADD,C2,UY2,UY1,C,-C
PCALC,MULT,TXUX,TX,C1,1,
```

```
PCALC,MULT,TYUY,TY,C2,1,
PCALC,ADD,T,TXUX,TYUY,1,1, ,
PCALC,INTG,TDS,T,S,1,
PCALC,ADD,J,WDY,TDS,1,-1, ,
PRPATH,WDY,TX,TY,TDS,J
```

VITA

The author, Hieu Chi Ma, was born near Ho Chi Minh City, Vietnam, on April 30, 1991. He received a Bachelor of Engineering in Civil Engineering from Ho Chi Minh City University of Technology in 2014. In 2015, he achieved the scholarship by AUN/SEED-Net for his Master degree in Civil Engineering at Chulalongkorn University under the supervision of Associate Professor Akhrawat Lenwari, Ph.D. His currently interest is in Fracture Mechanics and Finite Element Method.